NAVAL POSTGRADUATE SCHOOL
Monterey, California

THESIS

AN EXPERIMENTAL INVESTIGATION INTO THE DYNAMIC RESPONSE OF A STIFFENED FLAT PLATE LOADED IMPULSIVELY BY AN UNDERWATER SHOCKWAVE

by

Thomas R. Rentz

June 1984

Thesis Advisor: Y.S. Shin

Approved for public release; distribution unlimited

SECURITY CLASSIFICATION OF THIS PAGE (When Data Entered)

REPORT DOCUMENTATION PAGE	READ INSTRUCTIONS BEFORE COMPLETING FORM
1 REPORT NUMBER	2 GOVT ACCESSION NO. A151321 / 3 RECIPIENT'S CATALOG NUMBER
4 TITLE (and Subtitle) An Experimental Investigation into the Dynamic Response of a Stiffened Flat Plate Loaded Impulsively by an Underwater Shockwave	5 TYPE OF REPORT & PERIOD COVERED Master's Thesis; June 1984
	6 PERFORMING ORG. REPORT NUMBER
7. AUTHOR(s) Thomas R. Rentz	8 CONTRACT OR GRANT NUMBER(s)
9. PERFORMING ORGANIZATION NAME AND ADDRESS Naval Postgraduate School Monterey, California 93943	10. PROGRAM ELEMENT, PROJECT, TASK AREA & WORK UNIT NUMBERS
11 CONTROLLING OFFICE NAME AND ADDRESS Naval Postgraduate School Monterey, California 93943	12 REPORT DATE June 1984
	13 NUMBER OF PAGES 172
14. MONITORING AGENCY NAME & ADDRESS (if different from Controlling Office)	15. SECURITY CLASS (of this report) Unclassified
	15a DECLASSIFICATION DOWNGRADING SCHEDULE

16. DISTRIBUTION STATEMENT (of this Report)

Approved for public release; distribution unlimited

17. DISTRIBUTION STATEMENT (of the abstract entered in Block 20, if different from Report)

18. SUPPLEMENTARY NOTES

19 KEY WORDS (Continue on reverse side if necessary and identify by block number)

underwater shock, stiffened flat plate, tripping, EPSA, finite element computer code, ~~non-linear elasto plastic shell response~~, PATRAN-G, electronic instrumentation, strain gage, [illegible] pressure gage

20 ABSTRACT (Continue on reverse side if necessary and identify by block number)

The experiment conducted is in support of a broad-based study of underwater shock wave phenomena and the effects they have on ship's hull lethality. An air-backed flat plate with externally machined rectangular stiffeners and a clamped boundary condition was subjected to a shock wave loading generated by an eight pound TNT charge detonated underwater. The plate was instrumented to measure transient strains. The

DD FORM 1 JAN 73 1473 EDITION OF 1 NOV 65 IS OBSOLETE

S/N 0102-LF-014-6601

SECURITY CLASSIFICATION OF THIS PAGE (When Data Entered)

20. (Continued)

test structure acceleration and free field pressures were also measured. Preshot and postshot calculations were performed using the ~~finite element~~ finite central difference computer code, EPSA (Elasto Plastic Shell Analysis). This code was modified to predict the nonlinear elastoplastic shell response for the plate. The EPSA/~~DATRAN~~ interface program developed at NPS was utilized to produce color graphics which aided greatly in the analysis.

Approved for public release; distribution unlimited

An Experimental Investigation into the Dynamic Response of a Stiffened Flat Plate Loaded Impulsively by an Underwater Shockwave

by

Thomas R. Rentz
Lieutenant, United States Navy
B.S., United States Naval Academy, 1978

Submitted in partial fulfillment of the requirements for the degree of

MASTER OF SCIENCE IN MECHANICAL ENGINEERING

from the

NAVAL POSTGRADUATE SCHOOL
June 1984

Author: Thomas R. Rentz

Approved by: [signature]
Thesis Advisor

R. E. Newton
Second Reader

P. J. Marto
Chairman, Department of Mechanical Engineering

[signature]
Dean of Science and Engineering

ABSTRACT

The experiment conducted is in support of a broad-based study of underwater shock wave phenomena and the effects they have on ship's hull lethality. An air-backed flat plate with externally machined rectangular stiffeners and a clamped boundary condition was subjected to a shock wave loading generated by an eight pound TNT charge detonated underwater. The plate was instrumented to measure transient strains. The test structure acceleration and free field pressures were also measured. Preshot and postshot calculations were performed using the finite element/finite central difference computer code, EPSA (Elasto Plastic Shell Analysis). This code was modified to predict the nonlinear elastoplastic shell response for the plate. The EPSA/PATRAN-G interface program developed at NPS was utilized to produce color graphics which aided greatly in the analysis.

TABLE OF CONTENTS

LIST OF TABLES

LIST OF FIGURES

ACKNOWLEDGEMENTS

I would like to express my appreciation to Professor Young S. Shin for his assistance and the motivation he provided me. Special thanks go to Weidlinger Associates, particularly Dr. Raymond P. Daddazio for his patience. Many individuals here at the Naval Postgraduate School played important roles in carrying out the experimental part of the research. Most notable is Charles Crow for the hours he spent in fabricating the test structure. And finally, LT Hugh Reams, formerly of the Defense Nuclear Agency, deserves a well done for successfully transferring the technology to the school.

I. INTRODUCTION

This paper outlines in detail the work achieved to date at the Naval Postgraduate School in the area of underwater shock loading of plates. The objective of this work is three fold: first to obtain experimental data on the dynamic response of simple structures subject to underwater shock, secondly to compare the experimental results with the predicted results based on the existing computer code, and thirdly for the school as a whole to acquire the knowledge and technical expertise necessary to conduct these types of experiments. An anticipated result of the latter is to identify the problem areas and base technology needs in experiment and prediction methods. This paper discusses the first underwater shock test, which was an investigation into the associated phenomena of gross plate response and the tripping of rectangular stiffeners.

The tripping effect is a lateral, torsional instability of the stiffener as it becomes suddenly unstable and fails under a load. Tripping is also viewed as a buckling and warping of the stiffener. In either case, the response of such structures as a stiffened flat plate or a cylinder with ring stiffeners will change dramatically when the functional character of the stiffeners is reduced after they have

tripped. The need for this study and its applicability to the Navy is self-evident as stiffeners are incorporated in the structural design of all ships and submarines. The results of a previous series of tests on ship-type grillages have been described as "clearly demonstrating the significance of lateral-torsional instability (tripping) as a primary ductile failure mode for ship structure" [Ref. 1].

II. DESIGN AND FABRICATION OF THE TEST STRUCTURE

The purpose of this work was to conduct a series of experimental tests where plates of various stiffener types would be loaded by an underwater shock wave. The plate was geometrically similar to a ship's stiffened hull--or grillage--and air backed. This required a backing structure that was watertight and strong enough to be used throughout the test series. The plate was subjected to large deformations, well into plastic regime, to ensure a good tripping effect in the stiffeners. As an aid in setting up and validating each test, it was necessary to model the test plate using a finite element computer code. Therefore, to ease the modeling requirements, the structure was kept simple throughout the design process. Well defined geometric and material properties and good boundary conditions were specified. As in any experimental test, the number of uncertainties were kept as few as possible.

Needed for the plate material was a common and easily machinable metal with the material properties of being initially isotropic and exhibiting very little strain hardening. 6061-T6 aluminum was selected because it has these properties and is readily available in the sizes required. It is easily machined and can be welded as well.

Upon receipt of the material, a section of the blank was removed and tension test specimens made from it. The uniaxial tension tests were conducted to characterize the 6061-T6 aluminum as having a yield stress (σ_y) of 43200 psi and an ultimate stress (σ_{ult}) of 44900 psi. The recorded elongation is 11.5%. Data from these tests are presented in Appendix A.

As for the boundary conditions of the test panel, a clamped arrangement has proven in past shock tests to be most effective. The integral edge arrangement reported by E. A. Witmer and R. Wu [Ref. 2] was adopted. This involved machining the test panel out of larger blank stock and leaving a massive edge on all four sides. Previous designs for a clamped boundary of a panel to be shock tested had employed such schemes as serrated clamps, massive bolts, or hardened faces, all of which had slipped to a degree. It was this final design of an integral edge which exhibits essentially no slip during loading [Ref. 3].

The stiffeners were likewise integrally machined from the aluminum blank to eliminate any uncertainty that would arise from a welding procedure. All corners and intersections were rounded to remove any stress concentrators.

To model a typical ship's grillage requires the use of scaling laws. Based on discussions with Dr. R. P. Daddazio of Weidlinger Associates, Inc., there are two important parameters, β and λ, for scaling of the grillage.

$$\beta = (b/t)\sqrt{\sigma_y/E} \quad \text{and} \quad \lambda = (a/k\pi)\sqrt{\sigma_y/E} \qquad \text{(eqn 2.1)}$$

The two parameters are defined such that β is a measure of the plate's slenderness ratio and λ is a measure of the slenderness of the longitudinal stiffeners. Other variables are:

σ_y = material yield strength

E = Young's modulus

b = spacing of the longitudinal stiffeners

t = plate thickness

k = radius of gyration of longitudinal stiffener acting with an assumed effective width of plating denoted by b_e

a = spacing of the transverse frames

b_e = effective width of plating given by $b_e = b(\frac{2}{\beta} - \frac{1}{\beta^2})$

[Ref. 1].

The final dimensions of the test panel are as shown in Figure 2.1. A calculation of the β and λ as a check on the design is necessary. From reference 4 a survey of typical ship's grillages yields:

$$1 \leq \beta \leq 4.5 \quad \text{and} \quad .15 \leq \lambda \leq .9$$

Approximate engineering reference text values for the 6061-T6 yield strength and elastic modulus were used in this design process because the stock material was not on hand

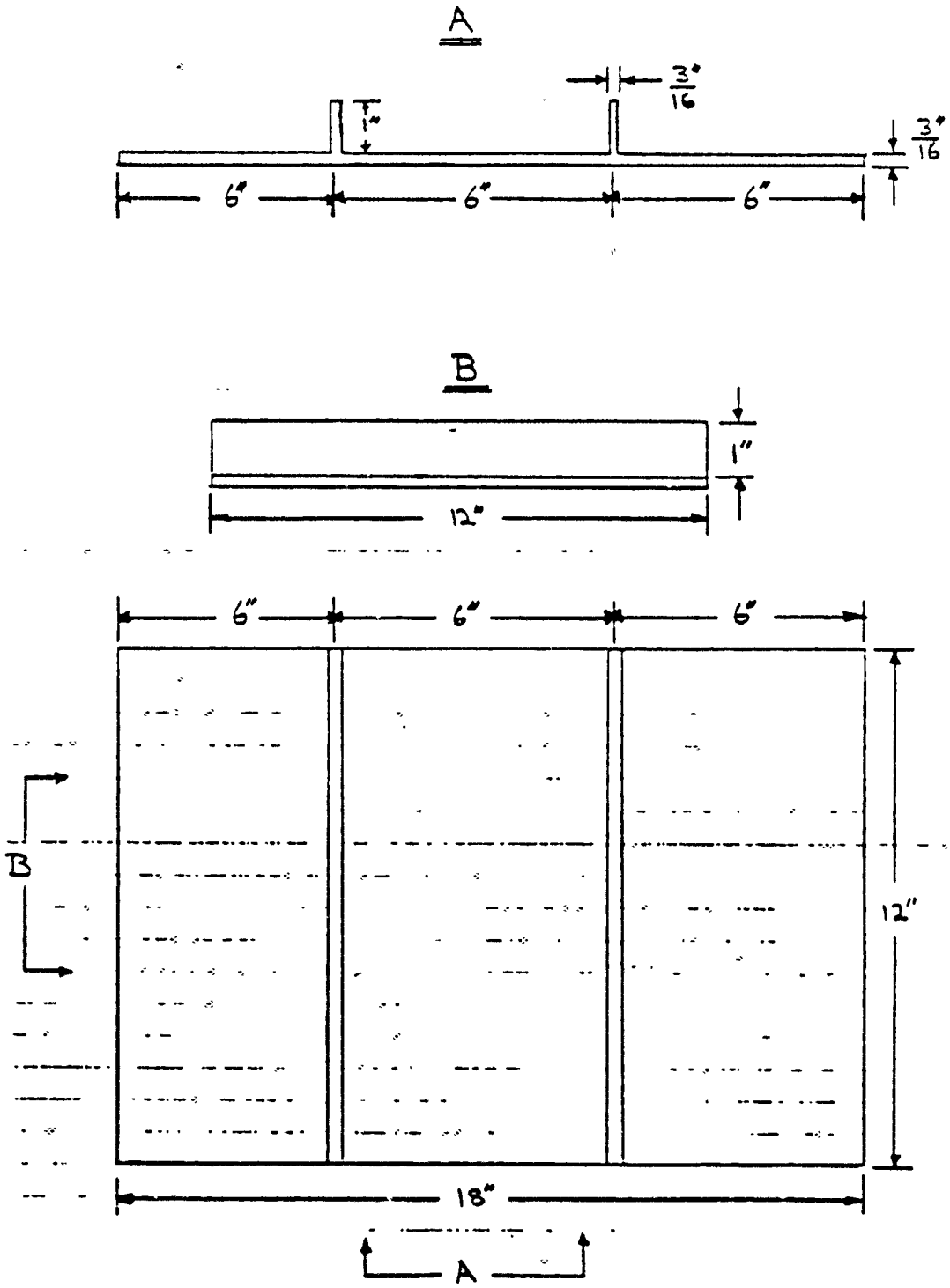

Fig. 2.1 Test Panel

for testing. For the following calculations, σ_y = 40 ksi and E = 10 x 10^6 psi.

For the rectangular stiffener in Figure 2.2

$$\beta = (\frac{b}{t})\sqrt{\frac{\sigma_y}{E}} = \left(\frac{6 \text{ inches}}{0.1875 \text{ inches}}\right)\left(\frac{40000 \text{psi}}{10 \text{ x}10^6 \text{ psi}}\right)^{1/2} = 2.02 \quad \text{(eqn 2.2)}$$

$$b_e = b(\frac{2}{\beta} - \frac{1}{\beta^2}) = (6 \text{ inches})(\frac{2}{2.02} - \frac{1}{2.02^2}) = 4.47 \text{ inches} \quad \text{(eqn 2.3)}$$

Neutral Axis Location,

$$Y_{na} = \frac{(0.5 + \frac{0.1875}{2})(0.1875)(1.0)}{(0.1875)(4.47 + 1)} = 0.109 \text{ inches} \quad \text{(eqn 2.4)}$$

$$I_{plate} = \frac{1}{12}(4.47)(0.1875)^3 + (4.47)(0.1875)(0.109)^2 \quad \text{(eqn 2.5)}$$

$$= 0.0124 \text{ in}^4$$

$$I_{stiffener} = \frac{1}{12}(0.1875)(1)^3 + (0.1875)(1)(0.485)^2 \quad \text{(eqn 2.6)}$$

$$= 0.0597 \text{ in}^4$$

Radius of Gyration,

$$k = \sqrt{\frac{I}{A}} = \left(\frac{0.0124 + 0.0597}{(0.1875)(4.47+1)}\right)^{1/2} = 0.265 \text{ inches} \quad \text{(eqn 2.7)}$$

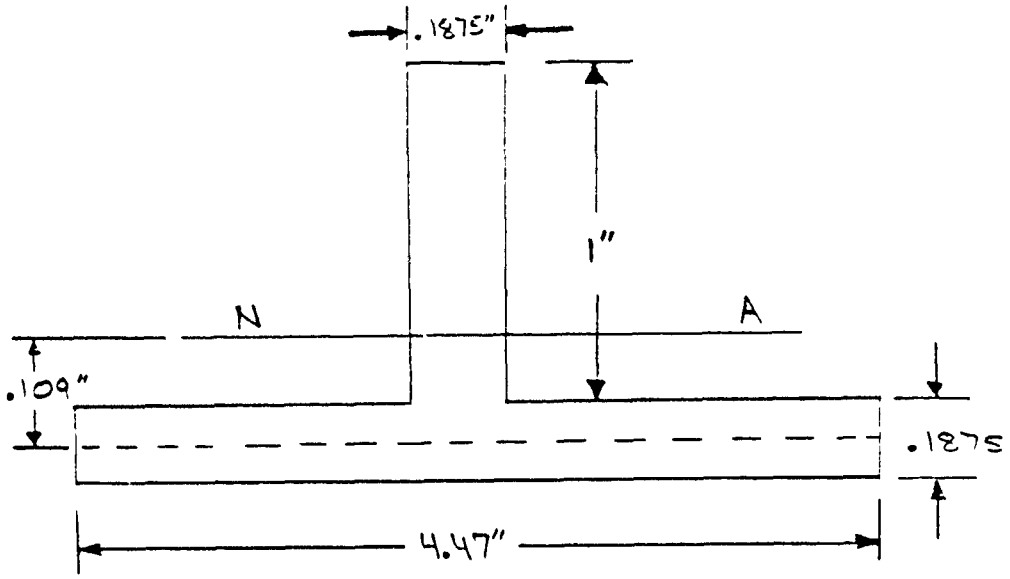

Figure 2.2 Stiffener Dimensions

$$\lambda = \left(\frac{a}{k\pi}\right)\sqrt{\frac{\sigma_y}{E}} = \frac{12 \text{ inches}}{(0.265 \text{ in})(\pi)}\left(\frac{40{,}000 \text{ psi}}{10 \times 10^6 \text{ psi}}\right)^{1/2} = 0.9 \qquad \text{(eqn 2.8)}$$

It is noted that $\beta = 2$ and $\lambda = .9$ fall within the range of a typical ship's grillage and the test panel is an acceptable model.

The final design is a panel 18 inches by 12 inches and 3/16 inch thick machined from a 2 inch thick aluminum blank measuring 33 inches by 27 inches. There are two stiffeners

located symmetrically about the centerline. This is to permit a computer modeling of only one quarter of the test panel which is a great savings in computational costs. The stiffeners are on the exposed external surface so that the loading conditions at the center will be compressive in nature; this is a requirement for tripping to occur.

The test structure is made in such a way that the plate may be simply turned over and secured to the backing structure should it be desired to test internally stiffened plates. A bolting arrangement between the test panel and the backing structure was designed to aid the clamped boundary conditions and to ensure a watertight seal throughout the loading. The final design is a double row of 64 bolts all around. They are 1 inch in diameter, A325 high strength structural steel in a friction-type connection under single shear loading. An eyebolt is located at each corner for ease in handling and rigging.

The design drawings for the test plate and the backing structure are in Appendix B and are to be referred to for more precise details and dimensions. A presentation of the calculations performed in the design of the bolting arrangements will be made here.

Figure 2.3 shows a bolt group located on the massive aluminum collar surrounding the test section. Bolt spacing is 3 inches.

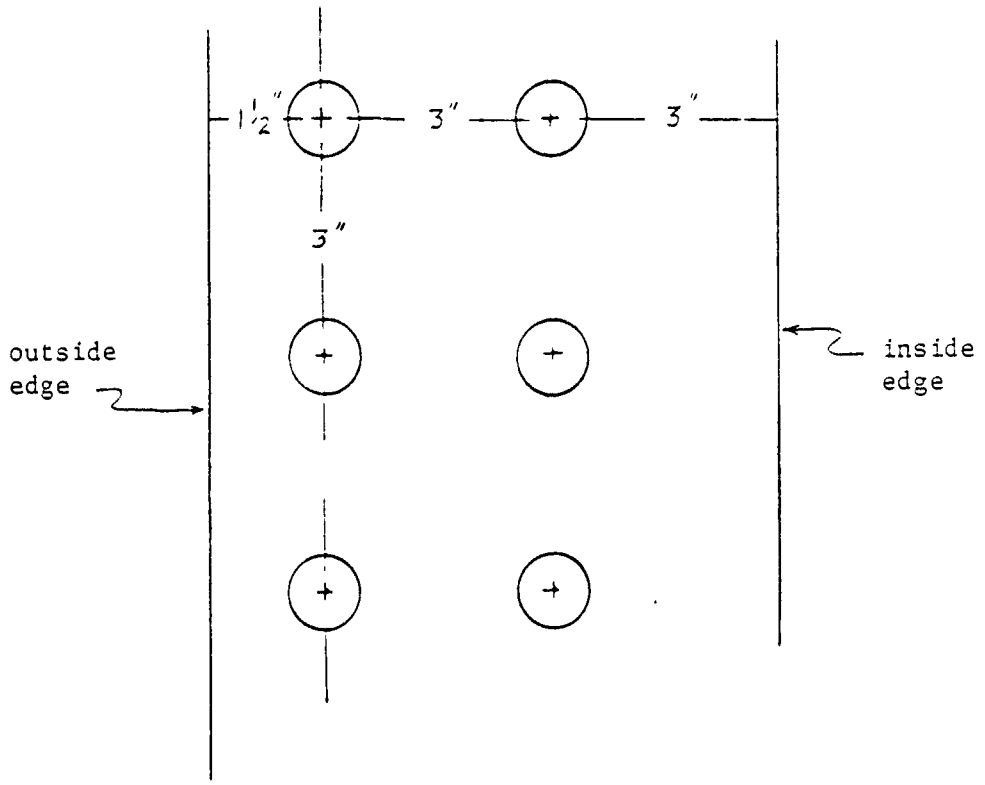

Figure 2.3 Bolt Group Spacing

Maximum bolt shear = (σ_y panel)(t panel)(bolt spacing)

= (40 Ksi)(3/16 inch)(3 inches)

= 22.5 Kips

Maximum moment at edge = $1/4\ \sigma_y t^2 b$

= $(1/4)(40\ \text{Kips})(3/16\ \text{inch})^2(3\ \text{in})$

= 1.05 Kip-in

This moment produces a tension in the bolt:

p=M/e = 1.05 Kip-in/3 inches = 0.3516 Kips.

To check the effect of this tension on bolt shear, the American Institute of Steel Construction Manaul [Ref. 5] was used.

Specification 1.6.3 on page 5-28 defines an allowable shear reduction factor due to tension in the bolt.

Shear reduction factor = (1-fA/T):

where f = average tensile stress

A = nominal body area

T = minimum bolt pretension, from Table 1.23.5

factor = (1-.3516/51) = 0.993

Table 1.5.2.1 lists the maximum shear stress allowed, Fv = 17.5 Ksi, so the allowable shear = (17.5 Ksi)(.993) = 17.38 Ksi. Therefore, the effect of tension in the bolt is negligible.

From the AISC manual page 4-5, Table 1D, the allowable shear load for a friction connection using one inch A325 bolts is

(2 bolts in line of shear) (13.7 Kips) = 27.4 Kips

Check with the maximum bolt shear, 22.5 Kips < 27.4 Kips, and find that the bolting arrangement is acceptable.

A second set of calculations for a bolting configuration where the plate is flipped over also proves satisfactory.

Maximum moment at the edge = $1/4(\sigma_y)(t)(b)(t)$

= 1/4(40 Ksi)(3/16)(3)(2)

= 11.25 Kip-in

Tension in the bolt, P=M/e = 11.25/3 = 3.750 Kips

Shear reduction factor = (1-fA/T)

k = (1-.375/51)

k = 0.927, still consider k negligible.

The backing structure shown in Figure 2.4 was designed using the methods described in [Ref. 6]. The entire structure is made of standard structural A36 steel, 1.25 inches thick. An O-ring gasket is fitted into the channel machined in the surface of the flange. A hull penetrator

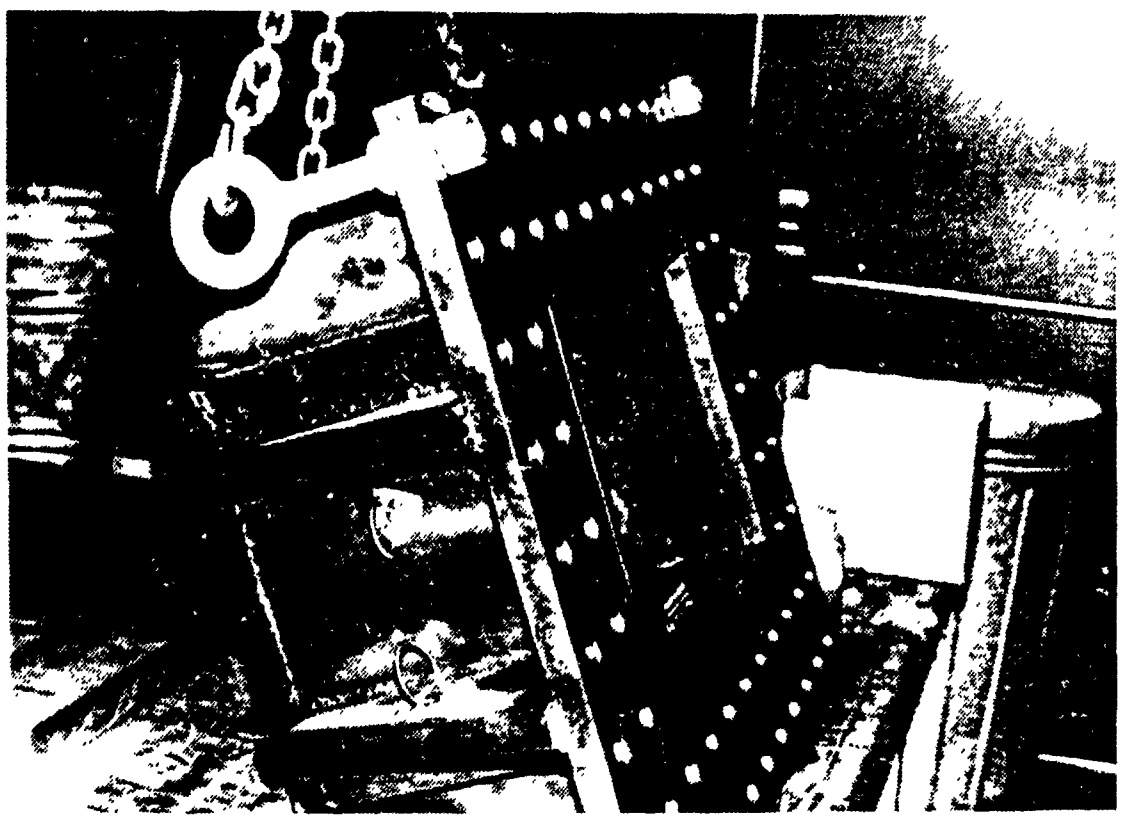

Figure 2.4 Backing Structure During Assembly

type connector is fixed to the bottom center to allow for internal instrumentation. A steel collar is welded around the exposed penetrator to prevent damage during handling and testing. The penetrator is a 24-pin model made by SEACON, part no. XSM-BCR. The mating connector used during the test is part no. XSM-CCP, with a 40 foot length of 16 gage cable attached. The backing structure weighs approximately 758 lbs. The test panel weighs 126 pounds, and the nuts and bolts weigh 111 lbs., for a total weight of the test structure of 1,000 pounds. This is obviously massive and has proven strong enough to withstand repeated shock tests. Figure 2.5 shows the assembled structure on the workbench.

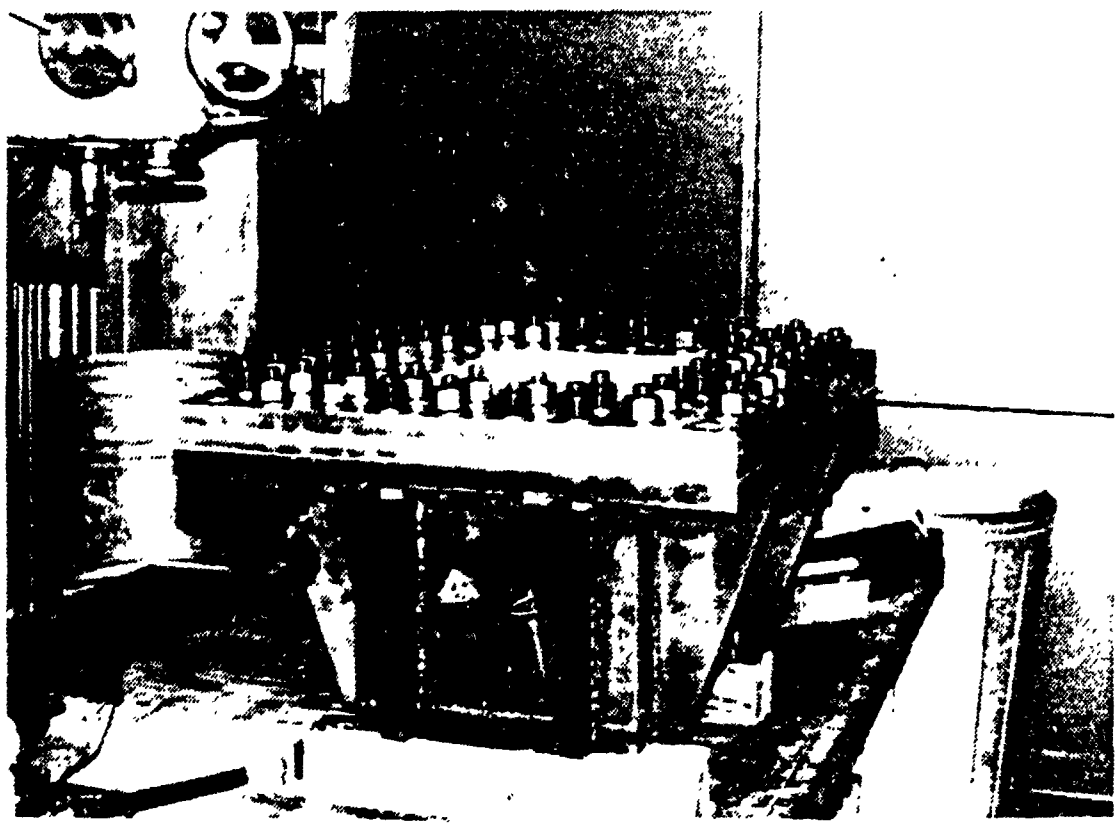

Figure 2.5 Backing Structure With Test Panel

III. TEST GEOMETRY

The inelastic response of the stiffened panel which this test is to examine requires that the plate undergo large deflections. These are on the order of four plate thicknesses. To achieve this result, calculations must be made which specify the appropriate charge weight and standoff distance. A treatment of the theory of underwater explosions will not be attempted in this paper, rather a prior knowlege is asumed concerning the characteristics of the pressure loading generated and the many secondary phenomena associated with underwater explosions.

The empirical formulas used to determine the charge weight and standoff are those derived by Robert H. Cole in his authoritative text, Underwater Explosions [Ref. 7].

To determine the pressure at a point as a function of time, an equation is written in a general form as

$$P(t) = Pmax(e)^{-t/\theta} \qquad \text{(eqn 3.1)}$$

where the maximum pressure is

$$Pmax = K_1(W^{1/3}/R)^{A_1} \text{ psi} \qquad \text{(eqn 3.2)}$$

and the exponential decay constant is

$$\theta = K_2(W^{1/3})(W^{1/3} / R)^{A_2} \text{ msec} \qquad \text{(eqn 3.3)}$$

While the forms of these equations have been accepted as correct and invariant, the coefficients K_1, A_1, K_2, and A_2 are determined from data taken from numerous tests and are redefined as more accurate data is obtained. Due to the fact that the values will differ with different types of explosives, the first step in determining a test geometry would be to specify the explosive. TNT was selected due to its frequent use in tests of this sort, and an eight pound charge was chosen due to its availability in the Navy requisitioning system. The coefficients for TNT are

K_1=22505 K_2=0.058 A_1=1.18 A_2=0.185

The values of W and R are the charge weight in pounds and the standoff distance in feet, respectively.

Now that the incident pressure loading on the plate is known as a function of time, the theories of mechanics of structures may be applied to determine the resulting deformation. Cole treats this topic through the use of energy methods and draws a distinction between elastic and plastic considerations of yielding surfaces. An equation is

derived that provides a value for the final deflection of a plate, $Z(t_m)$, by equating the plastic work to the kinetic energy acquired. The equation is given below, but the reader is referred to Cole for its derivation and the definition of its variables.

$$Z(t_m) = \frac{P_m a}{\rho_o c_o}\sqrt{\frac{2m}{\sigma_o h}}\,\beta^{\frac{1}{1-\beta}} = 2\sqrt{\frac{\beta}{\sigma_o h}}\,\beta^{\frac{\beta}{1-\beta}}\, a\, E^{1/2} \quad \text{(eqn 3.4)}$$

The preceding equations could have been used in an iterative fashion to determine the required charge weight, charge type and standoff to produce the necessary deformation (the four plate thicknesses is 4 x 0.1875 = 0.75 inches). However, this method of calculation was not pursued. Rather, a computer analysis was made using a finite element model of the test plate. This is a much more powerful method of analysis in terms of time and accuracy. Moreover, in addition to specifying plate deformations, regions of maximum stress and strain and the stiffener response may be investigated, dependent upon the computer code used. The strains predicted by the computer output were used to set the instrumentation levels at the test site. This is one example of the benefits to be gained in using such a finite element model. A discussion of this computer model and the results obtained is the topic of the next chapter.

The analysis indicated the best standoff distance between the eight pound charge and the test plate was nine feet.

As in any experimental investigation, the test environment must be as ideal as physically possible. The test conditions desired were that they be repeatable, that they concentrate on the effect of the shock wave loading, and that they remain clean and free from any of the secondary effects associated with underwater explosions. An attempt was made to eliminate or minimize such phenomena as bulk cavitation and cavitation closure, the reloadings from the explosive gas bubble pulse and bubble migration, and the surface cutoff and bottom reflection. To achieve all of these criteria requires a combination of correct test geometry and limiting the elapsed time of the investigation to a small window. Most of these phenomena are considered late time effects and are eliminated by only looking at the plate response during the first few milliseconds of pressure loading. Furthermore, this early time restriction allows for the modeling of the fluid/structure interaction in a most simple and convenient manner. The plate response may be determined by approximating the loading as a plane pressure wave. To consider the late time or even intermediate characteristics of the fluid/structure interaction would require entirely different approximations [Ref. 8].

One of these late time effects which can be destructive in nature is the reloading generated by the explosive gas bubble. There are two distinct phenomena caused by the gas sphere: an expansion and contraction cycle which generates additional pressure pulses and thereby reloads the structure, and the tendency for the bubble to migrate towards a structure if it is close enough, and to then collapse upon it and do destructive work. Fortunately, empirical equations have been determined which permit the calculation of the bubble radius as a function of time and the time of the first closure pulse. These two equations are similar in form to the pressure equation. The coefficients are determined by the type of explosive and the variables are the charge weight and the charge depth. The general equation and its associated coefficients for TNT are as follows:

Time of first closure pulse $T = K_5 \frac{W^{1/3}}{(D+33)^{5/6}}$ sec (eqn 3.5)

Maximum bubble radius $A_{max} = K_6 \frac{W^{1/3}}{(D+33)^{1/3}}$ ft (eqn 3.6)

$K_5 = 4.268$

$K_6 = 12.672$

An eight pound charge weight with a nine foot standoff distance has already been selected to produce the desired deformation. W = 8 lb. and charge depth in feet are run iteratively in these equations to satisfactorily meet two conditions. First, the time of the closure pulse is to be relatively late, well beyond the first few milliseconds. Secondly, the charge depth needs to be such that, as the bubble expands to its maximum radius, it will break the surface of the water and vent to the atmosphere before it contacts the plate. This venting action is considered instantaneous and the bubble is prevented from expanding or contracting further if it breaks the surface when it is near its maximum radius. A ratio of charge depth to maximum radius in the neighborhood of .50 to .75 will ensure a good venting action. A charge depth of four feet was determined to produce the desired results. The calculations are shown below.

$$T = (4.268)\ \frac{8^{1/3}}{(4+33)^{5/6}} = 0.421 \text{ sec}$$

$$A_{max} = (12.67)\ \frac{8^{1/3}}{(4+33)^{1/3}} = 7.60 \text{ ft}$$

$$4A/7.60 \text{ ft} = 0.526$$

A charge depth of four feet is 53% of maximum bubble radius and it will therefore vent.

Another underwater explosion phenomenon which can be eliminated through the proper test geometry is the bulk cavitation effect. The region of water that will cavitate is a function of depth and range from the explosion source. The cavitation is created when the reflected wave from the surface passes through the water directly behind the primary wave front. Figure 3.1 depicts the generation of bulk cavitation (courtesy of Weidlinger Associates).

The effect this cavitated region has on the structure is that the plate will experience essentially no pressure loading while it is surrounded by cavitated water. However, when the combined forces of atmospheric pressure and the weight of the water above the region overcome the cavitating forces, the cavitation suddenly closes back up to generate a reloading on any structure within the region. Although the pressure associated with this cavitation closure can be calculated and has been successfully done by Weidlinger Associates in a finite element code called CUE, these calculations are extremely involved. The best solution for the experimental test in question would be to remove the test structure from the cavitated region entirely. This necessitates the use of equations which define the extent to which cavitation will occur, based on charge size, type, and location.

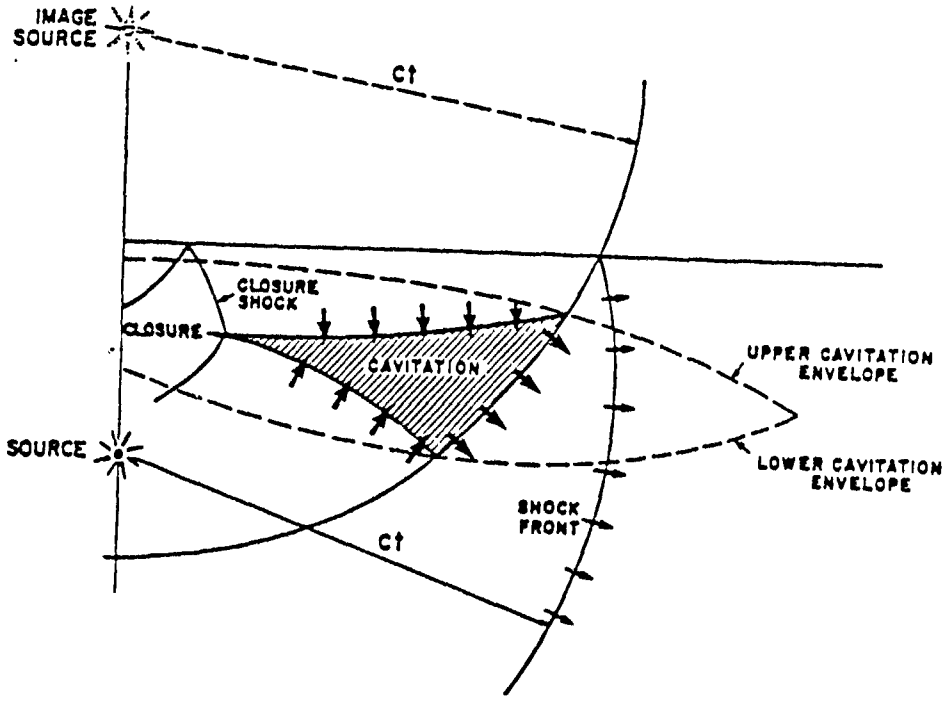

Figure 3.1 Development of Cavitation as Described by CUE

The equations ncessary to calculate this region of bulk cavitation are substantial in size. Computation of this region by computer is advisable and was done by means of another program written by Weidlinger Associates, Inc. for Tektronix 4051/2. The graphic output from this program is a range versus depth profile of the cavitated region and is shown in Figure 3.2.

The result of all calculations is a vertical charge/plate orientation with the charge located directly over a flat,

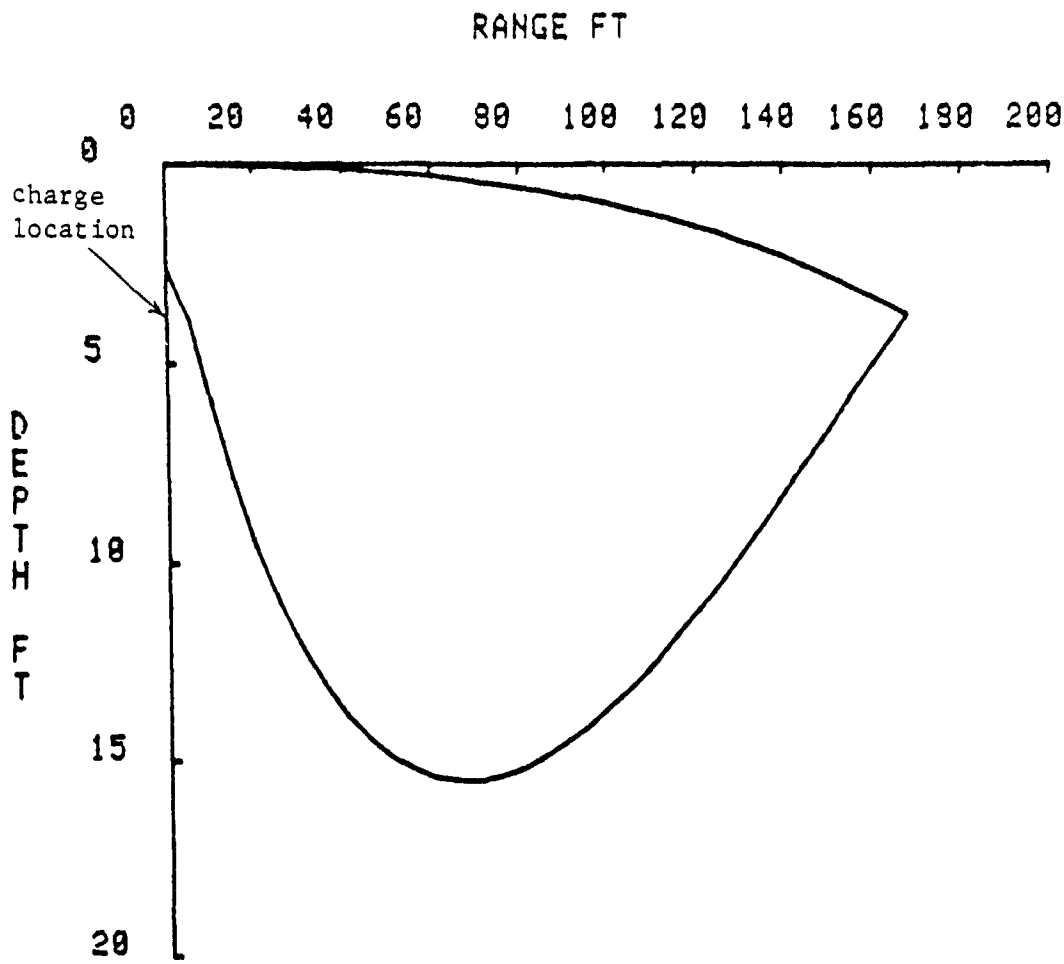

THE INCREDIBLE BULK

W = 5* D = 5

* 5lbs HBX; considered equivalent to 8 lbs TNT

Figure 3.2 Region of Bulk Cavitation

horizontal plate. The eight pound TNT charge would be suspended at a depth of four feet and the test structure nine feet beneath it at a depth of thirteen feet. Theoretically, this test geometry would create a test environment which is clean from those effects which are burdensome to calculate and reproduce while still producing the desired deformations in the plate.

The previously mentioned computer program written for the Tektronics 4051/2 by Weidlinger Associates is part of a library of programs available at the Naval Postgraduate School. A second program on this tape library is called "Undex Parameters" and outputs numerical data for most of the phenomena of interest in an underwater explosion. Copies of the output for this specific test geometry and the pressure history graph generated are presented on the following pages.

****

----- UNDEX PARAMETERS -----

****

TEST GAGE 1

CHARGE WEIGHT	8.0000	LBS. TNT
STANDOFF	9.0000	FT
CHARGE DEPTH	4.0000	FT
MODEL DEPTH	13.0000	FT
HORIZONTAL RANGE	0.0000	FT
PEAK PRESSURE	3947.5134	PSI
DECAY CONSTANT	0.1573	MSEC
SHOCK FACTOR	0.3143	
SHOCK FACTOR WITH CUTOFF	0.3143	
KEEL SHOCK FACTOR	0.3143	
KEEL SHOCK FACTOR WITH CUTOFF	0.3143	
ENERGY	226.9166	PSI-IN
ENERGY WITH CUTOFF	226.9166	PSI-IN
IMPULSE	0.7656	PSI-SEC
IMPULSE WITH CUTOFF	0.7656	PSI-SEC
CUTOFF TIME	1.6000	MSEC
BUBBLE PERIOD	0.4302	SEC
BUBBLE RADIUS	7.5625	FT
BUBBLE MIGRATION	7.2622	FT
PRESSURE REDUCTION FACTOR	0.1816	
BUBBLE PULSE PRESSURE	689.7383	PSI
BULK CAVITATION DEPTH	1.5750	FT
TIME OF CAVITATION CLOSURE	172.5546	MSEC
(CUTOFF TIME)/(DECAY CONSTANT)	10.1709	

Figure 3.3 UNDEX Parameters for Test Geometry

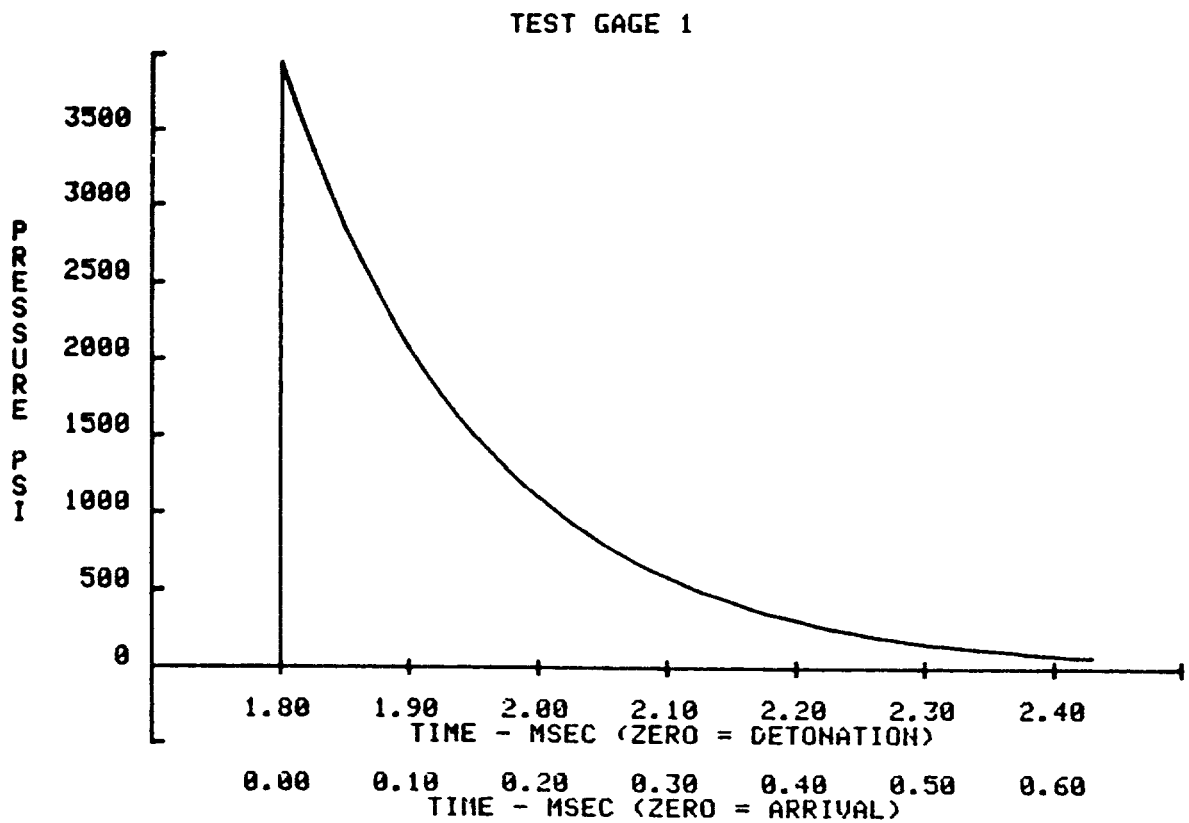

Figure 3.4 Theoretical Decay of Pressure Wave

IV. THE EPSA MODEL

The finite element computer code used to predict the gross plate reponse was the Weidlinger authored Elasto-Plastic Shell Analysis (EPSA) code. The theory underlying the analytic expressions used by the code may be found in the EPSA User's Manual [Ref. 12]. The version installed at NPS is run on a VAX-11/780 machine using the EPSA Guide [Ref. 9]. An interface between EPSA and the PATRAN-G graphics software was the subject of recent thesis work at NPS [Ref. 10]. This eased the task of interpreting the numerical output and has created a powerful tool for the analysis of underwater shock loading of structures (both cylinders and flat plates). Appendix C presents the necessary commands and procedures for executing an EPSA job on the NPS installation. Also presented here are examples of file editing and the use of library files.

EPSA is a central difference, finite element numerical scheme which will output nodal point and element response quantities at the specified number of time steps. Computation starts when the incident, spherical shaped pressure wave loads the first node it reaches based on the input geometry. Output quantities are the incident pressures, incident velocities, and the total pressure at

tne requested nodes. Also output are the requested element stresses and strains, nodal velocities and displacements. It was these displacements which were used to check the test geometry to ensure the necessary deformation was occurring during the initial loading. Also, as part of the other pre-shot calculations, the strains were output at the locations of the strain gages on the plate. The maximum value of strain was used to set the instrumentation levels prior to the test.

Because this test assumes that theory can only accurately predict the plate response for the first few milliseconds of shock wave loading, EPSA was run for this limited time frame. Modifications were made to the versions of EPSA at NPS so that only the early time effects are considered. The fluid-structure interaction used only a plane wave approximation; the later time effects within the code (the virtual mass approximation in the doubly asymptotic approximation) are turned off. Additionally, since EPSA was originally written to model cylindrical shells, either with or without internal stiffeners, modifications were made to permit the modeling of flat plates with external stiffeners.

The procedure for creating an EPSA input deck is covered in the User's Manual. Only those input calls which are different will be discussed. Figure 4.1 is the input deck

```
NPS PLATE- 2 REC STIF  STRN TOP
4000  1  0  0  0  100  0  0  4  4
.0000005     1  4000  100
1  1  17  1  16
16  10  4  1  1  0  27  20  26  14  1  1  0
0  0
10000000.  .3  .000255  40000.  .18750  0.0  0.00001
'stif' 1  0  1
-1   1   1
187  0
1  0  0  0.0  0.0
17  1  0  9.0  0.0
-17 17  10  0.0  0.6
0/
160  1  1  16  10
1   1  17  0  1  0  1  0
2   1  11  1  0  0  1  0
3   1  17  1  1  1  1  0
4   1  11  1  1  1  1  0
1   1  1  1  0.0  0.0  0.0
0.0  0.0  0.0  0.0  0.0  0.0  0.0  0.0/
1  1  1  1  1  2  1  1  3  17 1  1  17 1  2
17 1  3  6  7  1  6  7  2  6  7  3  17 11 1
17 11 2  17 11 3  12 7  1  12 7  2  12 7  3
1  11 1  1  11 2  1  11 3  6  1  1  6  1  2
6  1  3  12 1  1  12 1  2  12 1  3  17 5  1
17 5  2  17 5  3/
1  1  1  1  1  2  1  1  4  1  1  5  16 1  1
16 1  2  16 1  4  16 1  5  6  7  1  6  7  2
6  7  4  6  7  5  16 10 1  16 10 2  16 10 4
16 10 5  11 10 1  11 10 2  11 10 4  11 10 5/
11 5  10 10 1  9  11 1  10 12 1  9  12 10 10
16 5  9  16 5  10 16 1  9  16 1  10 11 1  10
10 1  10 12 8  9  11 8  10 10 8  9  16 1  7
16 1  8  11 1  11 11 2  11 11 3  11 11 4  11
11 5  11 11 6  11 11 7  11 11 8  11 11 9  11
11 10 11/
1  1  3  17 1  3  17 11 3  1  11 3  5  7  3
5  11 3  12 2  3  12 7  3  12 11 3  17 7  3
11 1  3  11 3  3  11 5  3  11 7  3/
0.5625   0.1875  1.000
11       1/
0/
9.0   0.0000945   60000.0
1   108.0   0.0    9.0
8.0   22505.0    1.18   0.058   -0.185  0.0008/
0   0   0   0   0
```

Figure 4.1 EPSA Input Deck for Preshot Analysis

used for the present analysis. Note that the timestep size is 5 x 10^{-7} seconds and the program is to run for 4,000 time steps. Therefore, the real time loading of the plate which is output is 2 milliseconds, and a run of this time size requires 1 hour and 32 minutes of CPU time on a VAX 11/780 computer.

The discretization of the plate and the axes for the i-j counting scheme discussed in the User's Manual are shown in Figure 4.2. A quarter model of the plate was generated to conserve computer resources. The quarter plate is 16 elements by 10 elements with 187 nodes; each element would physically measure 0.52 inches by 0.60 inches. An application of the Courant stability criterion for finite element codes shows the timestep size to be sufficiently small to avoid numerical instability. This is also shown in the Figure 4.2.

When modeling a structure and using the EPSA/PARTRAN-G interface, care must be taken so that the origin of the sheet is such that side four is either clamped or a rigid end cap of a cylinder. This is due to the method by which deformed meshes are generated by subtracting the rigid body motion of the structure from total displacements. The subroutine NEUDISP in the interface module subtracts the motion of the nodes on side four from the other nodes along corresponding rows. This anomaly only affects the PATRAN

EPSA DISCRETIZATION

1/4 PLATE MODEL

16 elements by 10 elements 640 for full plate

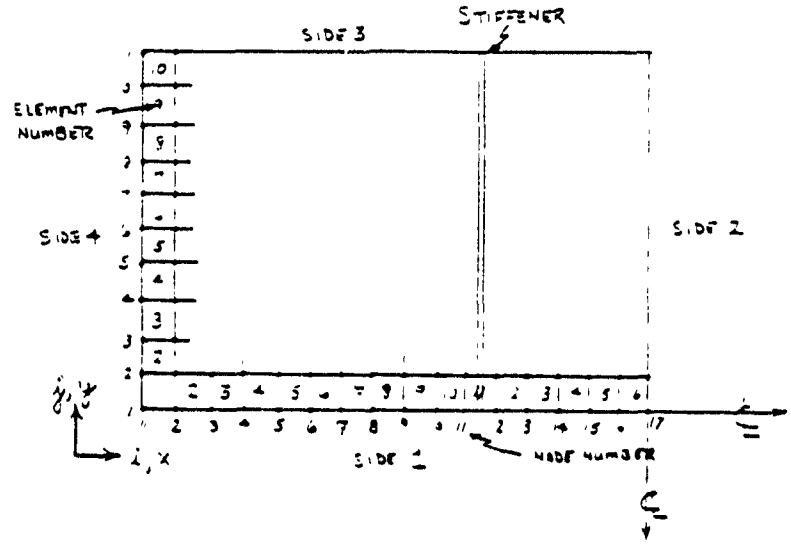

EACH ELEMENT : 0.5 INCHES

0.5625 INCHES

FOR COURANT STABILITY CRITERION,

TIME STEP SIZE, $\Delta t \leq \frac{1}{2} \delta_{min} \left(\frac{\rho}{E}\right)^{1/2}$

$$\delta_{min} = \sqrt{\left(\frac{0.5625}{2}\right)^2 + \left(\frac{.5}{2}\right)^2} = 0.4112$$

$$\Delta t \leq \frac{1}{2}(0.4112)\left(\frac{0.000255}{10 \times 10^6}\right)^{1/2}$$

$$\Delta t = 1.04\ \mu sec$$

Figure 4.2 Discretization Scheme for EPSA Model

deformed mesh; the EPSA results will be correct regardless of origin location.

To execute the plane wave approximation, the following variables for the input of Section VI of the User's Manual must be set to the values listed:

NCRTOT = -1

MAXTOT = 1

IFLSYM = 1

This satisfies GO TO loops which pass over the sections of the code which calculate the virtual mass approximation in the doubly asymptotic approximation. Additionally, to model a flat plate, the input value for the variable CURV(2) found in Section IV must be a small non-zero number, approximately 1.0×10^{-5}.

The modifications of EPSA which permit it to treat the case of external, rather than internal, stiffeners are contained within the code. Each time the other stiffener type is desired, changes must be made to the code itself. This involves an editing of the Fortran version of EPSA, followed by a compiling and a linking to a library file. Examples of this procedure are found in Appendix C. The EPSA User's Guide also outlines this procedure [Ref. 12]. The change required is in the subroutine RDSTIF. Twenty-four lines from the beginning, change CX=CX to CX= -CX when it is desired to change from an internal stiffener to an

external stiffener. CX is the distance from the centerline of the plate cross-section to the stiffener centroid. The type of stiffener being modeled by EPSA can be determined from the output file. In the first section following the input readback is a section listing sheet stiffener data. A negative value for CX confirms the desired case of an external stiffener.

Another update to the EPSA at NPS which is not reflected in the User's Manual permits the option to output strains at the top of a rectangular stiffener. To call for this output, the variable ITYPE found in Section XIII is set to 11. A copy of the changes made within the code to the subroutine CPTSTRN may be found on page 94 of reference 12.

An additional modification to EPSA allows for the input of a discrete pressure history for the loading. The discrete form of pressure field representation, as opposed to an exponentially decaying curve, is selected by setting the variable ICHRG = 2 in Section XVI. Card 3 now reads NSHAPE (up to a maximum of J = 25 points). Card 4 reads pairs of TC(J) and PC(J), where TC is an array of times in milliseconds after the arrival of the incident pressure wave and PC is the array of pressure which corresponds to the times in array TC. The final two values on card 4 are THEXP2 and TCUT2. An exponentially decaying tail may be added to the discrete pressure history. THEXP2 is the time

constant of exponential decay for this tail (corresponds to a theta value in milliseconds). If a decaying exponential tail is not desired, set THEXP2 $\leq$ 0.0. Figure 4.3 is an example of this option. TCUT2 is the value of surface cutoff by the negative reflected wave from the surface with time in milliseconds.

One other unique feature about executing an EPSA flat plate model is that there is no need to create a virtual mass array file. This fact is covered in the User's Manual by the example of the statically loaded beam. When modeling a cylinder and employing the VMA, a virtual mass array must be created in machine language by using either the interactive program ACESION, or the batch BASESION. For the EPM models (explosive power meter), this file is usually named EPM.VMA. When running a flat plate, simply return empty the call for a virtual mass file name.

As mentioned earlier, a discussion on the merging of PATRAN and EPSA and the commands necessary for its use was the topic of a previous thesis. Therefore, it will not be presented here, but a brief description of it and example of its use may be found in Appendix C. This merger causes EPSA to create special result files of numerical data during each run. These files are formatted such that they may be read by PATRAN. The neutral results file is written on FOR019.DAT and contains the finite element mesh generated by

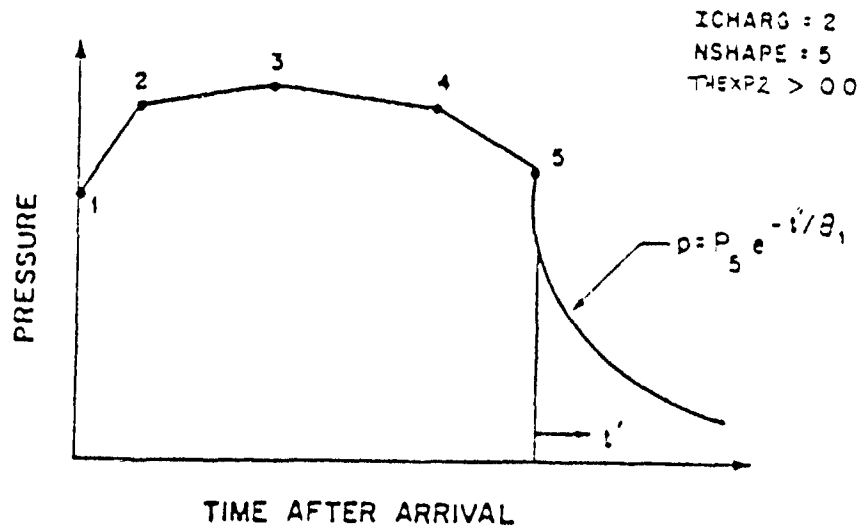

Figure 4.3 Discretized Pressure History Input

the EPSA input. The mesh is shown in Figure 4.4. This view assures the user that the input file is correct and the mesh is generated as desired. There are 187 nodes and 160 elements for the flat plate which models the upper left quarter of the test panel. The elements are numbered in Figure 4.4. Files FOR016.DAT and FOR018.DAT are the elemental results and nodal results files, respectively, and are used for post-processing. IN EPSA, an element result is either a stress or a strain and a node result is either a

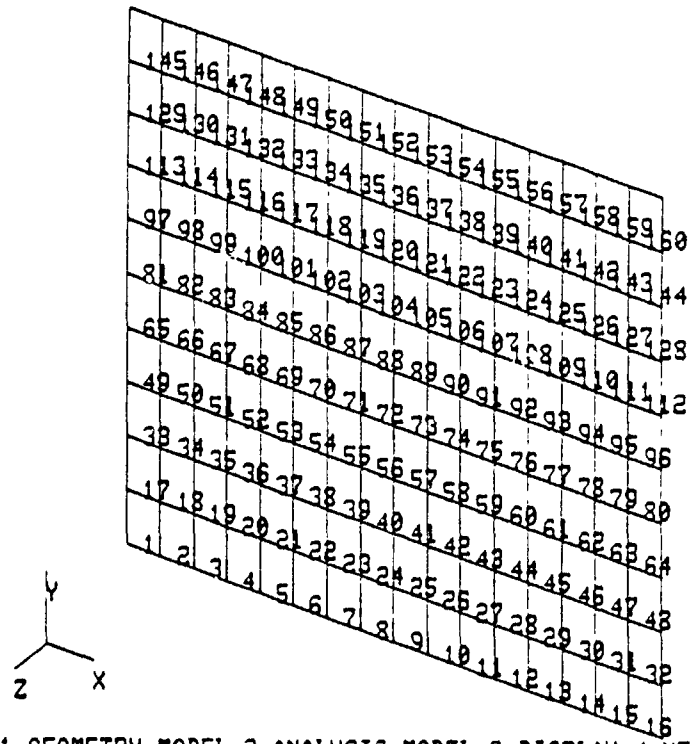

MODE? 1.GEOMETRY MODEL 2.ANALYSIS MODEL 3.DISPLAY 4.NEUTRAL SYS. 5.END
>

Figure 4.4 EPSA-Generated Finite Element Mesh

velocity or a displacement. The PATRAN graphics used for the preshot analysis were deformed mesh views of the plate and deformation contour level views. These were generated by running EPSA for 2 milliseconds of real time loading and specifying an eight pound TNT charge at a nine foot standoff. These views are presented in Figure 4.5 and Figure 4.6. A view of the stress contour levels is not shown here because the Von Mises stresses which were to be output by PATRAN (EPSA provides only σ_x, σ_y, and σ_{xy}) were

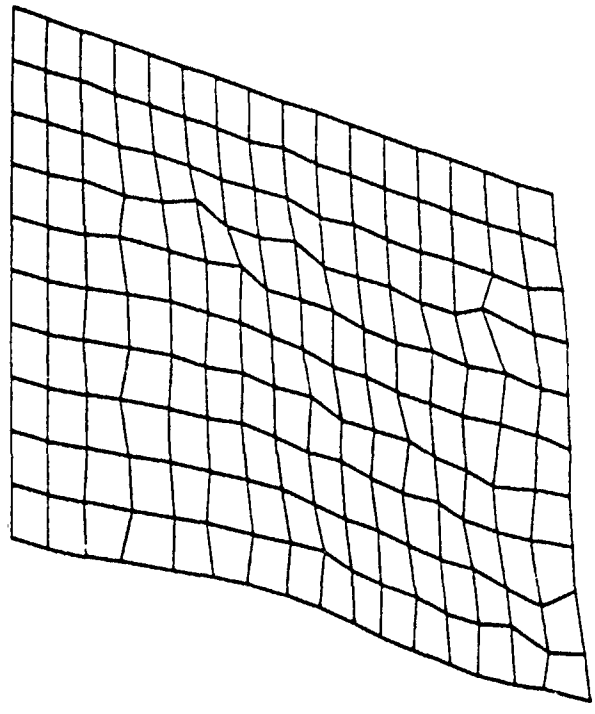

DEFPLT? 1.CLEAR SCREEN 2.UNDEFORMED MESH 3.DEFORMED MESH 4.END
>3

Figure 4.5 Deformed Mesh

not being calculated correctly and it was not possible to fix this until after the shot. The Von Mises stresses are shown in the results section.

As pictured above, the deformed mesh provides an excellent analysis tool; the areas of greatest deformation are easily identified.

During the post-processing, PATRAN will specify the greatest displacement and the node where it occurs. For the deformed mesh shown it is -.75 inches at node 17. A word of

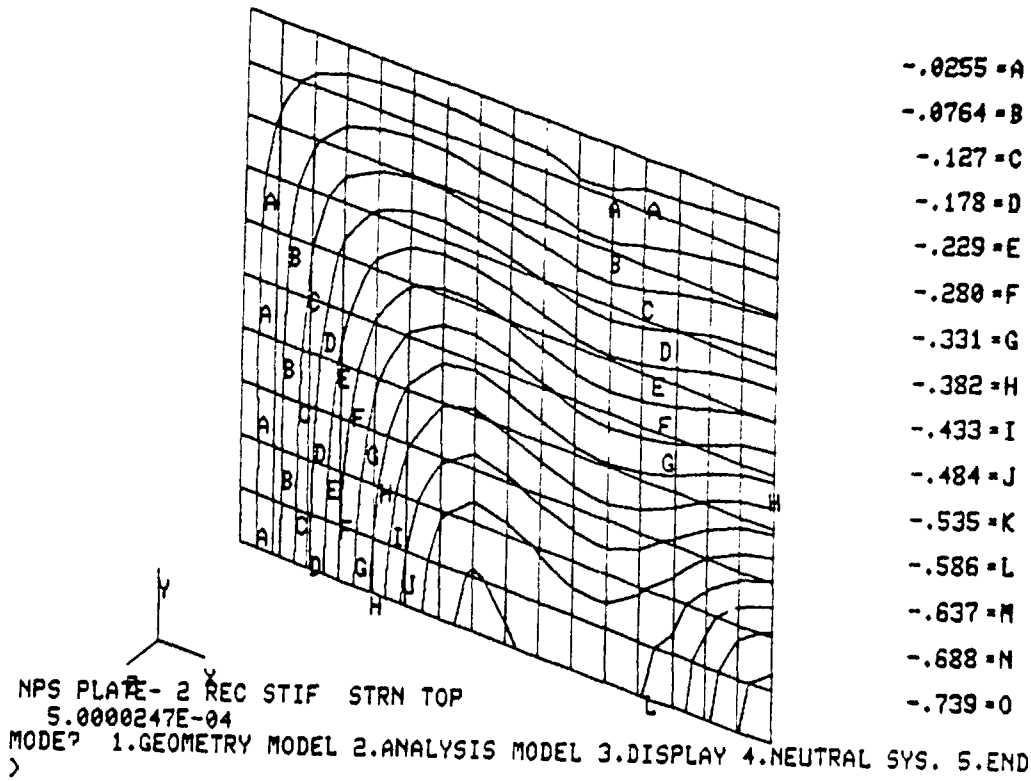

Figure 4.6 Deformation Contours

caution to the user: the deformed mesh is not scaled, but rather exaggerated so that the results may be prominent. This may be deceiving at times. Remember, the deformed geometry mesh is not proportioned exactly.

The contour level plots are another means of displaying the displacements of the plate. Although they may not provide as clear an image of the results as the deformed mesh, they do provide a more accurate analysis tool. With each contour line is an identifying letter which is

transcribed by the legend so that the precise amount of displacement may be read for any location on the plate from this one view. Here it can be seen that the area around node 17 is experiencing a displacement of at least -.739 inches.

These PATRAN views were checked against the EPSA output file and the displacements were verified. The requisite amount of plate deformation is occurring within the first few milliseconds of plate loading (again this is considered the only time frame which theory can predict acceptably well). From the EPSA printout of displacements, the greatest displacement during this time is -.974 inches at 1.5 milliseconds.

The final use of EPSA in the preshot analysis was the identification of maximums strains for setting instrumentation levels. To better understand how this is done, the EPSA output for strains corresponding to gage locations on the plate are shown in Figures 4.7, 4.8, and 4.9. The maximum strains are circled and a summary of these maximum strains at each of the gage locations is shown in Table I. The strain gage locations are shown in Chapter V.

PLATE GAGE # → 2 3 5 6 7 8 9 10 11 12

⊕ TENSION ⊖ COMPRESSION

STRAIN POINT HISTORIES

N	TIME	E02(11, 5)	E01(10, 1)	E02(11, 1)	E01(12, 1)	E02(12,10)	E01(16, 5)	E02(16, 5)	E01(16, 1)	E02(16, 1)	E02(11, 1)
1	0.500E-04	0.386E-03	0.573E-03	-0.639E-03	0.591E-03	0.268E-02	0.140E-03	-0.104E-04	0.972E-04	-0.518E-04	-0.639E-03
2	0.100E-03	-0.411E-03	-0.944E-03	-0.131E-03	-0.968E-03	0.458E-02	-0.324E-03	0.145E-02	-0.137E-02	0.595E-04	-0.131E-03
3	0.150E-03	-0.600E-03	-0.130E-02	-0.560E-03	-0.100E-02	0.583E-02	-0.162E-02	-0.184E-02	0.142E-02	0.870E-04	-0.560E-03
4	0.200E-03	-0.287E-03	0.140E-02	-0.109E-02	-0.201E-02	0.626E-02	-0.243E-02	-0.380E-02	0.206E-02	0.387E-02	-0.109E-02
5	0.250E-03	-0.176E-03	0.225E-02	-0.138E-02	0.364E-03	0.689E-02	-0.370E-02	-0.635E-02	0.624E-03	0.181E-02	-0.138E-02
6	0.300E-03	-0.229E-03	0.274E-02	-0.223E-02	0.802E-03	0.716E-02	-0.537E-02	-0.467E-02	-0.375E-02	-0.151E-02	-0.223E-02
7	0.350E-03	-0.403E-03	0.260E-02	-0.345E-02	0.239E-02	0.769E-02	-0.439E-02	-0.191E-02	-0.577E-02	-0.466E-02	-0.345E-02
8	0.400E-03	-0.631E-03	0.388E-02	-0.427E-02	0.994E-03	0.797E-02	-0.302E-02	0.204E-03	-0.894E-02	-0.757E-02	-0.427E-02
9	0.450E-03	-0.663E-03	0.274E-02	-0.540E-02	0.128E-02	0.824E-02	-0.174E-02	0.159E-02	-0.117E-01	-0.917E-02	-0.540E-02
10	0.500E-03	-0.255E-03	0.180E-02	-0.631E-02	0.133E-02	0.866E-02	-0.310E-02	0.264E-02	-0.153E-01	-0.953E-02	-0.631E-02
11	0.550E-03	0.177E-03	-0.298E-03	-0.613E-02	0.328E-02	0.904E-02	-0.571E-02	0.257E-02	-0.192E-01	-0.111E-01	-0.613E-02
12	0.600E-03	0.174E-03	0.190E-02	-0.565E-02	0.460E-02	0.921E-02	-0.988E-02	0.210E-02	-0.236E-01	-0.121E-01	-0.565E-02
13	0.650E-03	-0.853E-04	0.248E-02	-0.531E-02	0.656E-02	0.104E-01	-0.158E-01	0.210E-02	-0.291E-01	-0.892E-02	-0.531E-02
14	0.700E-03	-0.702E-03	-0.115E-02	-0.563E-02	0.919E-02	0.108E-01	-0.179E-01	0.846E-03	-0.327E-01	-0.638E-02	-0.563E-02
15	0.750E-03	0.211E-03	-0.274E-02	-0.735E-02	0.144E-01	0.106E-01	-0.149E-01	-0.332E-02	-0.359E-01	-0.133E-01	-0.735E-02
16	0.800E-03	0.367E-03	-0.126E-02	-0.946E-02	0.200E-01	0.992E-02	-0.797E-02	-0.117E-01	-0.464E-01	-0.250E-01	-0.946E-02
17	0.850E-03	-0.284E-03	0.161E-02	-0.936E-02	0.181E-01	0.101E-01	-0.423E-02	-0.128E-01	-0.469E-01	-0.765E-02	-0.936E-02
18	0.900E-03	-0.108E-02	0.310E-02	-0.906E-02	0.166E-01	0.112E-01	-0.798E-02	-0.100E-01	-0.280E-01	0.309E-01	-0.906E-02
19	0.950E-03	-0.100E-02	0.670E-03	-0.914E-02	0.215E-01	0.116E-01	-0.243E-01	-0.374E-01	0.454E-03	0.498E-02	-0.914E-02
20	0.100E-02	-0.118E-02	-0.141E-02	-0.591E-02	0.267E-01	0.117E-01	-0.333E-01	-0.630E-01	0.111E-01	0.321E-02	-0.591E-02
21	0.105E-02	-0.907E-03	0.825E-02	-0.545E-02	0.177E-01	0.120E-01	-0.212E-01	-0.283E-01	0.203E-01	0.313E-01	-0.545E-02
22	0.110E-02	0.112E-03	0.942E-02	-0.757E-02	0.114E-01	0.961E-02	0.237E-01	-0.218E-01	0.922E-02	0.299E-01	-0.757E-02
23	0.115E-02	-0.869E-03	-0.159E-02	-0.740E-02	0.124E-01	0.991E-02	0.163E-01	-0.588E-01	0.625E-02	-0.132E-01	-0.740E-02
24	0.120E-02	-0.132E-02	-0.954E-02	-0.456E-02	0.141E-01	0.995E-02	0.117E-01	-0.533E-01	0.848E-02	-0.547E-01	-0.456E-02
25	0.125E-02	-0.345E-02	-0.953E-02	-0.376E-02	0.977E-02	0.104E-01	0.874E-02	-0.173E-01	0.974E-02	-0.340E-01	-0.376E-02
26	0.130E-02	-0.417E-02	-0.130E-01	-0.457E-02	0.101E-01	0.991E-02	0.212E-02	0.755E-02	0.156E-01	-0.711E-02	-0.457E-02
27	0.135E-02	-0.408E-02	-0.134E-01	-0.545E-02	0.141E-01	0.115E-01	-0.531E-03	0.482E-02	0.645E-02	-0.202E-01	-0.545E-02
28	0.140E-02	-0.385E-02	-0.115E-01	-0.629E-02	0.130E-01	0.106E-01	-0.804E-02	-0.191E-01	-0.167E-01	-0.528E-01	-0.629E-02
29	0.145E-02	-0.455E-02	-0.583E-02	-0.691E-02	0.146E-01	0.945E-02	-0.107E-04	-0.193E-01	-0.170E-01	-0.542E-01	-0.691E-02
30	0.150E-02	-0.392E-02	-0.367E-02	-0.997E-02	0.149E-01	0.942E-02	-0.596E-03	-0.198E-01	-0.123E-01	-0.551E-01	-0.997E-02
31	0.155E-02	-0.447E-02	-0.836E-02	-0.933E-02	0.137E-01	0.935E-02	-0.153E-02	-0.230E-01	0.691E-02	-0.311E-01	-0.933E-02
32	0.160E-02	-0.389E-02	-0.752E-02	-0.959E-02	0.147E-01	0.874E-02	0.239E-03	-0.131E-01	0.268E-01	0.175E-02	-0.959E-02
33	0.165E-02	-0.557E-02	-0.850E-02	-0.892E-02	0.889E-02	0.837E-02	0.898E-02	-0.597E-02	0.184E-01	-0.907E-03	-0.892E-02
34	0.170E-02	-0.446E-02	-0.328E-02	-0.949E-02	0.108E-01	0.789E-02	0.110E-01	-0.496E-02	0.138E-01	-0.633E-02	-0.949E-02
35	0.175E-02	-0.433E-02	-0.554E-02	-0.986E-02	0.120E-01	0.691E-02	0.118E-01	-0.836E-02	0.119E-01	-0.139E-01	-0.986E-02
36	0.180E-02	-0.425E-02	-0.832E-02	-0.973E-02	0.143E-01	0.739E-02	0.975E-02	-0.154E-01	0.158E-01	-0.185E-01	-0.973E-02
37	0.185E-02	-0.543E-02	-0.692E-02	-0.959E-02	0.111E-01	0.628E-02	0.116E-01	-0.295E-01	0.222E-01	-0.173E-01	-0.959E-02
38	0.190E-02	-0.456E-02	-0.752E-02	-0.103E-01	0.122E-01	0.735E-02	0.155E-01	-0.334E-01	0.352E-01	-0.105E-01	-0.103E-01
39	0.195E-02	-0.480E-02	-0.627E-02	-0.992E-02	0.920E-02	0.756E-02	0.184E-01	-0.287E-01	0.348E-01	-0.708E-02	-0.992E-02
40	0.200E-02	-0.485E-02	-0.791E-02	-0.102E-01	0.122E-01	0.747E-02	0.211E-01	-0.189E-01	0.362E-01	-0.107E-02	-0.102E-01

Figure 4.7 Strains Predicted by EPSA for an 8 lb Charge

STRAIN POINT HISTORIES

		14	16	17	19	20	21	STRAIN ON TOP OF STIFFENERS 4,13			
N	TIME	EO2(10, 1)	EO1(12, 8)	EO2(11, 8)	EO1(10, 8)	E11(16, 1)	E12(16, 1)	(11,1) E1~~(12, 1)~~	(11,2) E1~~(12, 2)~~	(11,3) E1(12, 3)	(11,4) E1(12, 4)
1	0.500E-04	-0.518E-03	0.120E-02	0.335E-03	0.113E-02	-0.232E-03	-0.814E-04	0.103E-03	0.213E-03	0.111E-04	-0.914E-04
2	0.100E-03	-0.696E-04	0.271E-02	-0.271E-04	0.254E-02	0.101E-02	0.223E-03	-0.148E-03	-0.153E-03	-0.227E-03	-0.113E-03
3	0.150E-03	-0.569E-03	0.350E-02	-0.906E-04	0.327E-02	-0.172E-02	0.631E-03	-0.415E-03	-0.181E-03	-0.463E-03	-0.476E-03
4	0.200E-03	-0.779E-03	0.353E-02	-0.479E-03	0.425E-02	-0.181E-02	-0.226E-02	0.983E-04	-0.192E-03	-0.232E-03	-0.328E-03
5	0.250E-03	-0.105E-02	0.351E-02	-0.802E-03	0.415E-02	-0.774E-03	-0.143E-02	-0.588E-03	-0.410E-03	-0.418E-04	-0.106E-02
6	0.300E-03	-0.220E-02	0.339E-02	-0.109E-02	0.349E-02	0.342E-02	0.140E-03	-0.107E-02	-0.477E-03	-0.631E-03	-0.103E-02
7	0.350E-03	-0.418E-02	0.367E-02	-0.441E-03	0.272E-02	0.465E-02	0.272E-02	-0.179E-02	-0.727E-03	-0.675E-03	-0.118E-02
8	0.400E-03	-0.514E-02	0.349E-02	0.145E-03	0.235E-02	0.662E-02	0.559E-02	-0.212E-02	-0.132E-02	-0.941E-03	-0.995E-03
9	0.450E-03	-0.580E-02	0.331E-02	0.105E-02	0.264E-02	0.907E-02	0.667E-02	-0.229E-02	-0.127E-02	-0.102E-02	-0.109E-02
10	0.500E-03	-0.608E-02	0.350E-02	0.139E-02	0.238E-02	0.123E-01	0.763E-02	-0.202E-02	-0.147E-02	-0.157E-02	-0.164E-02
11	0.550E-03	-0.567E-02	0.364E-02	0.120E-02	0.167E-02	0.179E-01	0.888E-02	-0.756E-03	-0.151E-02	-0.912E-03	-0.120E-02
12	0.600E-03	-0.453E-02	0.270E-02	0.167E-02	0.209E-02	0.256E-01	0.939E-02	-0.803E-03	-0.143E-02	-0.567E-03	-0.594E-03
13	0.650E-03	-0.525E-02	0.230E-02	0.257E-02	0.303E-02	0.347E-01	0.690E-02	0.942E-03	-0.267E-02	-0.261E-02	-0.137E-02
14	0.700E-03	-0.597E-02	0.335E-02	0.120E-02	0.346E-02	0.413E-01	0.373E-02	0.324E-02	-0.442E-02	-0.220E-02	-0.318E-03
15	0.750E-03	-0.661E-02	0.560E-02	0.100E-02	0.476E-02	0.455E-01	0.946E-02	0.803E-02	-0.562E-02	-0.306E-02	-0.591E-03
16	0.800E-03	-0.859E-02	0.707E-02	0.205E-02	0.647E-02	0.488E-01	0.261E-01	0.850E-02	-0.466E-02	-0.499E-02	-0.348E-02
17	0.850E-03	-0.684E-02	0.668E-02	0.175E-02	0.628E-02	0.486E-01	0.208E-01	0.739E-02	-0.570E-02	-0.604E-02	-0.267E-03
18	0.900E-03	-0.790E-02	0.666E-02	0.254E-02	0.481E-02	0.332E-01	0.127E-01	0.611E-02	-0.259E-02	-0.428E-02	0.141E-02
19	0.950E-03	-0.740E-02	0.664E-02	0.295E-02	0.226E-02	0.336E-02	0.118E-01	0.144E-02	0.346E-03	-0.557E-02	0.322E-02
20	0.100E-02	-0.456E-02	0.496E-02	0.172E-02	-0.181E-04	-0.174E-01	0.478E-03	0.407E-02	0.241E-02	-0.310E-02	0.158E-02
21	0.105E-02	-0.542E-02	0.430E-02	-0.551E-04	-0.186E-02	-0.580E-02	-0.589E-01	0.146E-01	0.176E-02	-0.163E-02	0.144E-02
22	0.110E-02	-0.625E-02	0.389E-02	0.107E-02	-0.219E-02	0.301E-02	-0.420E-01	0.135E-01	0.764E-03	-0.422E-02	0.103E-02
23	0.115E-02	-0.831E-02	0.396E-02	0.133E-02	0.230E-02	-0.132E-02	0.131E-01	0.237E-02	0.241E-02	-0.419E-02	-0.142E-02
24	0.120E-02	-0.700E-02	0.464E-02	0.997E-04	0.217E-02	0.975E-02	0.130E-01	0.812E-02	0.545E-03	-0.604E-02	-0.117E-02
25	0.125E-02	-0.863E-02	0.641E-02	-0.745E-03	-0.878E-03	0.144E-01	0.747E-04	0.100E-01	0.266E-02	-0.564E-02	0.123E-02
26	0.130E-02	-0.835E-02	0.651E-02	-0.856E-03	0.142E-02	0.174E-01	-0.468E-02	0.869E-02	0.313E-02	-0.771E-02	-0.221E-03
27	0.135E-02	-0.774E-02	0.365E-02	-0.680E-03	0.162E-02	0.199E-01	0.494E-02	0.872E-02	0.170E-02	-0.951E-02	0.561E-03
28	0.140E-02	-0.562E-02	0.167E-02	-0.768E-03	0.142E-02	0.328E-01	0.218E-01	0.721E-02	-0.196E-03	-0.102E-01	0.184E-02
29	0.145E-02	-0.735E-02	0.349E-02	0.860E-05	-0.105E-02	0.388E-01	0.215E-01	0.125E-01	0.104E-03	-0.406E-02	0.244E-02
30	0.150E-02	-0.866E-02	0.315E-02	0.732E-03	-0.223E-02	0.345E-01	0.205E-01	0.136E-01	0.208E-03	-0.345E-02	0.214E-02
31	0.155E-02	-0.971E-02	0.413E-02	0.197E-02	-0.377E-02	0.153E-01	0.169E-01	0.100E-01	0.140E-02	-0.256E-02	0.155E-02
32	0.160E-02	-0.934E-02	0.220E-02	0.311E-02	-0.387E-02	-0.109E-01	0.249E-02	0.848E-02	0.368E-02	-0.266E-02	0.548E-03
33	0.165E-02	-0.985E-02	0.169E-02	0.395E-02	-0.417E-02	-0.364E-02	0.163E-02	0.868E-02	0.500E-02	-0.336E-02	0.471E-03
34	0.170E-02	-0.790E-02	0.118E-04	0.341E-02	-0.331E-02	0.885E-02	0.309E-02	0.143E-01	0.380E-02	-0.501E-02	0.107E-02
35	0.175E-02	-0.883E-02	0.116E-03	0.468E-02	-0.657E-02	0.239E-01	0.236E-02	0.148E-01	0.402E-02	-0.378E-02	0.161E-02
36	0.180E-02	-0.103E-01	0.167E-02	0.408E-02	-0.503E-02	0.327E-01	0.245E-02	0.159E-01	0.321E-02	-0.526E-02	0.866E-03
37	0.185E-02	-0.844E-02	0.150E-02	0.399E-02	-0.618E-02	0.323E-01	-0.584E-03	0.149E-01	0.399E-02	-0.382E-02	0.131E-02
38	0.190E-02	-0.105E-01	0.569E-03	0.381E-02	-0.852E-02	0.173E-01	-0.127E-01	0.159E-01	0.346E-02	-0.419E-02	-0.449E-03
39	0.195E-02	-0.995E-02	0.177E-03	0.321E-02	-0.953E-02	0.177E-01	-0.155E-01	0.159E-01	0.469E-02	-0.349E-02	-0.277E-02
40	0.200E-02	-0.101E-01	-0.412E-03	0.328E-02	-0.784E-02	0.978E-02	-0.194E-01	0.169E-01	0.436E-02	-0.301E-02	-0.187E-02

Figure 4.8 Strains Predicted by EPSA for an 8 lb Charge

ON TOP OF STIFFENERS (11,5)

STRAIN POINT HISTORIES

N	TIME	E1(12, 5)	(11,6) E1(12, 6)	(11,7) E1(12, 7)	(11,8) E1(12, 8)	(11,9) E1(12, 9)	(11,10) E1(12,10)
1	0.500E-04	-0.135E-03	-0.186E-03	-0.257E-03	-0.187E-03	0.690E-04	0.853E-04
2	0.100E-03	-0.151E-03	-0.102E-03	-0.252E-03	-0.106E-03	0.356E-03	0.187E-03
3	0.150E-03	-0.110E-03	-0.170E-03	-0.219E-03	0.193E-03	0.385E-03	0.136E-03
4	0.200E-03	-0.486E-03	0.340E-04	-0.215E-04	0.280E-03	0.676E-03	0.301E-03
5	0.250E-03	-0.708E-03	0.120E-03	0.258E-04	0.455E-03	0.768E-03	0.465E-03
6	0.300E-03	-0.486E-03	-0.155E-03	0.267E-03	0.603E-03	0.867E-03	0.673E-03
7	0.350E-03	-0.704E-04	-0.172E-03	0.504E-03	0.941E-03	0.856E-03	0.589E-03
8	0.400E-03	0.386E-04	0.141E-03	0.904E-03	0.113E-02	0.933E-03	0.595E-03
9	0.450E-03	0.131E-03	0.148E-03	0.109E-02	0.116E-02	0.966E-03	0.544E-03
10	0.500E-03	0.163E-04	-0.318E-03	0.666E-03	0.123E-02	0.106E-02	0.760E-03
11	0.550E-03	-0.581E-03	-0.623E-03	0.532E-03	0.118E-02	0.106E-02	0.670E-03
12	0.600E-03	-0.138E-03	-0.308E-03	0.927E-03	0.561E-03	-0.141E-03	0.382E-03
13	0.650E-03	0.176E-02	-0.274E-03	-0.101E-03	-0.139E-03	-0.172E-02	-0.602E-03
14	0.700E-03	0.236E-02	-0.239E-03	0.109E-02	0.466E-03	-0.327E-02	-0.105E-02
15	0.750E-03	0.760E-03	-0.116E-02	0.190E-02	0.203E-02	-0.379E-02	-0.116E-02
16	0.800E-03	-0.273E-02	-0.367E-02	0.131E-02	0.172E-02	-0.422E-02	-0.195E-02
17	0.850E-03	-0.184E-02	-0.695E-02	-0.658E-03	-0.377E-03	-0.422E-02	-0.197E-02
18	0.900E-03	-0.296E-03	-0.753E-02	-0.457E-04	-0.235E-02	-0.567E-02	-0.181E-02
19	0.950E-03	-0.170E-02	-0.511E-02	0.243E-02	-0.255E-02	-0.377E-02	-0.198E-02
20	0.100E-02	-0.201E-02	-0.282E-02	0.242E-02	-0.367E-02	-0.558E-02	-0.189E-02
21	0.105E-02	0.762E-03	0.294E-03	0.223E-02	-0.328E-02	-0.669E-02	-0.319E-02
22	0.110E-02	-0.117E-02	-0.158E-02	0.240E-02	-0.190E-02	-0.414E-02	-0.266E-02
23	0.115E-02	-0.290E-02	-0.137E-02	0.162E-02	-0.142E-02	-0.166E-02	-0.255E-02
24	0.120E-02	-0.236E-02	-0.385E-02	0.328E-02	-0.201E-02	-0.303E-02	-0.367E-02
25	0.125E-02	0.288E-02	-0.307E-02	0.478E-02	-0.178E-02	-0.550E-02	-0.406E-02
26	0.130E-02	0.229E-02	0.655E-03	0.902E-02	-0.239E-03	-0.649E-02	-0.284E-02
27	0.135E-02	0.377E-03	-0.616E-03	0.714E-02	-0.194E-02	-0.645E-02	-0.327E-02
28	0.140E-02	0.345E-03	-0.165E-03	0.627E-02	-0.314E-02	-0.500E-02	-0.242E-02
29	0.145E-02	0.623E-03	0.195E-02	0.641E-02	-0.159E-02	-0.593E-02	-0.419E-02
30	0.150E-02	0.137E-04	-0.136E-02	0.725E-02	-0.291E-02	-0.648E-02	-0.318E-02
31	0.155E-02	0.285E-03	0.579E-03	0.634E-02	-0.331E-02	-0.547E-02	-0.416E-02
32	0.160E-02	0.197E-03	0.129E-02	0.551E-02	-0.503E-02	-0.652E-02	-0.485E-02
33	0.165E-02	-0.169E-03	0.146E-02	0.493E-02	-0.547E-02	-0.598E-02	-0.318E-02
34	0.170E-02	-0.535E-03	0.139E-02	0.488E-02	-0.616E-02	-0.627E-02	-0.294E-02
35	0.175E-02	-0.115E-03	0.140E-02	0.289E-02	-0.657E-02	-0.642E-02	-0.409E-02
36	0.180E-02	0.146E-02	0.257E-02	0.315E-02	-0.566E-02	-0.667E-02	-0.413E-02
37	0.185E-02	0.587E-03	0.142E-02	0.271E-02	-0.603E-02	-0.704E-02	-0.408E-02
38	0.190E-02	-0.579E-03	0.421E-03	0.122E-02	-0.692E-02	-0.575E-02	-0.335E-02
39	0.195E-02	-0.301E-02	0.415E-03	0.188E-02	-0.688E-02	-0.594E-02	-0.357E-02
40	0.200E-02	-0.317E-03	0.489E-03	0.267E-02	-0.721E-02	-0.519E-02	-0.258E-02

Figure 4.9 Strains Predicted by EPSA for an 8 lb Charge

TABLE I

Summary of EPSA Predicted Strains

Gage Number	EPSA Number	Max Strain (μstrain)	Time (sec)	Percent (%)
1	16	+7070	0.80	0.7
2	19	-9530	1.95	0.9
3	18	-7210	2.00	0.7
4	17	+4680	1.75	0.5
5	15	-3170	2.00	0.3
6	12	-10300	1.90	1.0
7	13	+16900	2.00	1.7
8	14	-10300	1.80	1.0
9	11	-55100	1.50	5.5
10	10	-46900	0.85	4.7
11	8	-33300	1.00	3.3
12	9	-63000	1.00	6.3
13	6	+26700	1.00	2.7
14	3	-13400	1.35	1.3
15	4	+16900	2.00	1.7
16	7	*	*	*
17	1	-3170	2.00	0.3
18	2	-5570	1.65	0.6
19	5	-10300	1.90	1.0
20	20	+48800	0.80	4.9
21	21	-58900	1.05	5.9

V. TESTING AT WEST COAST SHOCK FACILITY

With the design and manufacture of the test structure completed, a satisfactory test geometry determined, and a pre-shot analysis accomplished with a computer model, the next step in the experiment was to determine what instrumentation would be necessary, and where and how to attach it.

The usual suite of instrumentation for an underwater shock test consists of pressure gages in the free-field to sense the pressure loading generated by the charge, strain gages on the test surface to output strain and deformation, and velocimeters and accelerometers on the structure to measure the velocity and acceleration imparted by the impulsive load. The decision on the instrumentation was made after liaison with the test facility because it was a function of what they could support with their equipment.

The West Coast Shock Facility (WCSF) was selected as the site for the test due to several factors. First and foremost was that they are the only licensed facility on the West coast where a test of this type can be performed in a controlled manner. Moreover, the shock facility is located only 120 miles north of Monterey in the South Bay of San Francisco. WCSF is a Navy activity which reports to the

Supervisor for Shipbuilding, Conversion and Repair, San Francisco. The facility has experience in conducting tests on this small scale, although the majority of their work is in the area of shock-qualification tests for the Navy. The latter involves the use of the standard Floating Shock Platforms (FSP) and much larger charges. Design engineers and an instrumentation technician were available to the Naval Postgraduate School to assist with the details of a viable solution to the necessary test geometry and the instrumentation of the structure. Presented on the next page is a sketch of the actual floation and rigging network as conceived by the design engineers.

Figure 5.1 shows the actual test geometry. Floation for the test structure was provided by the two pneumatic fenders (cylindrical shaped). The strong back I-beam was removed prior to the shot, as it was used solely for positioning the rig into the water. A wire rope was run from the pier and shackled to the backing structure as a safety measure. This would be used to retrieve the structure from the bottom should the explosion part the supporting lines. Once the test rig was submerged and the strong back removed, the outhaul was taken across the water by boat to a parallel pier and drawn tight by a winch. The test was conducted between these two piers, approximately 100 feet from the nearest one, and in about 50 feet of water. The tide was high and little to no current was present.

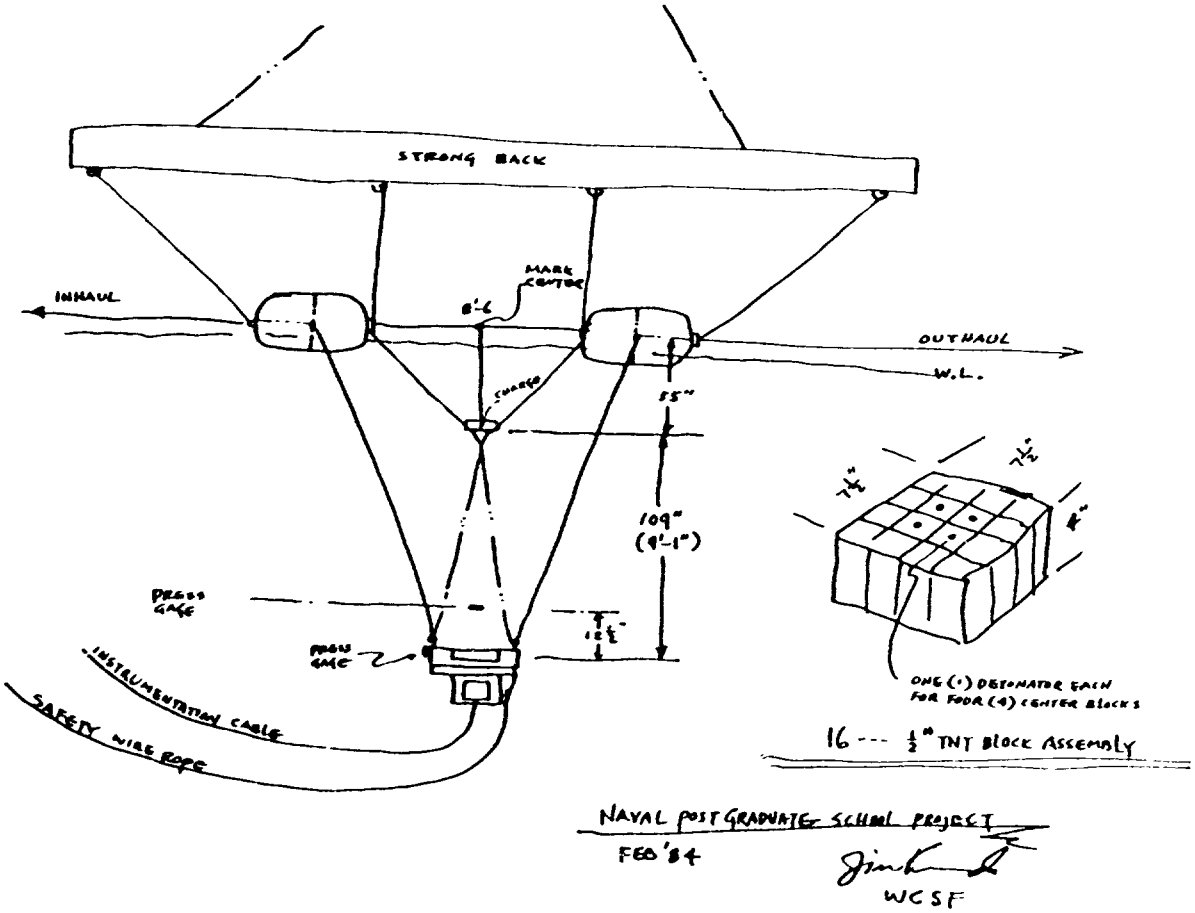

Figure 5.1 Test Rig at West Coast Shock Facility

The shock facility could support the test with 2 FM tape recorders which would allow for 24 tracks of data recording (14 tracks per recorder, 12 tracks for data, with one track for voice/countdown and one track for a one KHz time signal). It was decided that the 24 tracks be divided among two pressure gages, one accelerometer, and twenty one strain gages. No velocimeter was used during the test because there was not enough space inside the air-backing structure where it would be mounted.

The accelerometer used was an Endevco peizoresistive gage, model 2262-2000, with a range of ±2000 g. Ordinarily, an accelerometer would be mounted into the back of the plate so the acceleration imparted to it may be recorded. Additionally, this acceleration could be integrated to obtain a plate velocity, and integrated again for displacement. A calculation of the theoretical plate acceleration was made using the Taylor Flat Plate Theory to see if it was within the limit of the gage. The procedure found in [Ref. 13] was followed.

$$V_{max} = \frac{2P_o\theta}{m(1-\beta)} \left[e^{\frac{-\beta T_{max}}{\theta}} - e^{\frac{-T_{max}}{\theta}} \right] \qquad \text{(eqn 5.1)}$$

where $m = \{(12x18x.1875)+2(12x1x.1875)\,in^3 \times [.0002538\ \frac{lbf\text{-}sec^2}{in^4}]$

$$= 0.01142 \frac{\text{lbf-sec}^2}{\text{in}} \times 12 \text{ in/ft} = 0.137 \text{ slugs}$$

$$\text{m per sq. ft.} = 0.137 \text{ slugs}/1.5 \text{ ft}^2 = 0.0913 \frac{\text{lbf-sec}^2}{\text{ft}^3}$$

$$P_o = 22505 \left(\frac{8^{1/3}}{9} \right)^{1.18} = 3814.9 \text{ psi}$$

$$\theta = (0.058)(8^{1/3})\left(\frac{8^{1/3}}{9} \right)^{-0.185} = 0.1532 \text{ msec}$$

$$\beta = \frac{\rho c \theta}{m} = \frac{(2)(5000 \text{ ft/sec})(0.1532 \times 10^{-3} \text{ sec})}{(0.0913 \text{ lbf-sec}^2/\text{ft}^3)} = 16.77$$

$$T_{max} = \theta \left(\frac{\ln \beta}{\beta - 1} \right) = (0.1532 \times 10^{-3}) \left(\frac{\ln 16.77}{16.77 - 1} \right) = 0.0274 \times 10^{-3} \text{ sec}$$

$$V_{max} = \frac{2(3814.9 \times 144)(0.1532 \times 10^{-3})}{(0.137)(1-16.77)} \left[e^{-\frac{16.77}{0.1532}(0.0274)} - e^{\left(\frac{-0.0274}{0.1532}\right)} \right]$$

$$= 61.25 \text{ ft/sec}$$

$$\text{average acceleration, } \bar{a} = \frac{V_{max}}{T_{max}} = \frac{16.25 \text{ ft/sec}}{0.0274 \times 10^{-3} \text{ sec}} = 2.24 \times 10^6 \text{ ft/sec}$$

or 69,000 g's

This is in excess of the Endevco accelerometer's rating or of any accelerometer. The plate is too light and the

impulse too severe to attach an accelerometer to it. The other alternative was chosen and the accelerometer was screw-mounted into the base of the backing structure. In this manner, responses of the entire test structure were monitored, and as discussed later, with good results.

Locations for the twenty-one strain gages were determined based on the following considerations: symmetry, maximum plate response, stiffener response, and finite element discretization. Gages were located in the X and Y directions so that the recorded output could be compared to the EPSA output. Pairs of gages were positioned in the center cavity of the panel to record maximum plate response and a pair was positioned on the underside of the plate, internal to the backing structure, to check outer fiber strains against an exterior pair of gages. The balance of the strain gages were divided among the stiffeners and the plate. They were mounted on the top of the stiffeners and on the sides, both in the Y direction only.

Figure 5.2 shows the strain gages fixed to the exterior surface of the test panel. The strain gages used were Micro Measurements type EA-06-250BG-120, 120 ohm, rated at 3% to 5% strain limit in tension or compression. The cement used was Permabond 910. For a complete description of the bonding technique, refer to Appendix D.

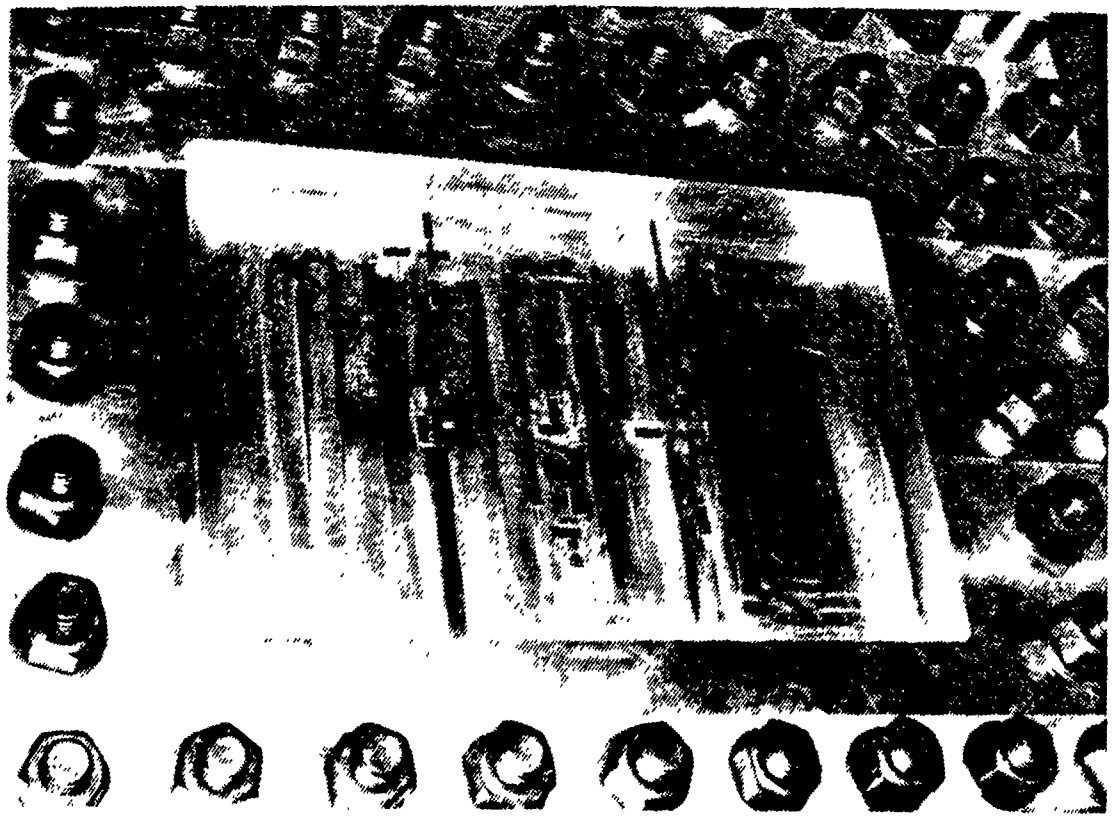

Figure 5.2 Photograph of Strain Gages Bonded to Test Panel

Figure 5.3 on the following page is another view of the strain gage locations and the position of the accelerometer.

An adhesive sealant was required to secure the strain gage lead wires to the plate. On this aspect, the advice of the engineers at the Underwater Explosion Research Division of DTNSRDC Norfolk, VA was followed. A saltwater resistant epoxy was applied directly on the gages and the wires. This smoothed out while setting to allow for good hydrodynamic flow. The material is a dichromate sealant manufactured by

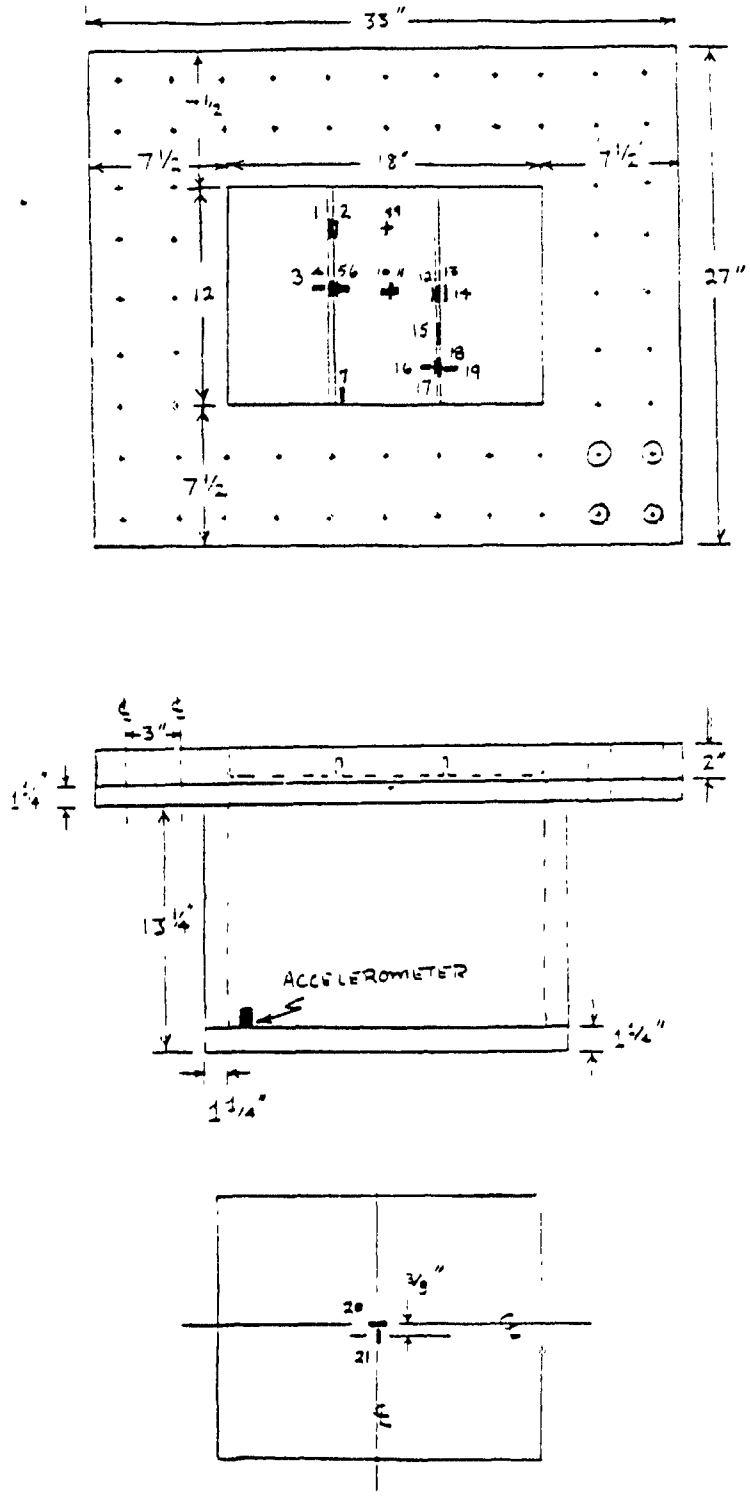

Figure 5.3 Instrumentation Plan of Test Structure

Products Research Corporation and labelled 1422A1, the last digit being a 1 hour work life.

The locations of the free field pressure gage are shown on the test geometry sketch, Figure 5.1. One is located a foot above the center of the plate and suspended by elastic shock cord and manila line. A good view of this arrangement is provided by the photo in Figure 5.4. The location of this gage was selected so that it would sense the same pressure wave which loads the plate. This was considered an important enough criteria to locate the gage above the plate, even though the reflected positive wave from the plate surface would reload the gage at approximately 0.4 msec.

The second pressure gage should therefore be located away from the test structure, preferably out in the free field, on an arc of the same radius as the plate. Rigging limitations prevented this arrangement, so it was positioned at the same radius as the plate by clamping it to the side of the test panel. A mounting block, three inches thick was fixed to the panel so the gage would be somewhat removed from the boundary effects that the incident pressure wave would create at the fixed edges of the panel.

The pressure gages used were one quarter inch tourmaline crystal gages, manufactured for the Navy at the Naval Surface Weapons Center. They are rated for a reliable

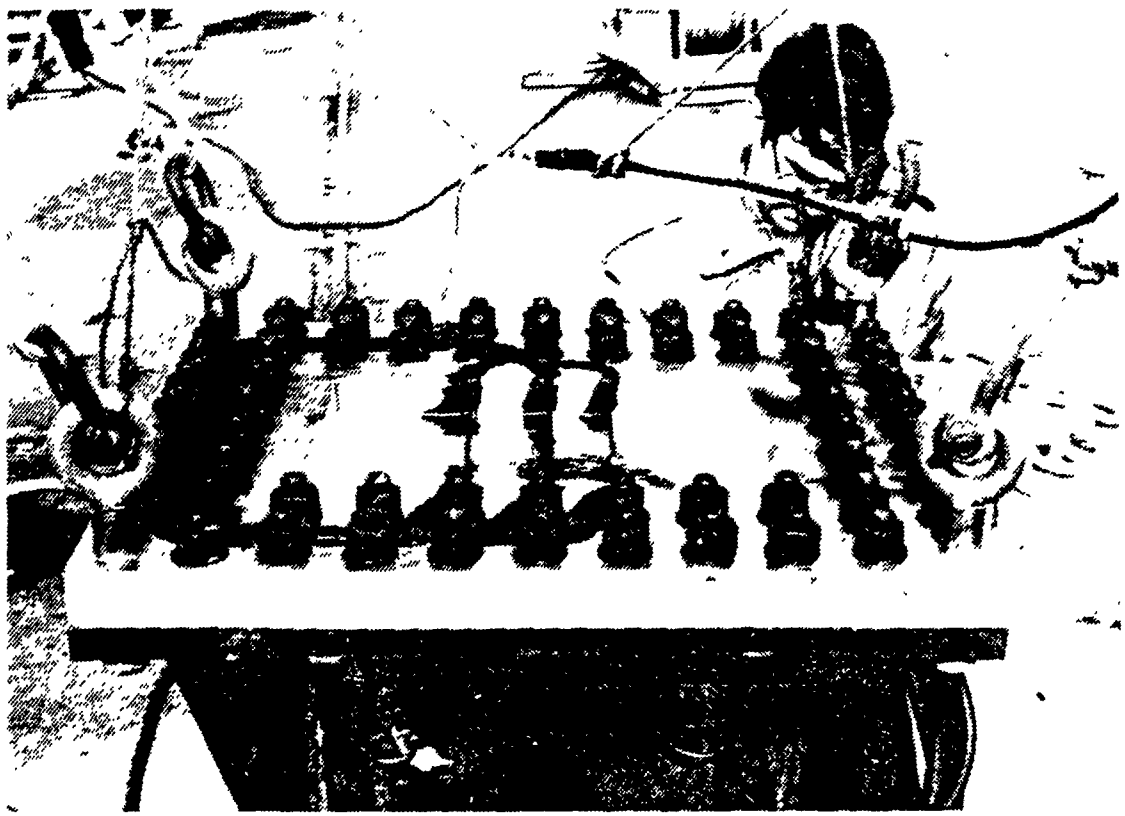

Figure 5.4 Test Rig Fully Instrumented

sensing of pressures up to 10,000 psi, although greater pressures have been accurately measured with this type of gage. The Naval publication listing the specifications for the tourmaline gage [Ref. 15] indicates that the quarter inch diameter gage is an adequate size gage for the test. As presented on page 16 of the report, the method of determination of proper gage diameter is:

θ, for explosive charge = .15 msec

t_D, transit time of shock wave across gage = .25 inch/

60,000 in/sec

$= 4.167 \times 10^{-6}$ sec

$1.5t_D$, to account for oil filled boot = 6.25×10^{-6} sec

$\theta/1.5t_D = 24$

and from the chart on page 17,

R_p = the pressure response ratio

= the apparent pressure/actual peak pressure

= .9793

This is well within the acceptable correction limit of 15%. The pressure gage greatly affects the accuracy of the peak pressure measurement due to its finite size and, therefore, orientation of the gage is important. The publication indicates that all measurements and calibrations of the tourmaline gages are based on a sideways or horizontally positioned gage. It was not until after the test was it realized that the second gage, located on the side of the box in a vertical orientation, was not in the ideal position.

After the test structure was positioned in the water, the explosive charge was taken out to it and the detonators inserted. The charge was run down to depth and secured in position by a lanyard in the rigging. This insured a center position over the plate. The eight pound TNT charge for which all preshot calculations were made was ordered by the

WCSF. Although it is considered a standard stock item for the Navy, it proved difficult to obtain. Moreover, when it was received, its physical condition was judged to be so deteriorated that it was destroyed. A counter-proposal was made to use what was available: sixteen 1/2 pound TNT charges, which could be bundled together to form one charge. This configuration is shown in the lower right hand side of Figure 5.1. It was fixed with an exploding bridge wire (EBW) detonator inserted in each of the four center charges. The test was conducted on February 29th, 1984. Figures 5.5 through 5.9 show the shot sequence and the two post shot views of the structure.

A listing of the instrumentation and the equipment used, the recording set-up and a wiring schematic may be found in Appendix E. All of the equipment listed is the property of the West Coast Shock Facility and is maintained there.

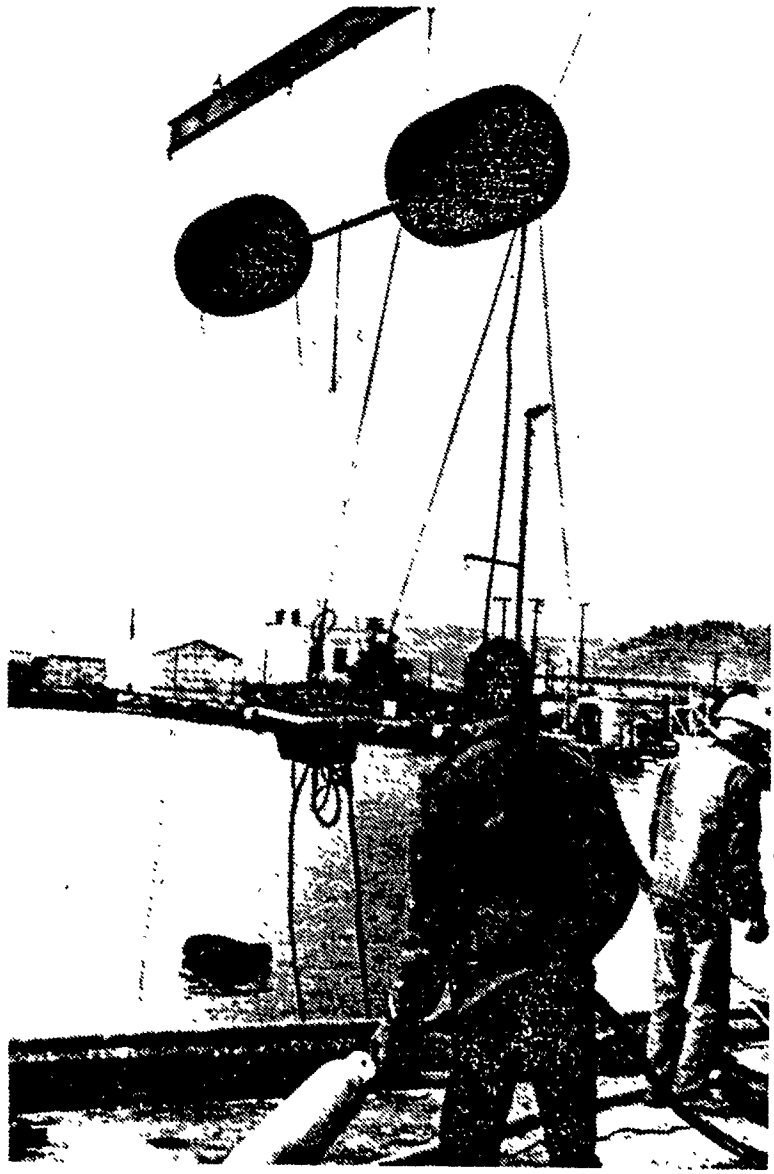

Figure 5.5 Lowering the Rig into the Bay

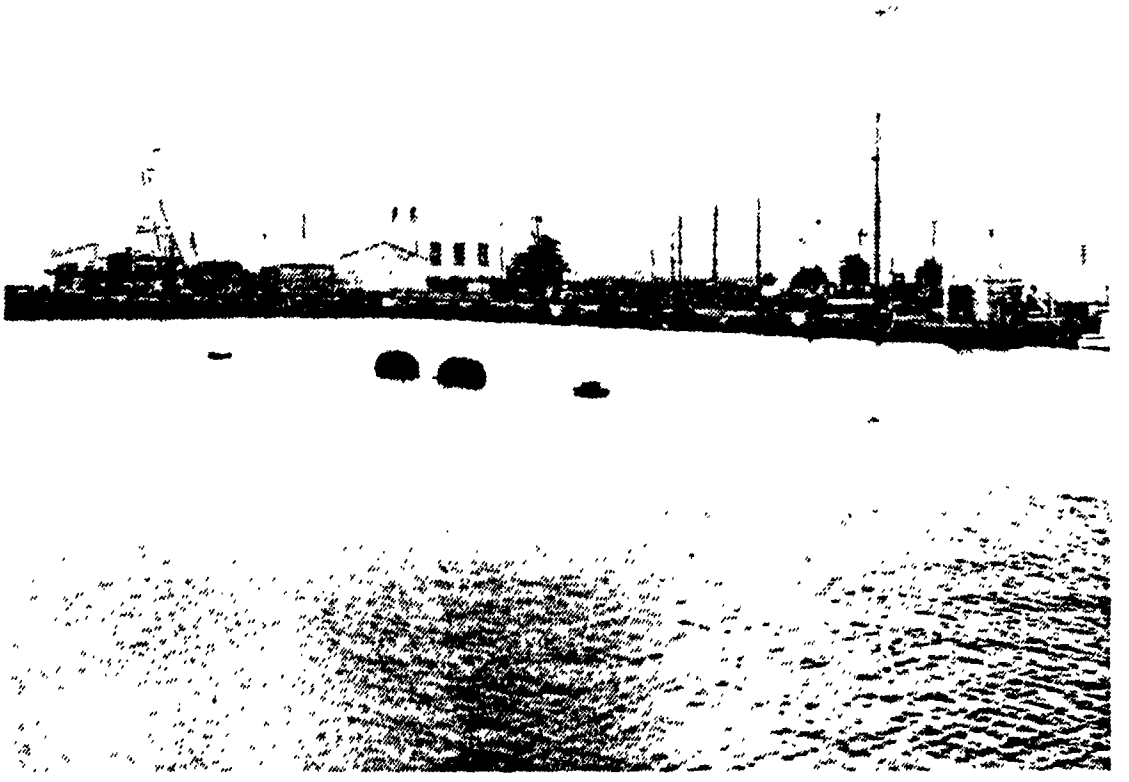

Figure 5.6 Test Rig in Position

Figure 5.7 Water Plume from Shot

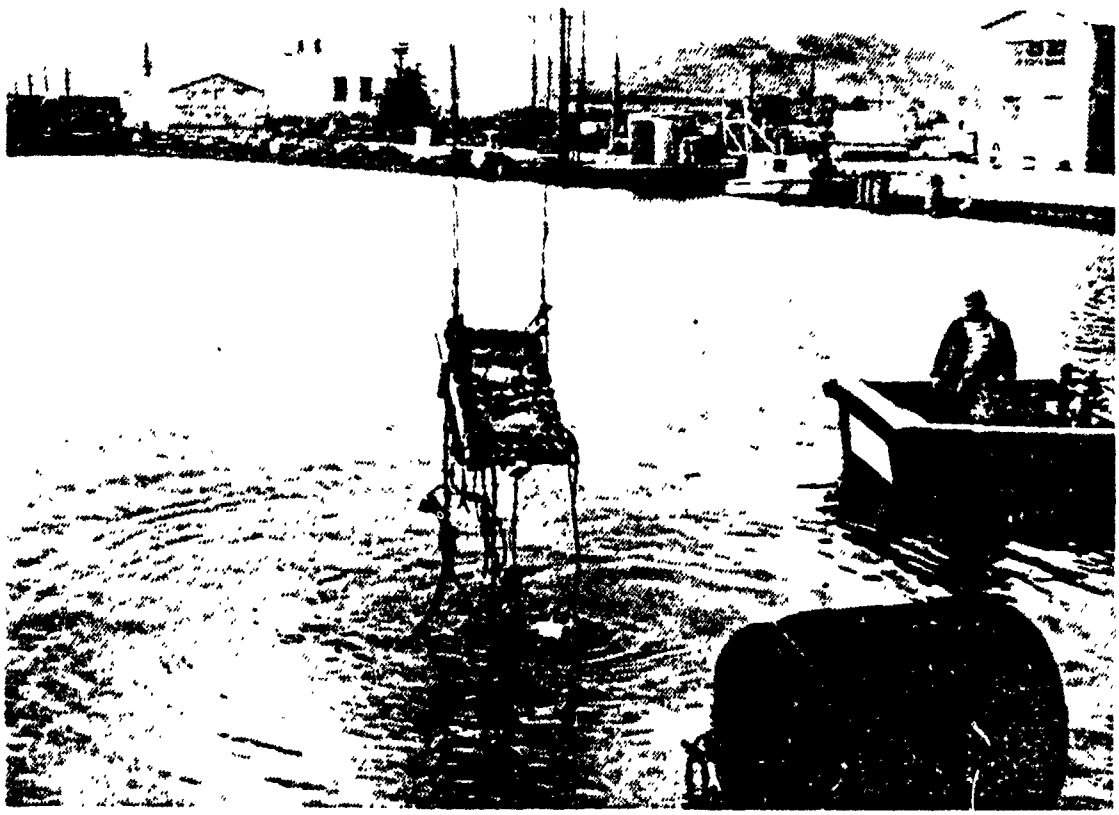

Figure 5.8 Post Shot View of Test Rig

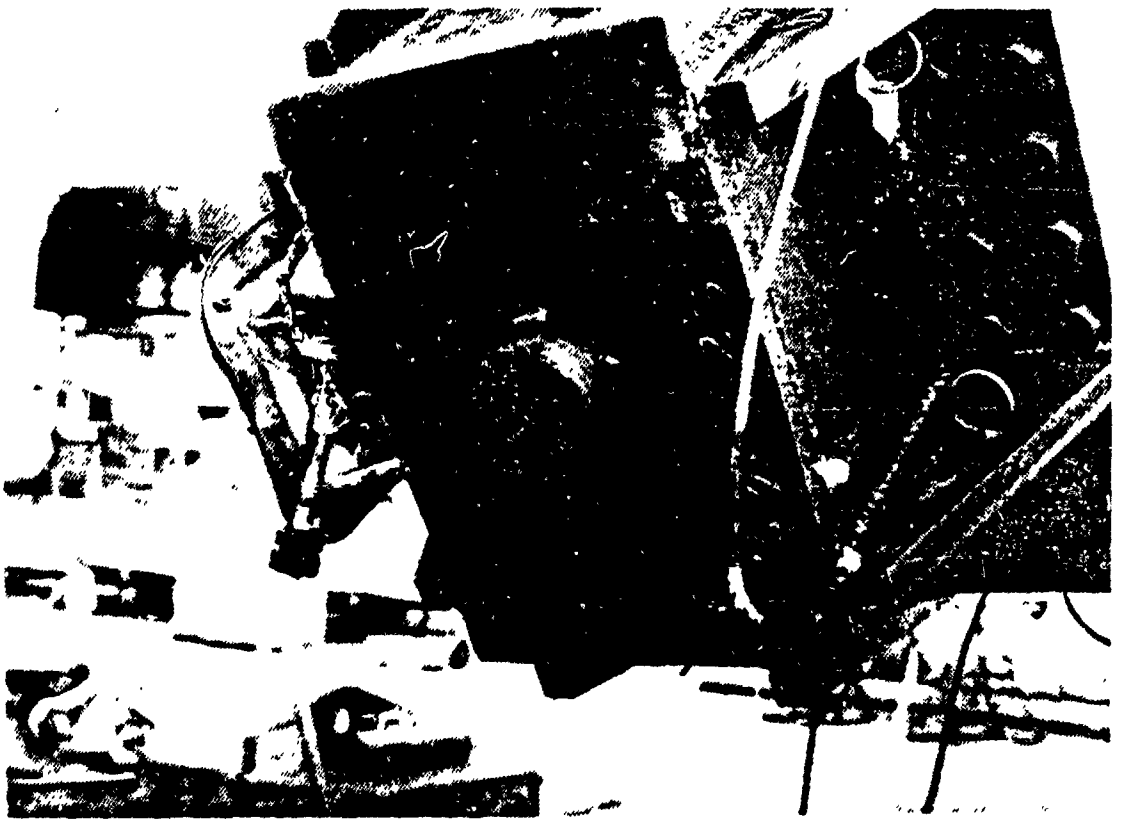

Figure 5.9 Post Shot Damage

VI. RESULTS AND INTERPRETATION OF DATA

This chapter will present the physical results of the test, then the data obtained, followed by a discussion on the limitations of the instrumentation, then the lessons learned from the test and methods of improving future tests of this nature.

Large deformations of the plate were achieved and the pattern, as seen in Figure 6.2 is as anticipated: symmetrical, with the greatest deformation in the center measuring 1.45 inches. EPSA predicted 1.24 inches as the maximum displacement at the center node at a very early time, 1.8 msecs. A precise measurement of the final deformation was performed after the shot. A deformation measurement rig was designed by the model maker, C. Crow, at NPS which would support a dial indicator depth gage as it was traversed across the plate. The readings obtained are presented in Figure 6.1 on the following page. These were taken before the plate was removed from the backing structure to preclude any relaxing that may occur when the plate is removed from its rigid support.

EPSA's results are considered very good. It must be understood that EPSA did not take into consideration any of the possible secondary effects which may have loaded the

POST SHOT MEASUREMENT

IDENTIFICATION NUMBERS

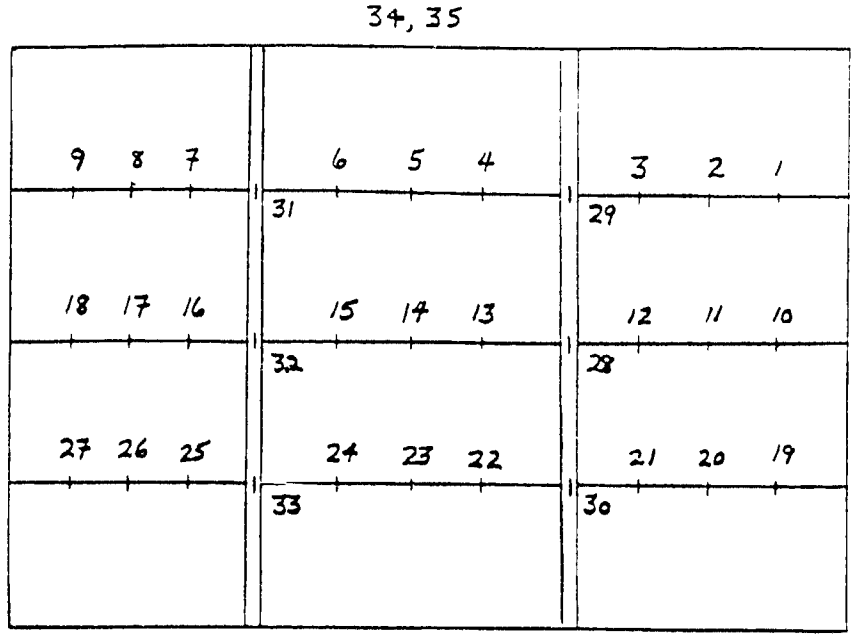

1) 0.226	12) 0.855	23) 0.978
2) 0.466	13) 1.376	24) 0.912
3) 0.689	14) 1.453	25) 0.587
4) 1.122	15) 1.304	26) 0.431
5) 1.186	16) 0.887	27) 0.221
6) 1.125	17) 0.609	28) 1.153
7) 0.687	18) 0.306	29) 0.909
8) 0.473	19) 0.221	30) 0.703
9) 0.234	20) 0.428	31) 0.909
10) 0.293	21) 0.591	32) 1.149
11) 0.599	22) 0.918	33) 0.739

34) Length of tear 3.0

35) Maximum displacement difference along tear 0.478

All measurements in inches

Figure 6.1 Post Shot Deformation Measurements

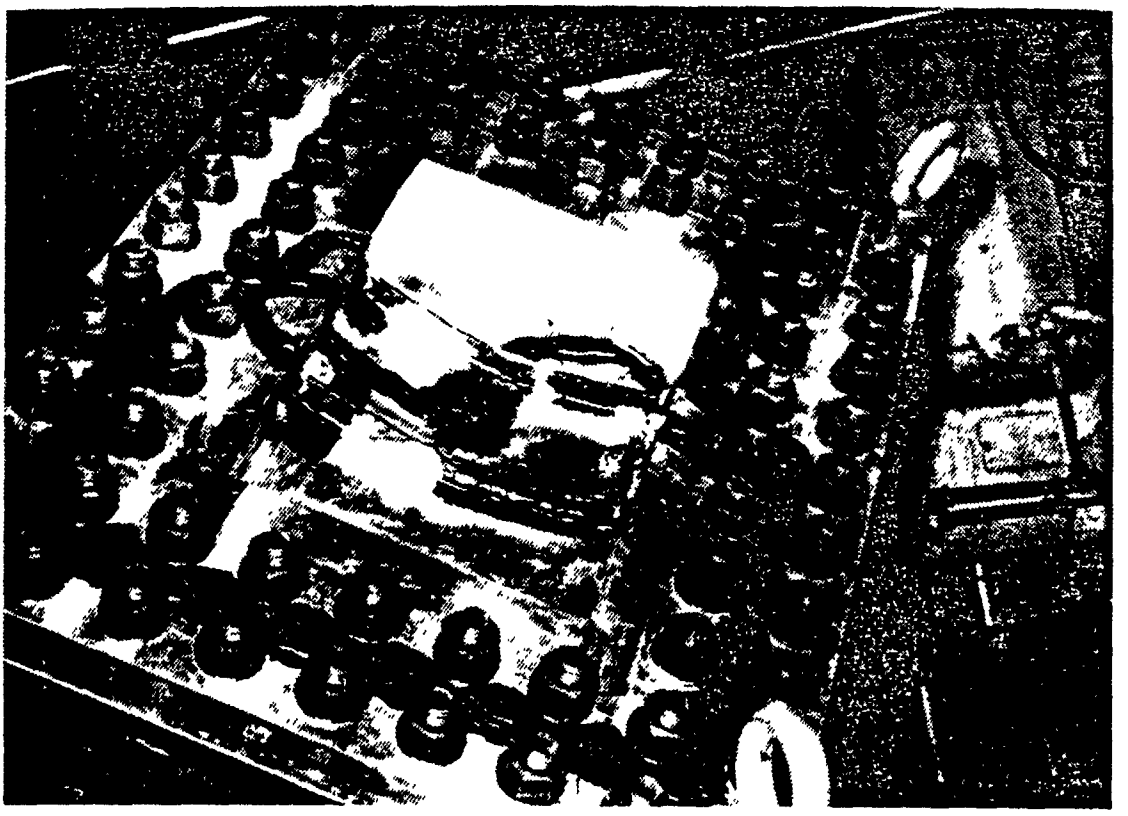

Figure 6.2 Panel Deformation

plate, most notably the afterflow loading generated by an accretion of water particles on the plate. Moreover, some unpredicted plate responses also occurred which otherwise would have allowed the plate to deform to a greater extent. There was an unexpected shearing of the stiffeners from the edges at each end, as seen in Figure 6.3. The other response that was not planned, but considered a likely occurrence should the loading be excessive, was a tearing of the plate at the center cavity. A close-up photo of the

Figure 6.3 Stiffener Sheared at End

tear is shown in Figure 6.4. The only other physical damage to the test structure was a parting of two shackles which attached wire ropes to one of the pneumatic fenders, a severe deformation of the brass terminal connection box on the side of the backing structure, and a shearing of the threads on the hardened plastic connector in the base. Some of these effects can be seen in previous Figure 5.9.

Another view of the deformed plate, Figure 6.5 shows the deformation pattern and the stiffeners with only a slight

Figure 6.4 Tear Along Edge of Center Cavity

out-of-plane twist. It is evident that the tripping effect desired did not take place. Also to be noticed in the photo are that a few of the strain gages became detached from the stiffeners during the test. One of them is seen lifted above the stiffener surface. Not shown is the shearing of the lead wires which were laid on top of the stiffeners; they parted at the same instant each of the stiffener ends sheared.

Figure 6.5 Stiffener Deformation

After the shot, an accurate EPSA prediction of stresses in the plate was finally produced. Figure 6.6 shows the Von Mises stress levels for the quarter plate model at time 1.2 msec after the shock wave loads the plate. The maximum stress is 55305 psi, well above the yield stress of 43200 psi. It is located at the top of the center cavity, suggesting that the plate should tear first at this point of maximum stress. The experimental results confirm this.

A shearing of the stiffener at the ends is not indicated by the stress plot. To understand why requires a description

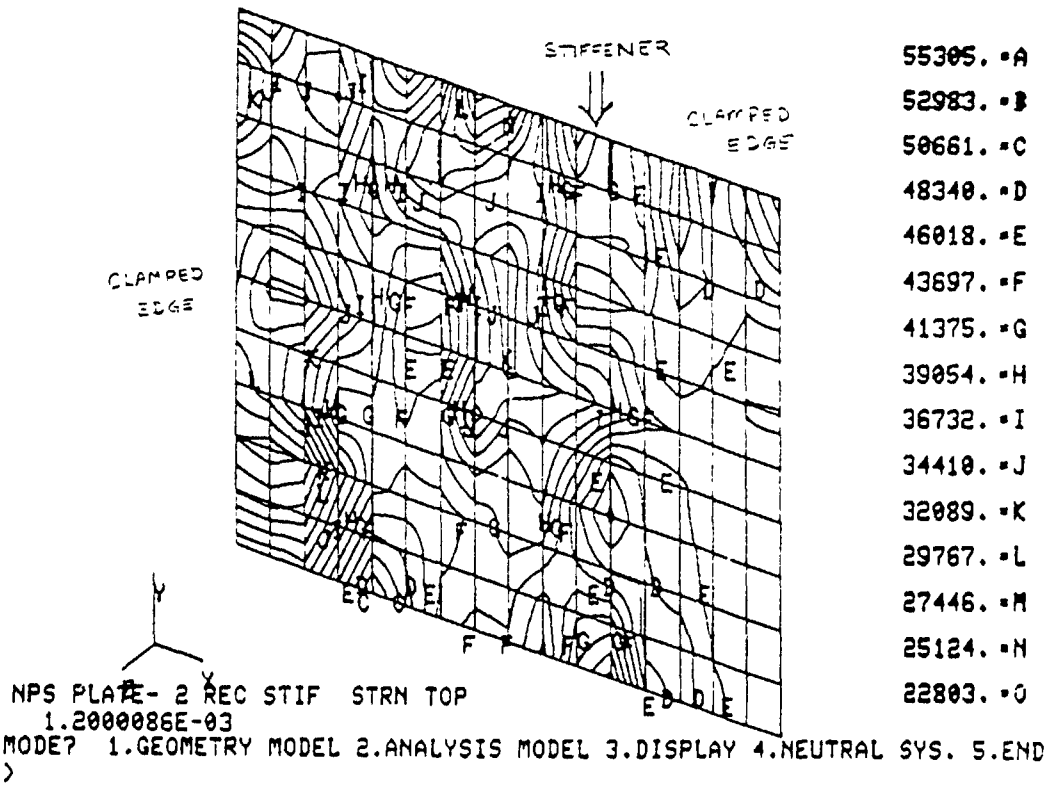

Figure 6.6 Von Mises Stresses Predicted by EPSA

of the way EPSA treats stiffened elements. To model the stiffener running through a column of elements, EPSA determines the mass of the 1 inch by 3/16 inch stiffener and adds the corresponding amount to the shell elements in the column. The orthotropic nature of a stiffened element is handled in the following manner. For each of these elements, strain increments are used to compute stress resultants in the shell. These same strain increments are transformed to the centroid of the stiffener. Using constituitive equations for a beam, these strains are

converted to stresses in the stiffener. Finally, these stress resultants are used to modify the membrane forces and bending moment in the plate element in the direction which the stiffener runs. The final result is a single stress at the midthickness of the plate. With the current method of EPSA output, stresses cannot be evaluated at the extreme fibers of a stiffener, nor at the fixed boundary where shearing occurred. It should be noted, however, that Weidlinger Associates have developed EPSA II which does output the necessary stresses throughout a stiffener. It also allows for the modeling of several different stiffener types.

Success was achieved in that data was recorded on all twenty-four channels. As to the quality and the worth of the data, that is still to be determined. A description of the appearance of some typical recordings are contained herein, along with reproductions of the traces, but there is insufficient room in this paper to include all data histories.

Data reduction at the test site consisted of a tape playback into a Visicorder unit. All of the strain gage histories, pressure and accelerometer histories were displayed on visicorder paper, along with the calibration signal for each of the above and a one kHz time signal. Appendix E describes the instrumentation and recording procedure. Tape playback was at 7 1/2 ips and Visicorder speed was 80 ips. This was for an initial look at the data

and for later reference. Xerox copies were made of the Visicorder sheets because they fade when exposed to light. Next, the shock facility instrumentation technician brought down to NPS one of the Ampex 1300 tape recorders and the magnetic tapes. The tapes were played back into an HP-5451C Fourier Analyzer and recorded onto a hard disk. This allowed for a local analyzing of the data, graphing on the HP plotter unit, and fitting of the response curves with the time code signal and calibration levels. Most importantly, transfer of the data to the Fourier Analyzer permitted a selective processing in the frequency domain and the permanent storage of the records at NPS.

The recorded histories from the two pressure gages appear as though the ratings of the instrumentation may have been exceeded. Also, it appears as if there is a signal driving the instrumentation beyond its maximum setting of 10,000 psi and causing its output to maintain this peak throughout the time of shock wave loading. Figure 6.7 is a reproduction of the Visicorder output. Shown are the traces for pressure gages one and two, located one foot above the panel and on the side of the panel respectively, and for the 1 kHz time signal. Calibration of the amplitude in the time domain was performed by a simple procedure of laying measurements on a 3 in. x 5 in. card from the calibration signals and the 1 kHz time signals, then transferring them to the pressure history.

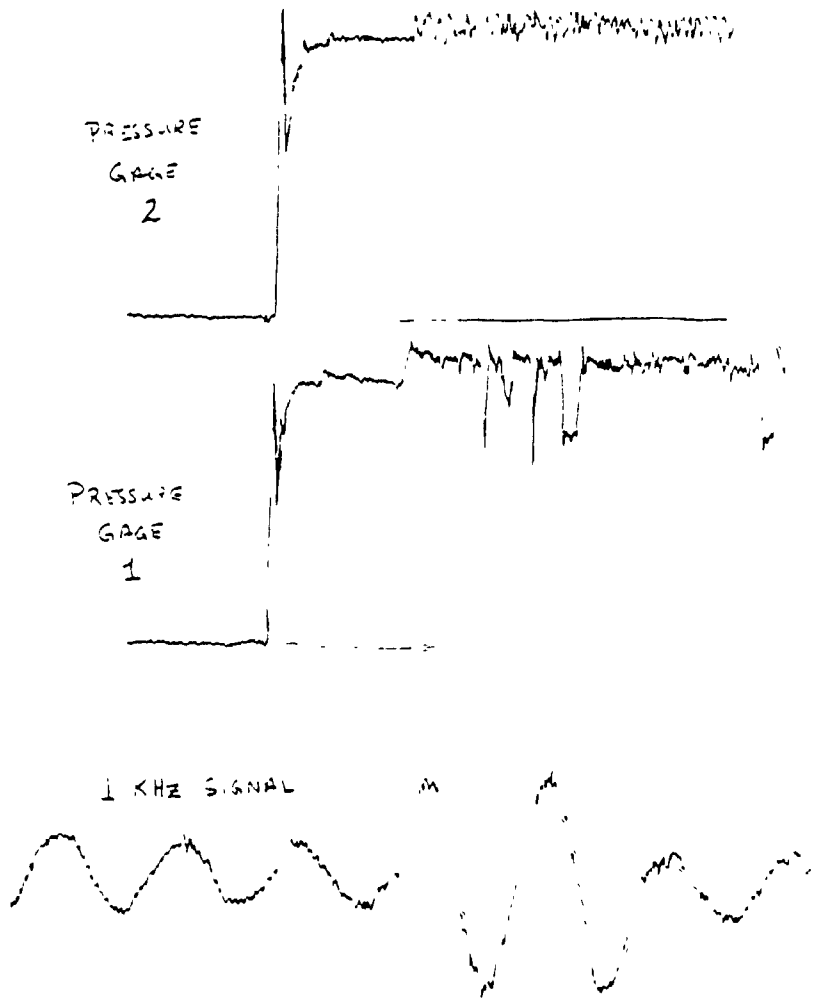

(Double amplitude is characteristic)

Figure 6.7 Visicorder Output

At the test site, the recording charge amplifiers were set to a maximum of 10,000 psi--exactly what seems to be recorded on both gages. As shown earlier, theory predicted an incident pressure from an eight pound spherical TNT charge to be 3950 psi. One would suspect that the actual pressure developed by the use of 16 one-half pound charges may have been somewhat greater. Post shot inspection revealed physical damage to both pressure gages. The leads inside the oil-filled sensing boot had become detached on one gage and the four tourmaline crystals in the other gage were delaminated. The time at which this damage occurred is unknown and such damage would have caused erratic readings.

Other damages for the excessive amplitudes include the possibility of a calibration error in the instrumentation or, as reported in the Compendum of Underwater Explosions Research [Ref. 15], the multiple charges have a much enhanced effect over a normal, homogenous charge of equal weight. The pressures from each of the charges may be additive when they are detonated sympathetically. There is much research left to be done in this area of what is called the multiple charge effect. For example, the pressure generated by a single one-half pound charge and sensed at eight feet away is:

$$P = 22505(0.5^{1/3}/8)^{1.18} = 1473 \text{ psi}$$

When using sixteen of these charges and they are arranged in such a manner that sympathetic detonation is induced, 16 x 1473 = 23,569 psi. This is enough pressure to saturate amplifiers and damage pressure gages. In view of this, some of the questions raised include whether or not some or all the charges were detonated sympathetically, or if there could have been a delayed effect due to the geometry of the TNT block. The author fully believes that the shape and height of the plume was very different from that of a standard spherical charge. There may have been a concentrating or jet effect of the pressure due to the stacking and the geometry of the charges. To quote directly from Cole, page 229, "...it can be expected that charges that do not have spherical symmetry will give rise to a shock wave which is not symmetrical, and differences in form of the wave at different points around the charge are in fact observed."

This statement leads one to question what shape of pressure history curve would be generated from the rectangular block of TNT used during the test. Fluid non-linearities also affect the propagation of a shock wave and are difficult to predict, model, or reproduce. As an added note, the equivalent weight of TNT required to produce 10,000 psi incident pressure at eight feet is 65 pounds. Questions such as those raised above can only be answered

through further experimentation and proper pressure field measurements. Cole concludes his chapter on pressure waves by stating that, "while an exponential curve is a simple and convenient approximation to the form of an underwater shock wave, it is by no means a perfect representation, and in some circumstances, is a rather poor one." The question of what was the true pressure loading experienced by the plate may never be known. The data records are presented in the report for possible future insight and understanding.

Without the knowledge of the loading history of the plate an accurate prediction/comparison of the strains induced in the plate is impossible. A best fit correlation was attempted between the recorded strains and those predicted by EPSA for the two possible loading extremes; the smallest being an eight pound charge and the greatest being a sixty-five pound charge. The next pages show these strain history comparisons for several gages using an eight pound charge. The details of how these strain histories were generated by EPSA are included in Appendix C.

As can be seen from the strain comparison (Figures 6.8 through 6.11), nothing generated by the computer seems to come close to agreeing with the recorded data. All twenty-one of the strain records are difficult to interpret. There is an excessive amount of high frequency noise imposed on what may be a valid strain signal within the first few

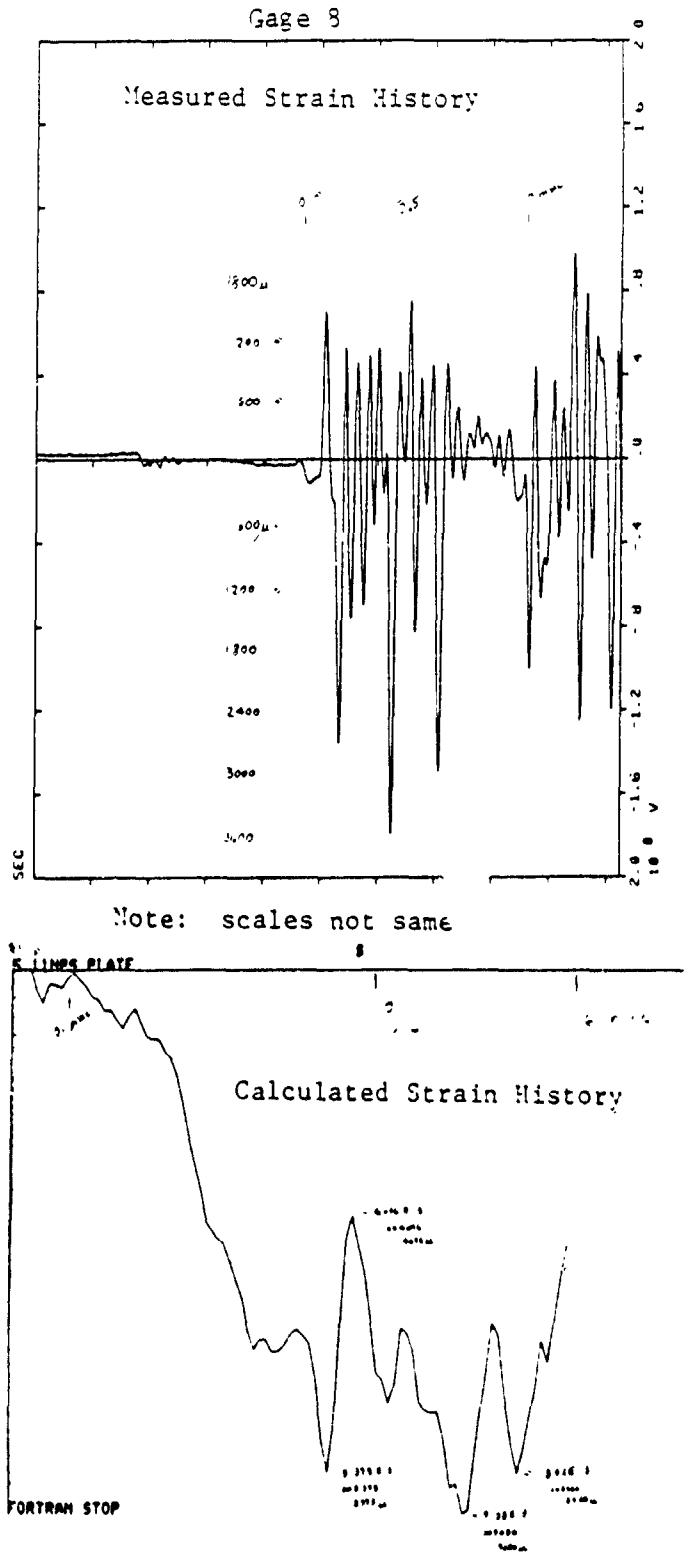

Figure 6.8 Gage 8 - Recorded Strain and EPSA Predictions

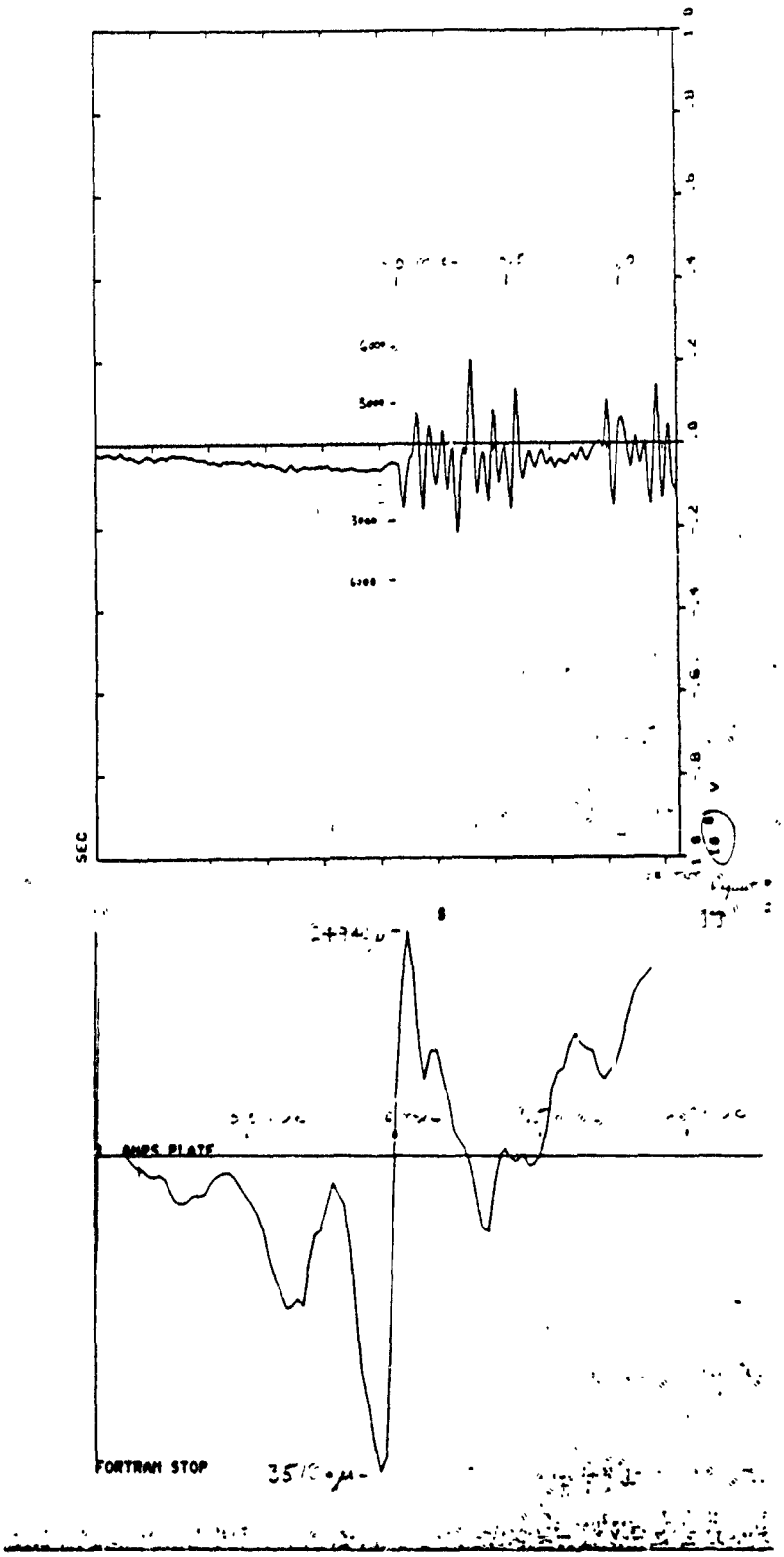

Figure 6.9 Gage 11 - Recorded Strain and EPSA Predictions

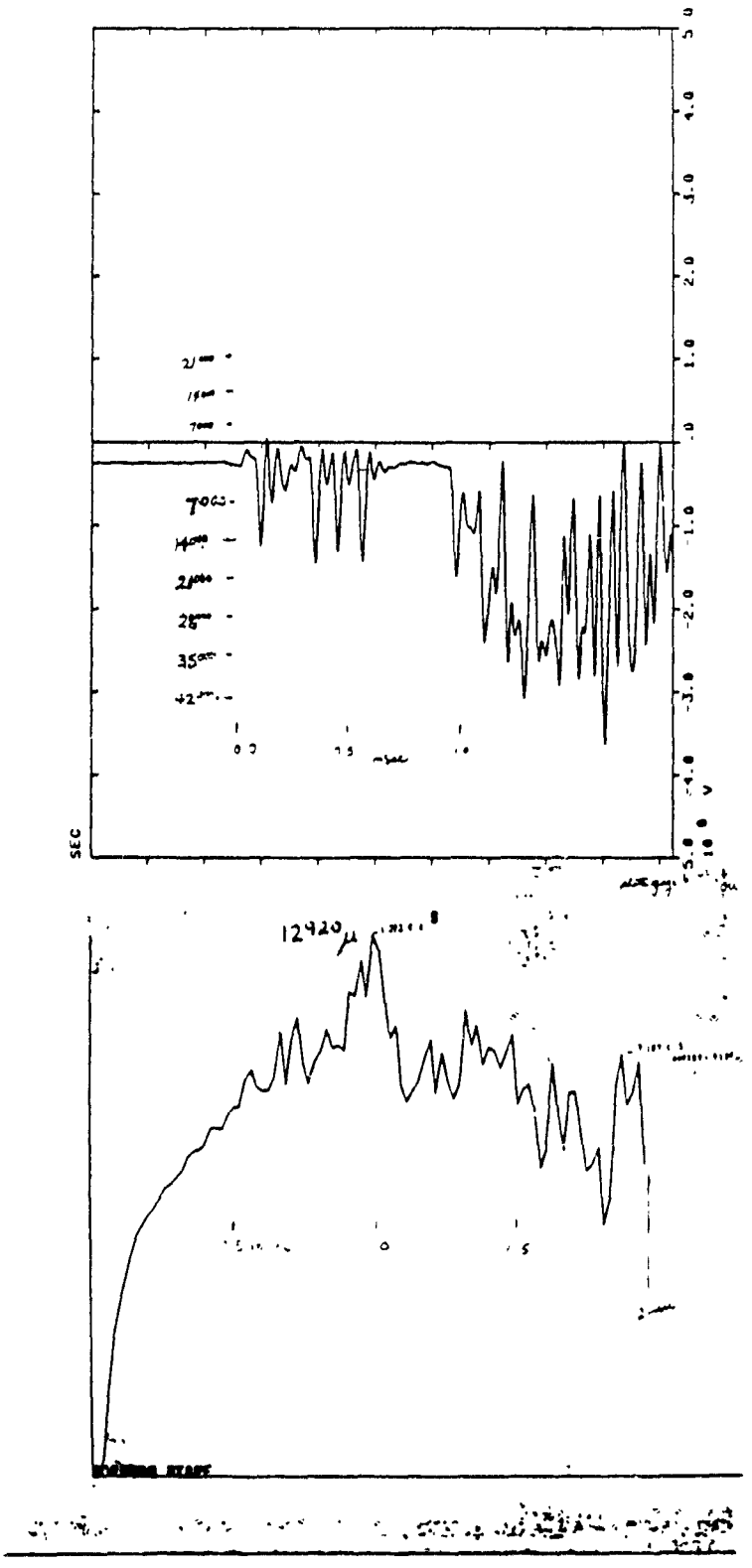

Figure 6.10 Gage 16 - Recorded Strain and EPSA Predictions

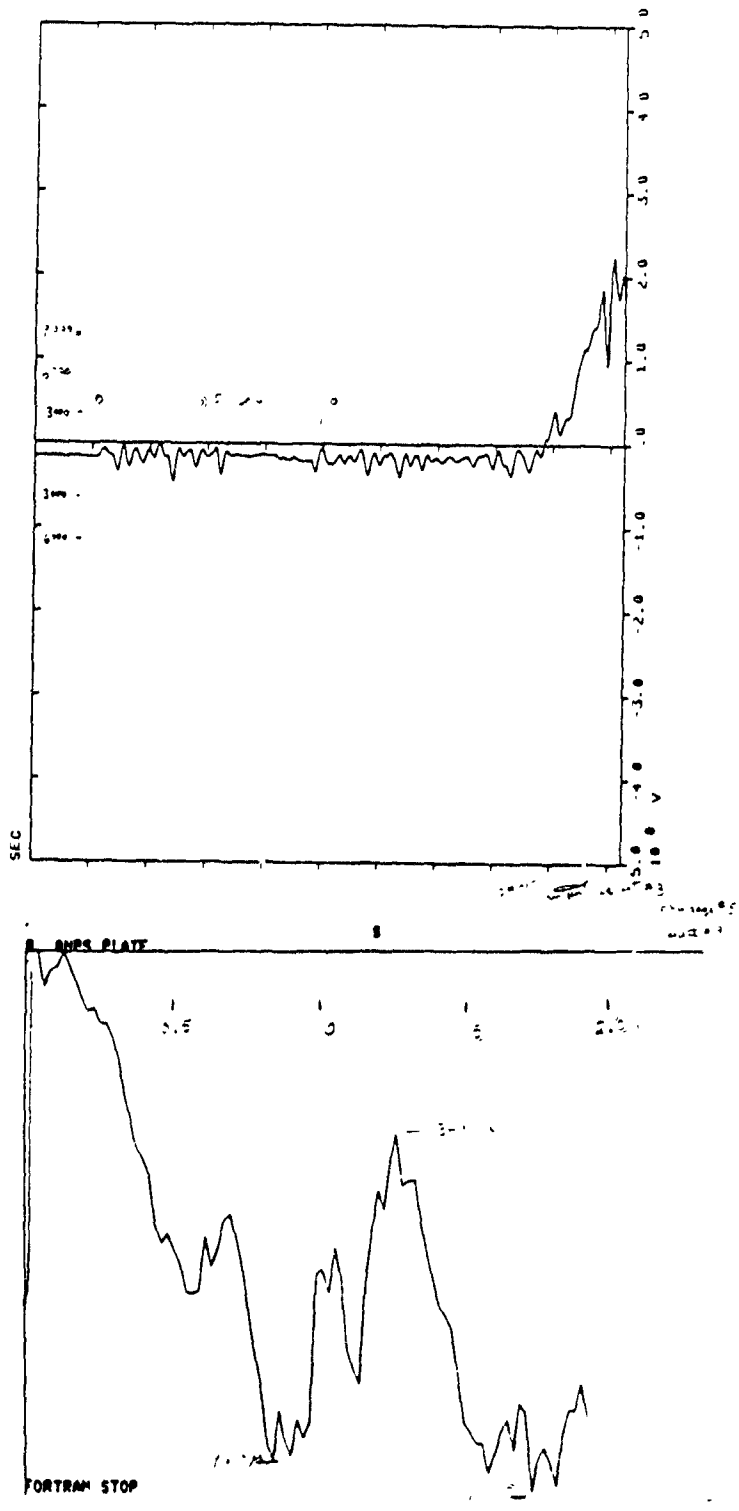

Figure 6.11 Gage 19 - Recorded Strain and EPSA Predictions

milliseconds. However, this noise could not be filtered out electronically by the HP-5451C Fourier Analyzer. Curve fitting could be attempted, but to even do this would lead to suspect results. Erroneous signals were surely generated as the lead wires to the gages were pulled and twisted. They were glued to the plate surface which was undergoing large deformations in very early times. Also, the lead wires which ran across the stiffeners were parted when the stiffeners sheared. Moreover, severe damage was done to the leadwire connection box on the side of the backing structure; wires were stripped and broken as the shock wave opened the box to the environment. Recommendations to avoid some of these problems in future tests are included later in this chapter. Appendix F contains select strain histories. Presented in Table II are the results of the strain gage analysis, with no conclusions drawn. Only the amplitudes of the first two peaks are tabulated; the validity of the subsequent recording is questionable. It is thought that the first sharp peak in the strain histories is the firing pulse signal. This is not shown in Figures 6.8 though 6.11, but may be seen in the data located in Appendix F.

The one instrument record which is readable and shows good results is the accelerometer history. This is shown in Figure 6.12 with the integrated velocity and displacement records. The HP-5451C Fourier Analyzer was used to perform

TABLE II

Strain Readings from Gages

Gage Number	Firing Pulse (μstrain)	Rise Time (msec)	Duration msec)	First Peak (μstrain)
1	-2250	0.09	0.11	+2000
2	-1440	0.07	0.10	+1200
3	-1650	0.10	0.12	+750
4	-400	0.05	0.10	+800
5	-1350	0.07	0.10	+950
6	-750	0.06	0.11	+1200
7	-2800	0.08	0.10	+1300
8	-800	0.08	0.12	+1400
9	+500	0.05	0.05	-1000
10	+1200	0.04	0.06	-2100
11	+2200	0.06	0.10	-2500
12	+800	0.05	0.07	-2200
13	+800	0.03	0.06	+1200
14	*	*	*	*
15	-1200	0.07	0.09	+1000
16	-12000	0.04	0.07	+2000
17	-1200	0.03	0.04	-1000
18	-4750	0.07	0.10	-1000
19	-3000	0.04	0.08	+700
20	*	*	*	-1000
21	*	*	*	*

* Amplitude too small to read.

No attempt was made to preserve the sign (+ or -) during transciption.

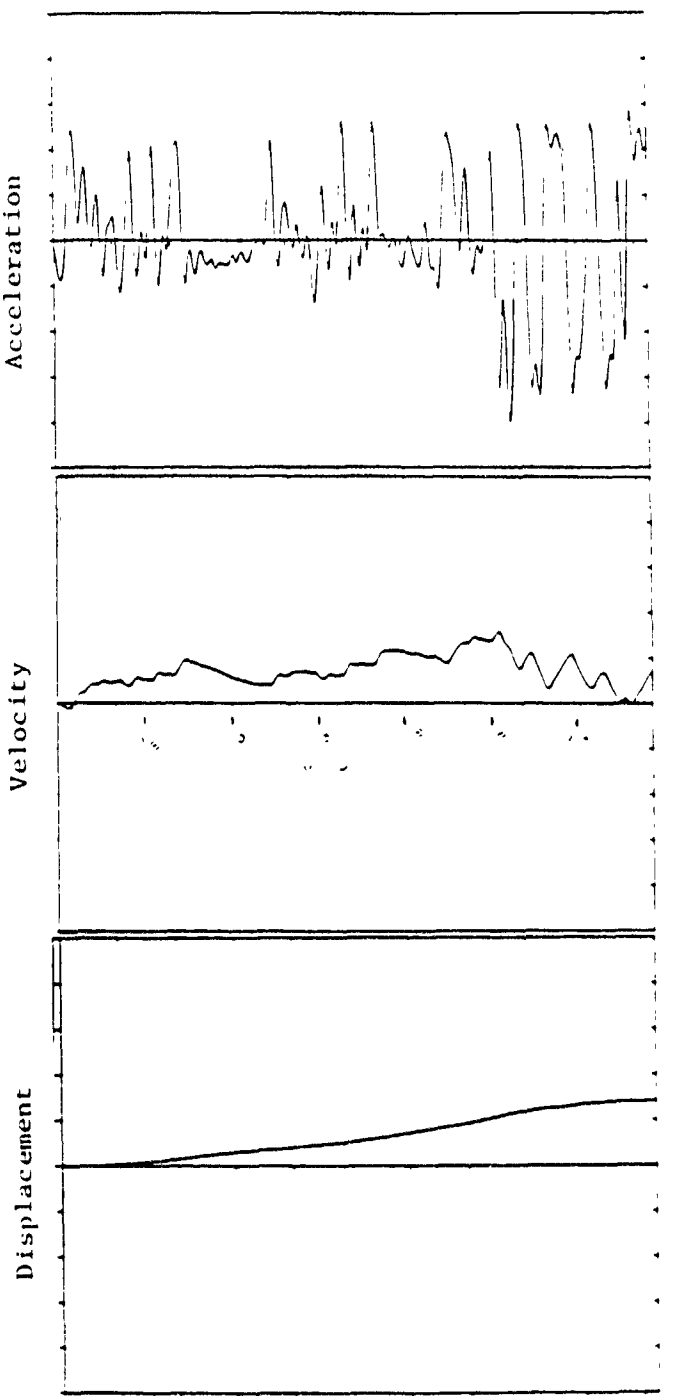

Figure 6.12 Accelerometer Histories

the integrations. The three records appear as they should: the integration of an impulse is a step and the integral of a step is a ramp function.

Each of the instrument records in Appendix F clearly shows the firing pulse impressed on the electronic signal. This indicates that the wiring configuration was such that it was particularly susceptible to noise pickup and electrical interference. The first singular voltage spike is identified as the firing signal because it appears in each of the records in similar form. It is followed by a "dead-time" on each record where no other signals occur for at least 1.8 msec. This time corresponds to that necessary for the shock wave to travel nine feet from the charge to the plate. The shape of the firing pulses, and of many of the other sharp peaks on the records, are too similar and cause one to question why. An explanation is found in the Shock and Vibration Handbook by Harris and Crede [Ref. 16]. It presents a thorough discussion on how improper or inadequate sensing, recording, and playback equipment will limit the frequency of signals which can be accurately measured. For example, listed on page 17-15 of the reference, the upper limit of FM magnetic tapes is 5000 Hz, a light beam galvanometer is limited to 50,000 Hz, an AC carrier amp with demodulator is 5000 Hz, and the same for an AC power supply. These numbers are representative only, and

the equipments are not the same as those used during the test. However, the characteristic rise time for an impulse shock wave is five or six milliseconds (as limited by the tourmaline 1/4 inch gage). This means that the electronic equipment must be sensitive to 200 kHz. The tape recorders used were Ampex 1300's which are rated at 20 kHz as a response time. This is precisely the recorded rise times for the firing pulses and peak signals on the data records. Table II also lists the rise times for these signals. It is evident that the limitations of the equipment were exceeded during this shot. What should be used for tests of this nature are FM tape recorders with a much better response time, such as an Ampex 2200 or a Honeywell 101. A note of caution, however, is that the higher the frequency of the recording, the poorer the signal to noise ratio. Considerations must be given to a proper arrangement of filters and playback speeds to obtain the best records. Oscilloscope photography has provided good response histories in past experiments. This method should always be considered a possibility.

To properly set up the electronics for an underwater explosion test is an art in itself. Many lessons were learned and some of them will be briefly mentioned as items that should be considered in any future tests:

-There must be a zero time signal on one of the data channels. This is necessary during the analysis phase so

the time code, the gage histories, and the zero time can be lined up to measure small differences in arrival times.

-If clipping of the signals is present, ensure that it is not caused by the playback electronics being oversensitive.

-For the tourmaline pressure gage calibration, the Q-step method described by Cole (pages 182-3) is highly recommended.

-There are corrective techniques to back out actual peaks in signal records should they be rounded due to equipment limitations. One of these methods is discussed by Ronald Tussing in his text on page 33 [Ref. 14].

-The firing circuit should be coupled to a transformer so as not to be grounded with the other gages. In this test, magnetic/inductive pickup through the cables is thought to have caused the firing signal to be impressed on the other lines and perhaps creating a signal of such magnitude as to overdrive the amplifiers. In future tests it is essential that the cable used to transmit the firing voltage be positioned as far away from the recording lines as possible.

A chapter in Harris and Crede's text is titled, "Interference and Noise in Transmission Cables". It brings out many important considerations and the means to correct them. For example, on page 12-21, it defines electrical

interference or pickup as, "Noise components superimposed on the desired signal due to the proximity of the connecting cable to the electromagnetic field of an electrical disturbance"... "and 'static-type' disturbances from switching transients are the worst offenders." A solution offered is the use of properly shielded cables and the correct grounding of the circuit in relation to the electronic equipment.

Another source of signal interference mentioned by the text comes from the movement of the signal carrying-cables. On page 12-26 it cautions that, "Noise is generated when the cable is suddenly squeezed, bent, struck, or mechanically distorted. Peak noise voltages from this source were frequently as large as the actual acceleration signals being recorded." A shock test is a dynamic phenomena and lead wires to instrumentation will be twisted and pulled as the shock wave impinges on them and as the plate deforms. There seems to be almost no way to eliminate this problem, however there may be methods to reduce the effect this has on the signal. Rather than fixing the strain gage lead wires directly to the plate with the PRC adhesive/sealant, it is recommended that a sheath or tube arrangement be devised to permit the lead wires to move as the plate deforms. This should be done at least in the immediate area of the test panel where large displacements will occur.

Additional considerations must be given to the use of the correct type of strain gage. There are special high-elongation gages which can measure up to 10% strain with accuracy. Also pointed out in Reference 16 is that the dynamic type gage will have the greater gage factor and provide maximum possible electrical signal for a given strain. The use of an iso-elastic foil will have a greater gage factor than constantan and therefore a greater resistive charge for a given strain.

Another important aspect of the use of strain gages is that they are bonded properly to the test specimen. As pointed out by Harris and Crede on page 17-5, the proper functioning of a strain gage is completely dependent on the bond. One must use the manufacturer's recommended cement and follow the directions closely. Incorrect strains will result if the bond is not completely over the entire area of the gage, or if it becomes partly or fully detached during the test.

The recording of transient strains under dynamic loads is a mostly difficult task, as brought out by the work at M.I.T. by Dr. Witmer [Ref. 17]. In a series of shock tests performed at the Aeroelastics and Structures Research Lab, only about 0.2 msec of data was the best that could be obtained. Although the severity of the impulse for the experiments was much greater than that for the underwater

shock test, the environment was much more controlled. The problems most often encountered were gage detachment and lead wire rupture. A very helpful procedure for the bonding of strain gages is presented by Dr. Witmer in his report, particularly with regard to the use of backing material to cover the gage. His procedure is included in Appendix D for future reference.

As a final caution in this discussion on the instrumentation of a shock test, it would be wise to thoroughly check out the electronic recording set-up just prior to the test so that it is well known what will be the character of the signals, as distinct from interference noise. Suggested is a simple procedure of turning off all power supplies and striking the plate to see the strain gage response within the elastic regime. It is also most important for the individual conducting the test to have a complete understanding of both the nature of the test (including underwater shock phenomena, material response of the test structure, the desired results, etc.) and the electronic measuring and recording of the data. Both of these go hand-in-hand and must be tailored to provide meaningful data.

One final recommendation for future work in this area is a redesign of the test panel to allow for better tripping of the stiffeners. A single stiffener in the longer direction of the test section will provide a greater area for a

stiffener to suffer compression. Also, investigation into the effects of detaching the ends of the stiffener so it is free to fall flat would be of interest. In any case, it's hoped that the work to date has paved the way for further research in this field of study.

APPENDIX A

UNIAXIAL TENSION TEST DATA FOR 6061-T6 ALUMINUM

Uniaxial tension tests were performed to characterize the material properties of the 6061-T6 Aluminum. A rectangular section of the material was cut from the end of the blank and six round test specimens were machined from it. Figure A.1 shows the dimensions of a specimen. The specification used was ASTM E8-69 for sm ll-sized round tension test specimens proportioned to a standard 2.0 inch gage length. The charts from the six tests are reproduced as Figures A.2 through A.7. Of the six, only four tests are considered valid. On test #1, the chart speed was too slow; it was increased from 2.0 inches per minute to 20.0 while the drive speed was kept at 0.2 inches per minute. For test #2, the original diameter was not measured accurately and the results are only approximate. Tests #3 and #6 are good and the results are listed below.

Test Number	Outside Diameter (inches)	Yield Stress (psi)	Ultimate Yield Strength (psi)	Elongation from Chart (%)
1	--	--	--	--
2	est. 0.250	44600	46300	12.3
3	0.251	43250	44866	10.68
4	0.255	42980	44742	12.04
5	0.251	43148	44866	12.04
6	0.248	43267	45026	11.36
Average of last four		43200	44900	11.50

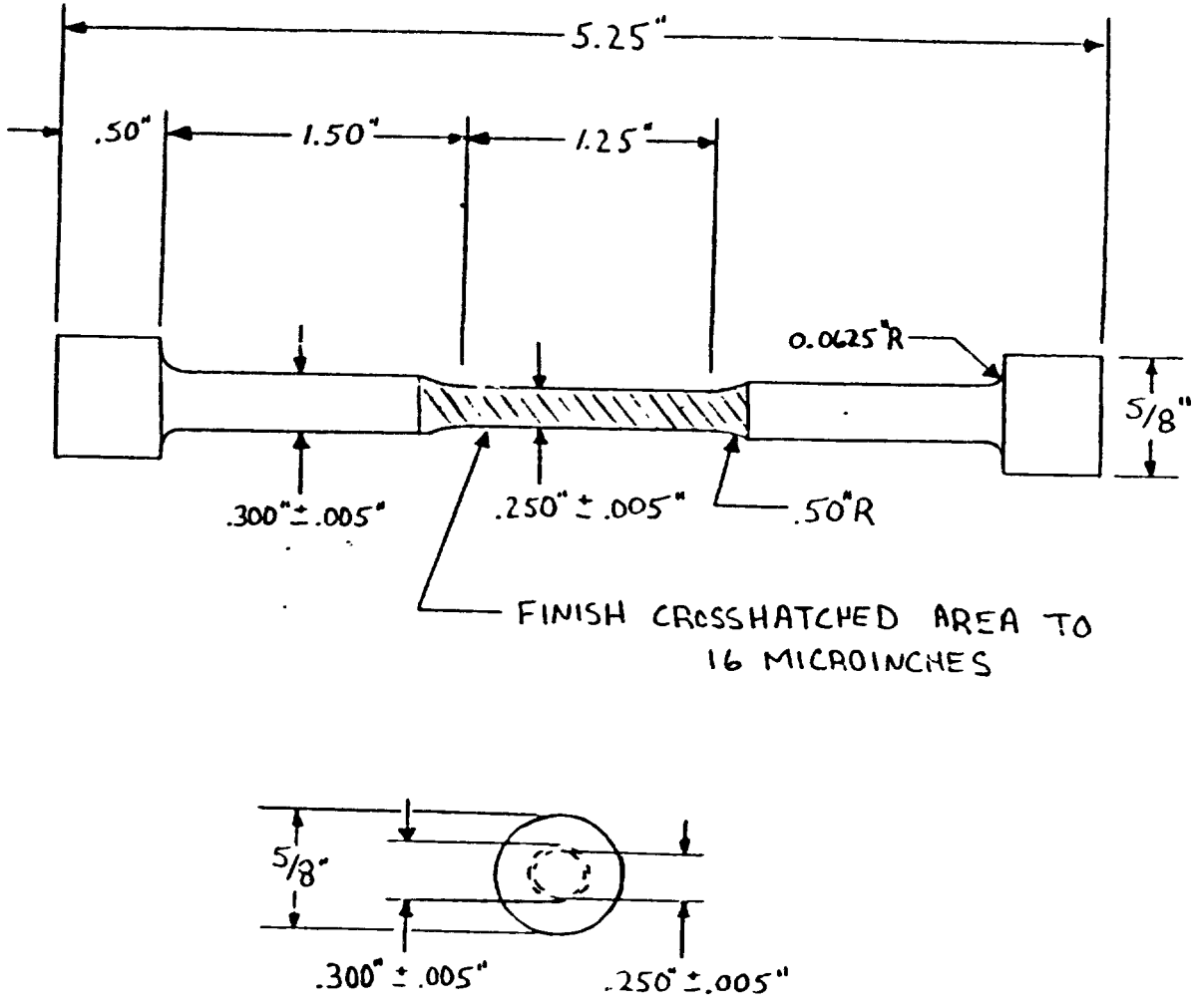

Figure A.1 Tension Test Specimen Dimensions

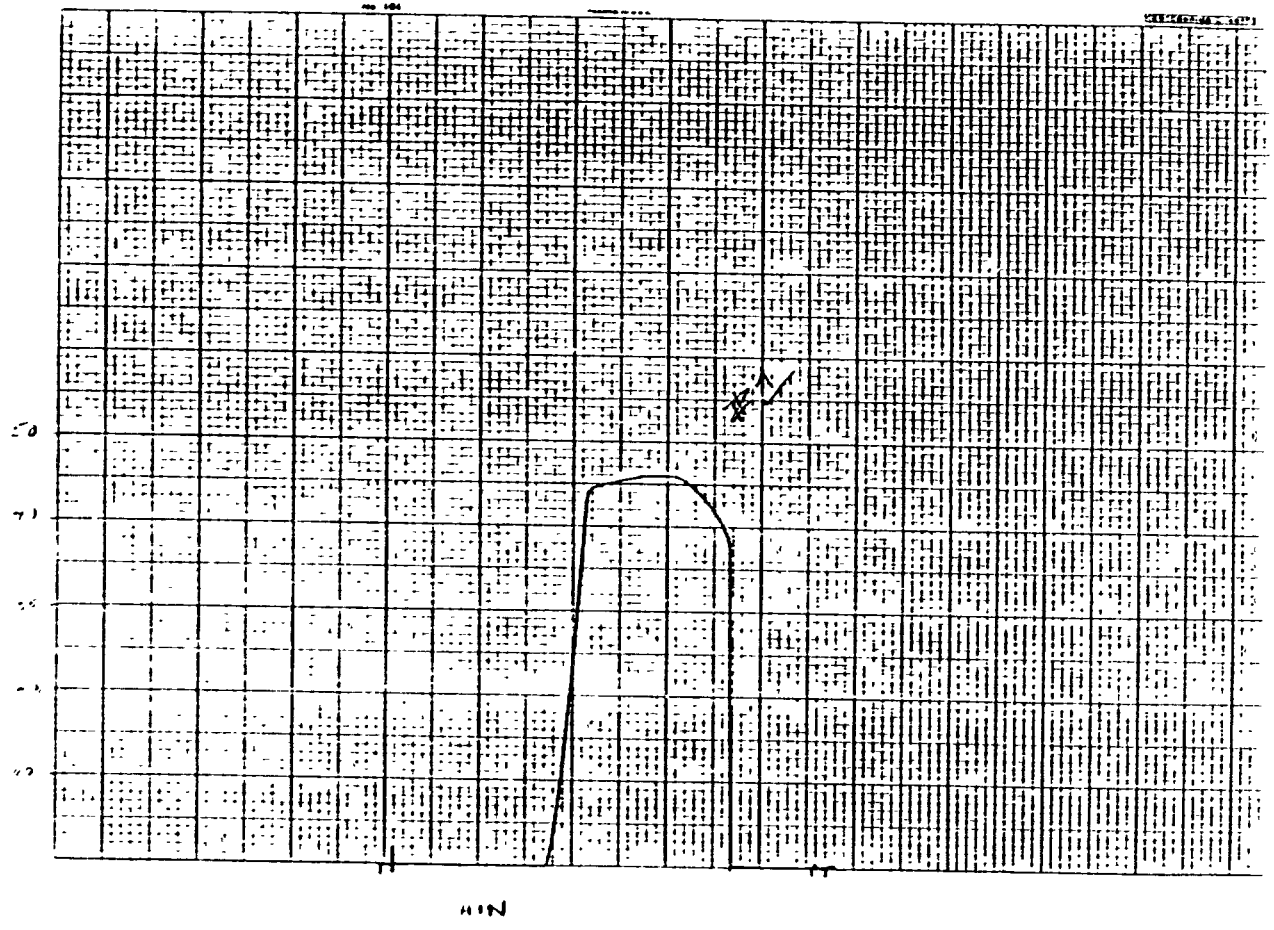

Figure A.2 Recording Chart - Test 1

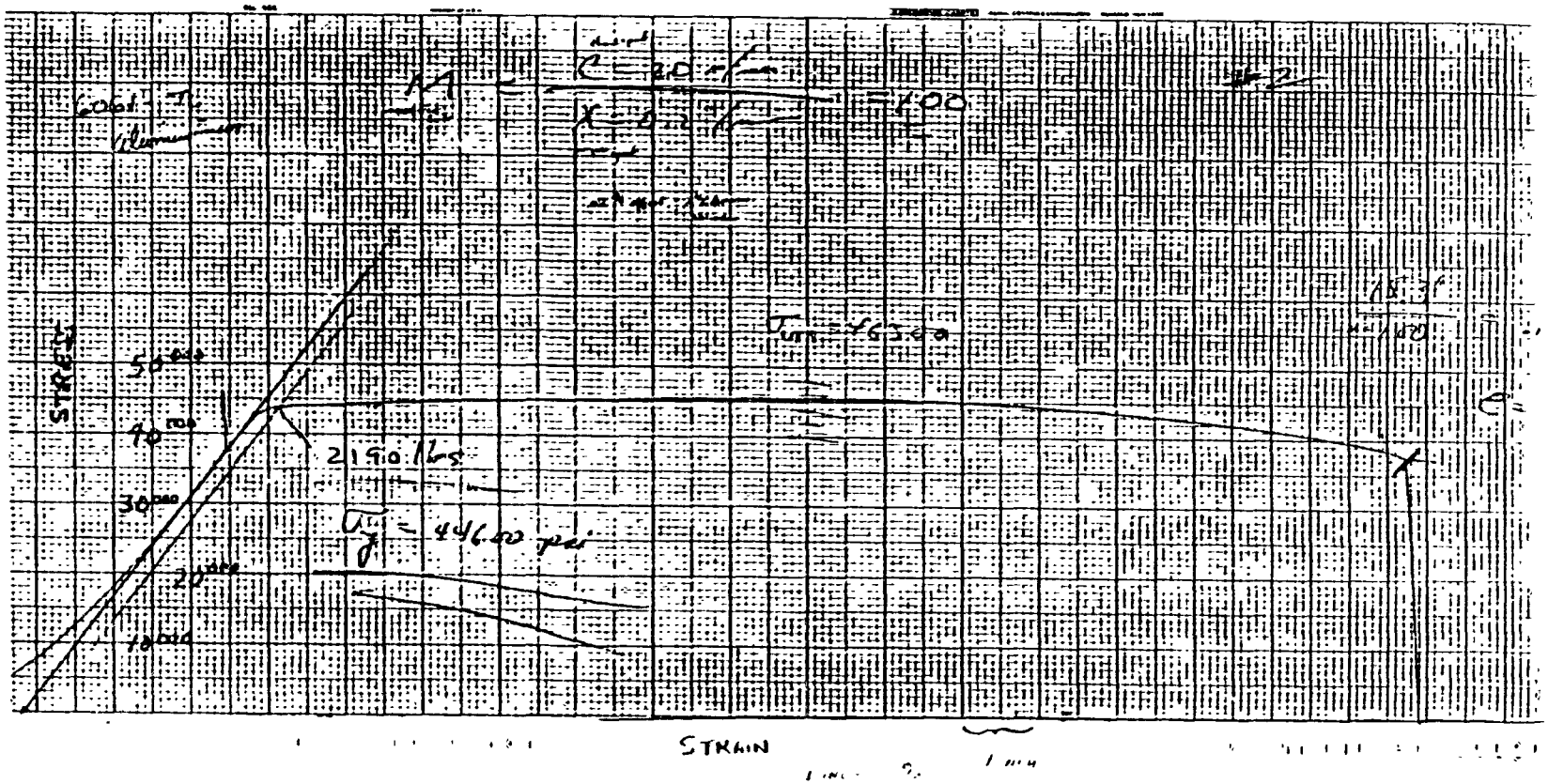

Figure A.3 Recording Chart - Test 2

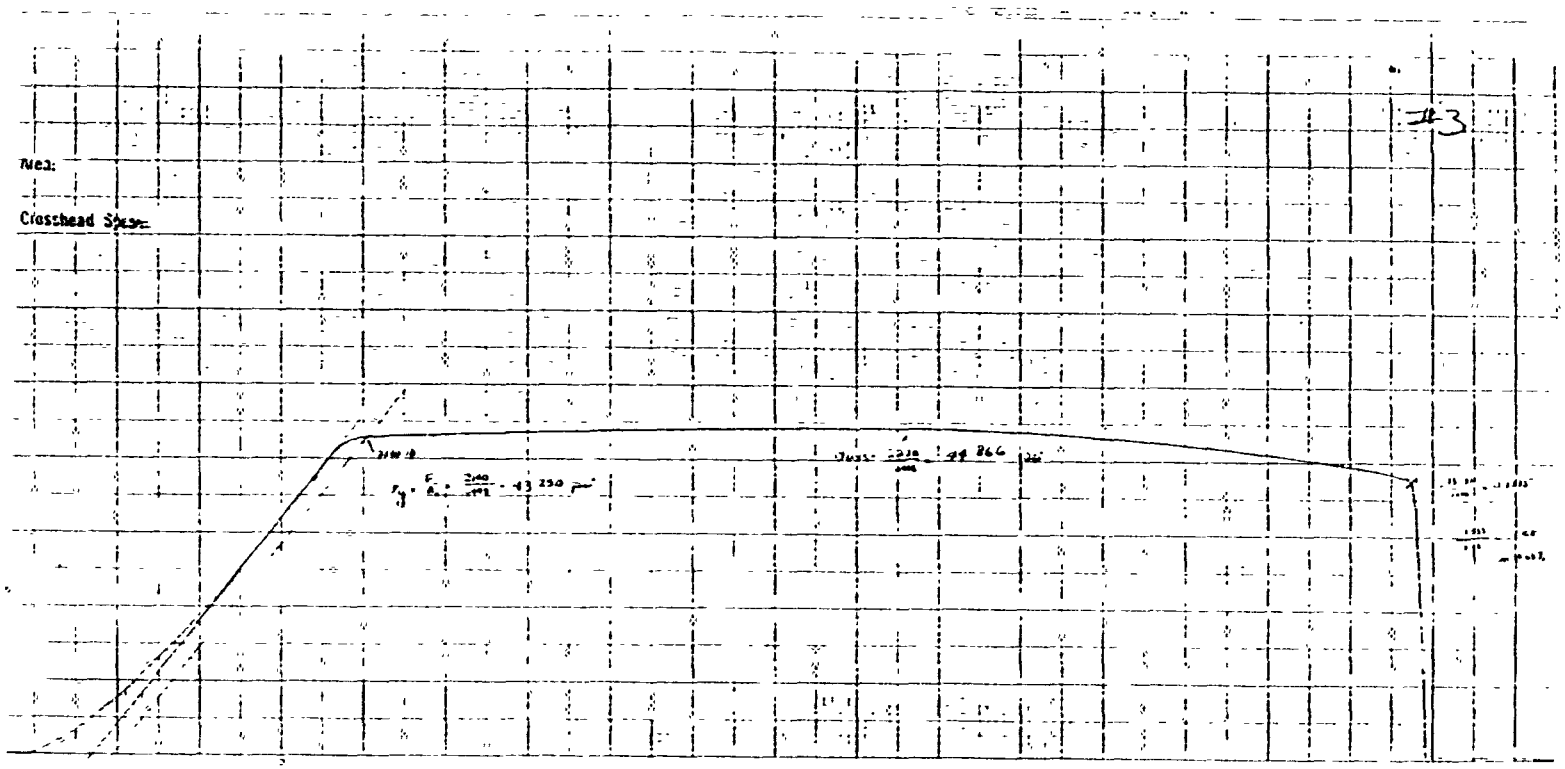

Figure A.4 Recording Chart -- Test 3

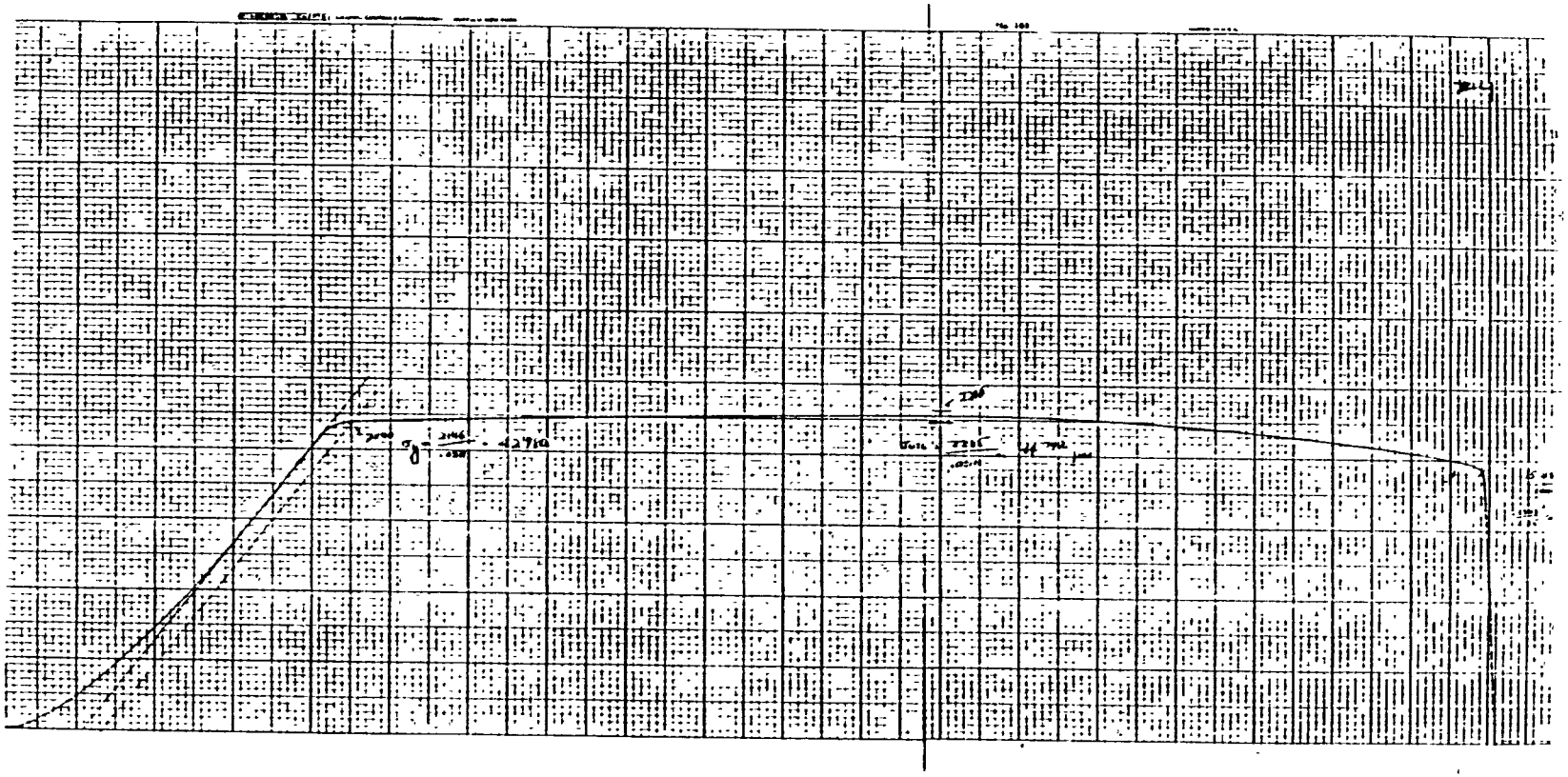

Figure A.5 Recording Chart - Test 4

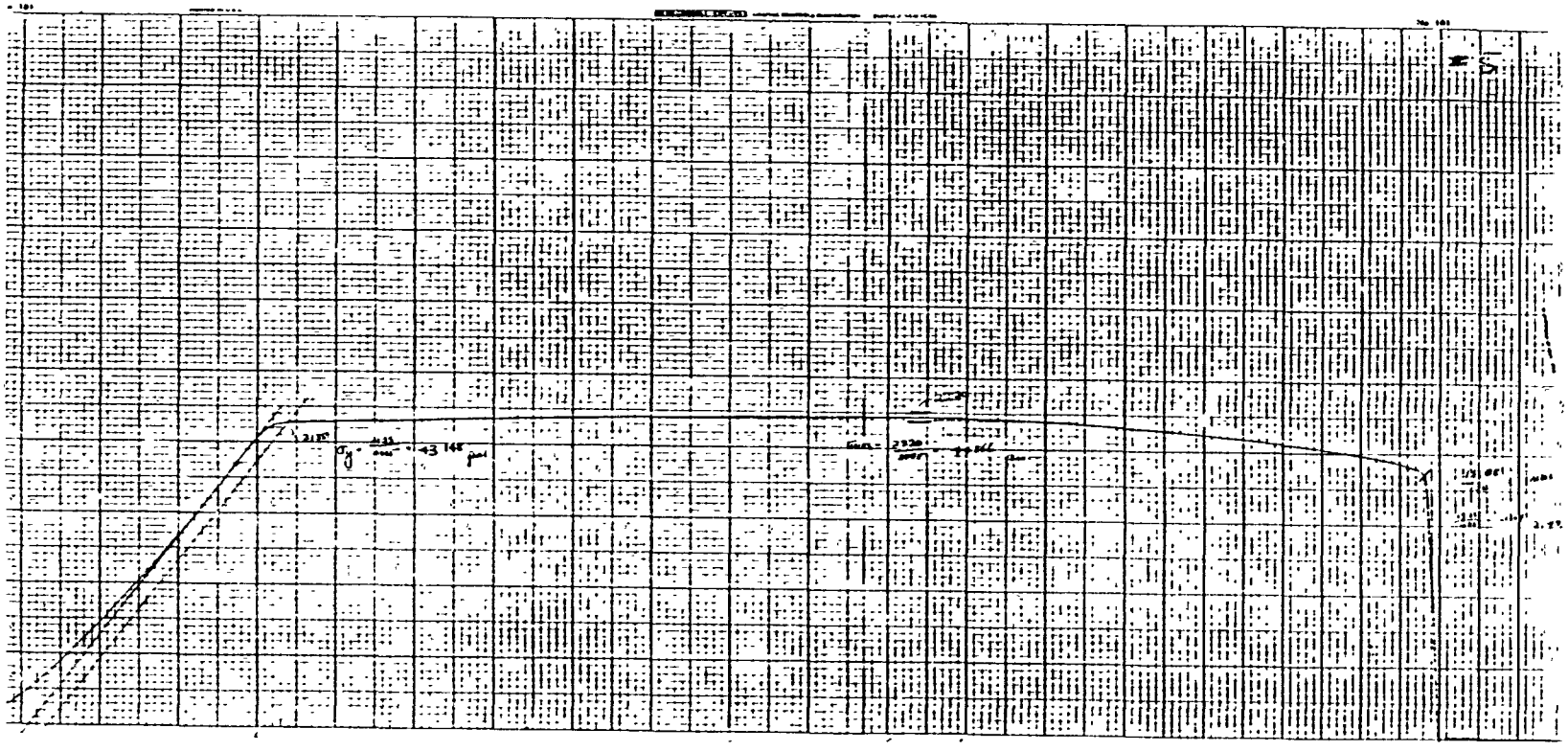

Figure A.6 Recording Chart - Test 5

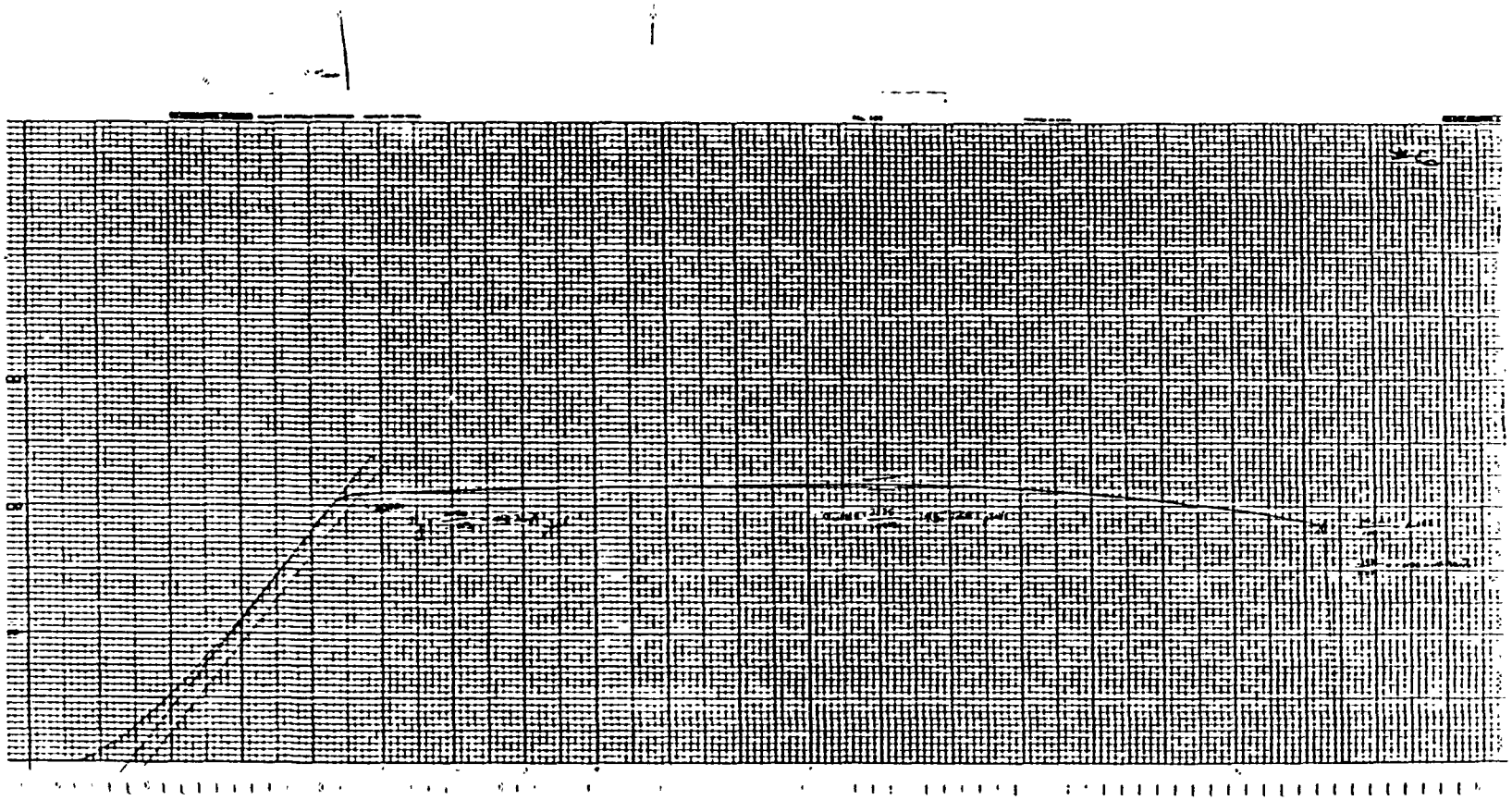

Figure A.7 Recording Chart - Test 6

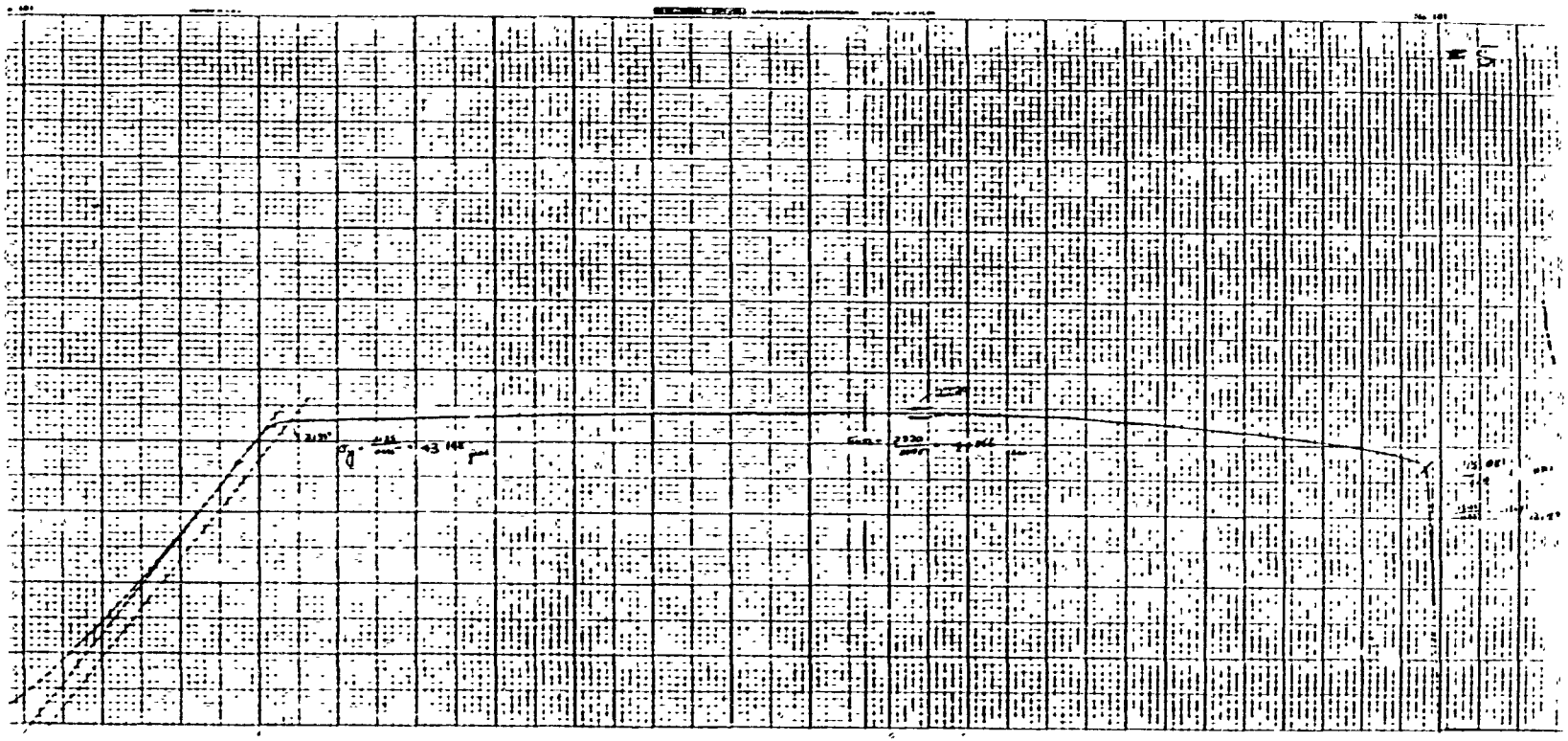

Figure A.6 Recording Chart - Test 5

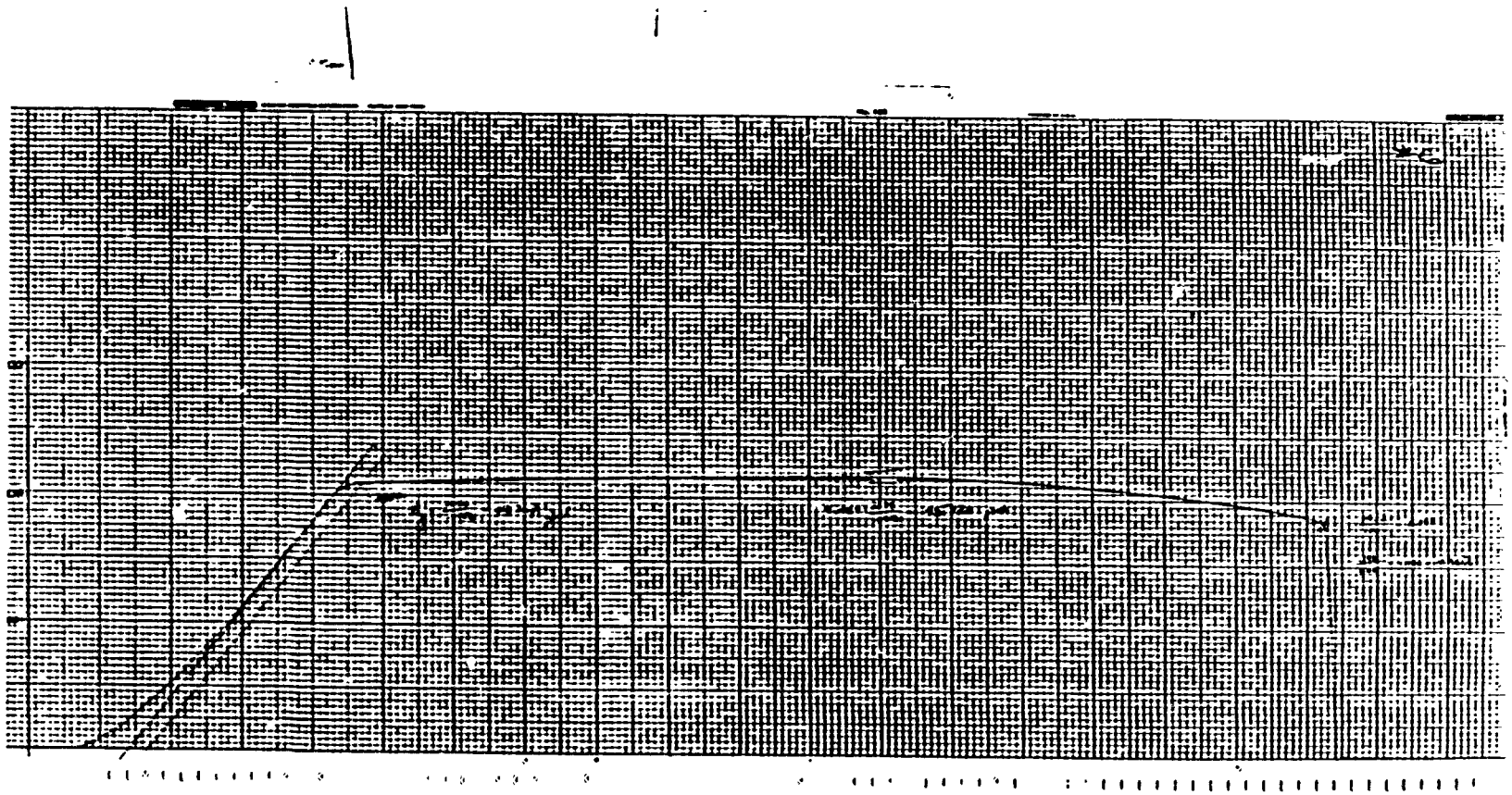

Figure A.7 Recording Chart - Test 6

APPENDIX B

DESIGN DRAWINGS OF THE BACKING STRUCTURE AND TEST PANEL

The drawings used for the manufacture and assembly of the test structure at the Naval Postgraduate School are found on the following pages. Also shown are the sketches used to order the plate cut to size.

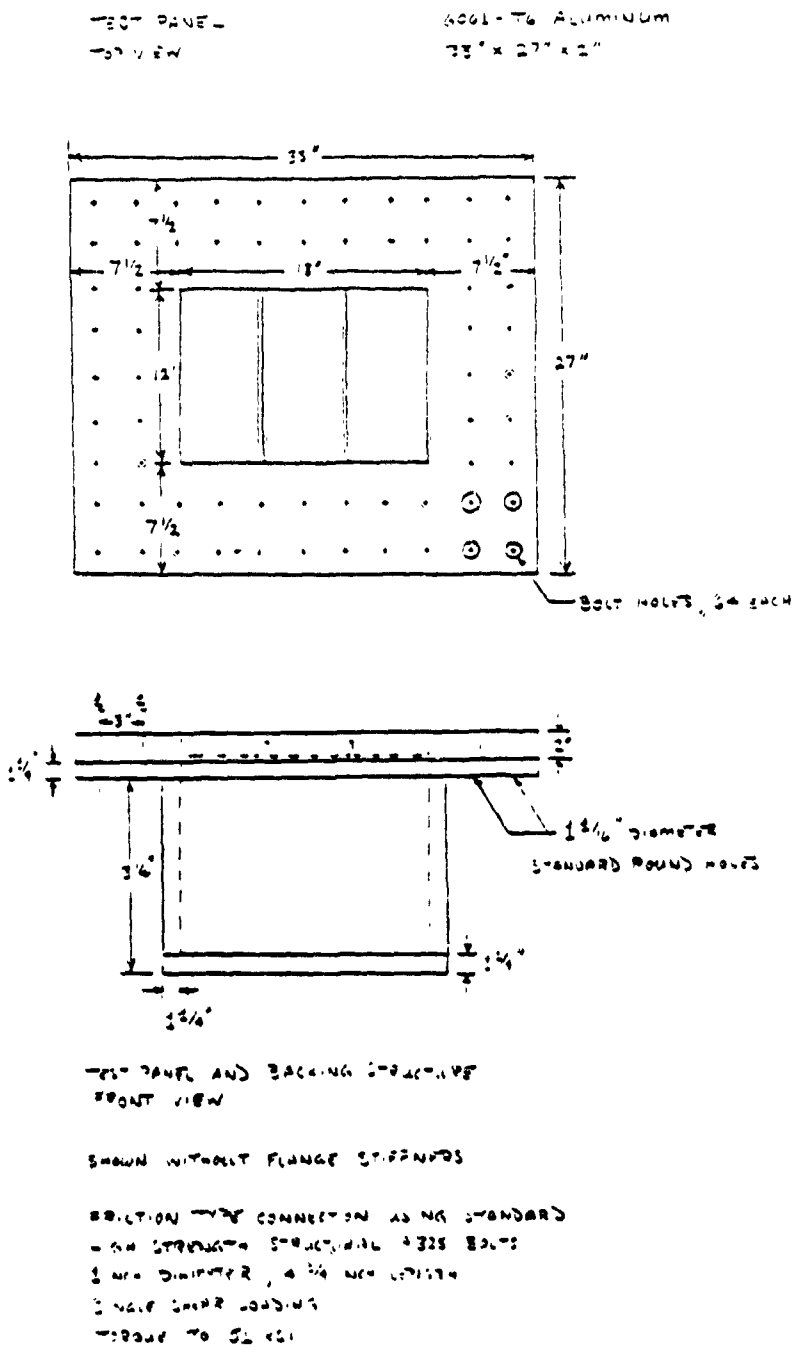

Figure B.1 Test Panel and Backing Structure

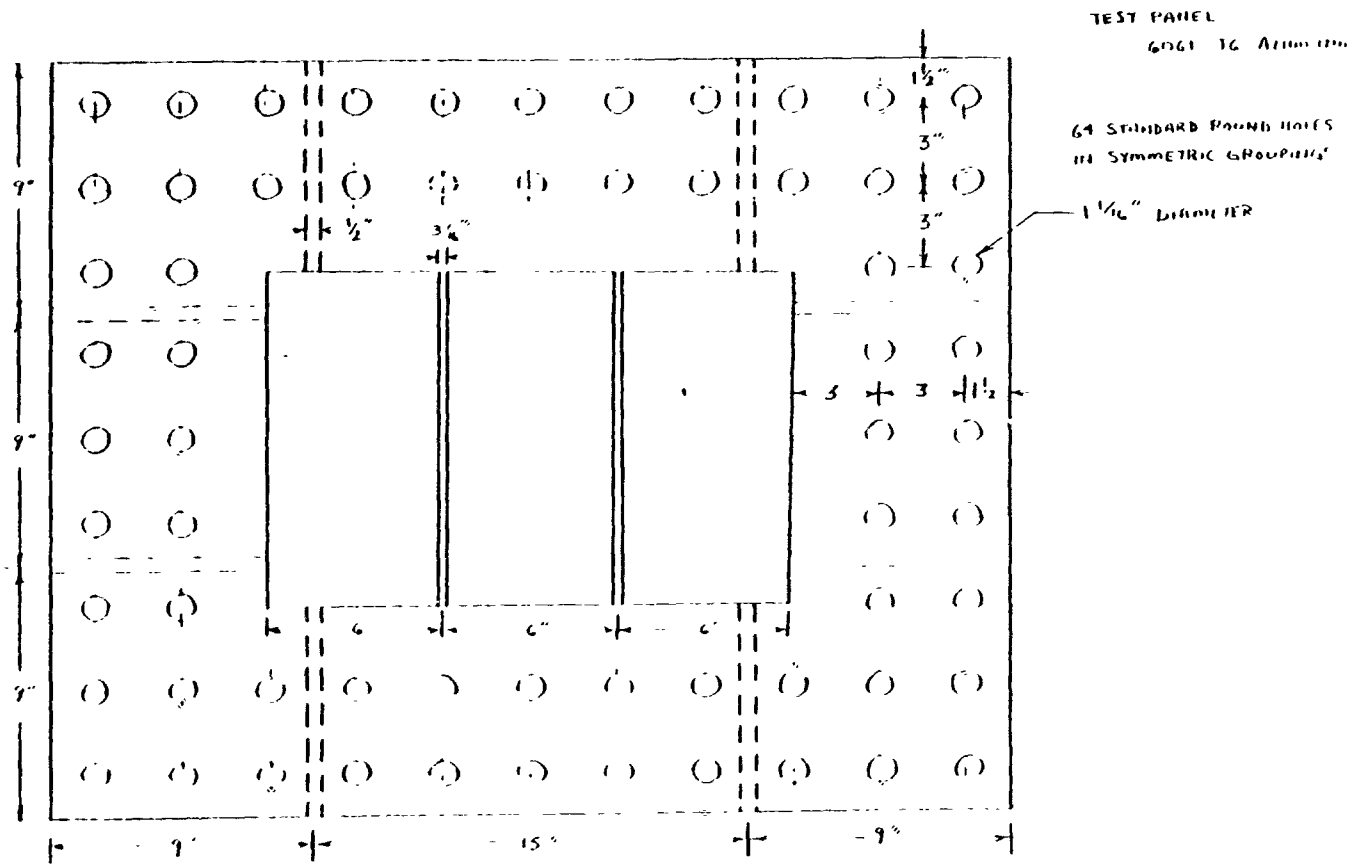

Figure B.2 Test Panel

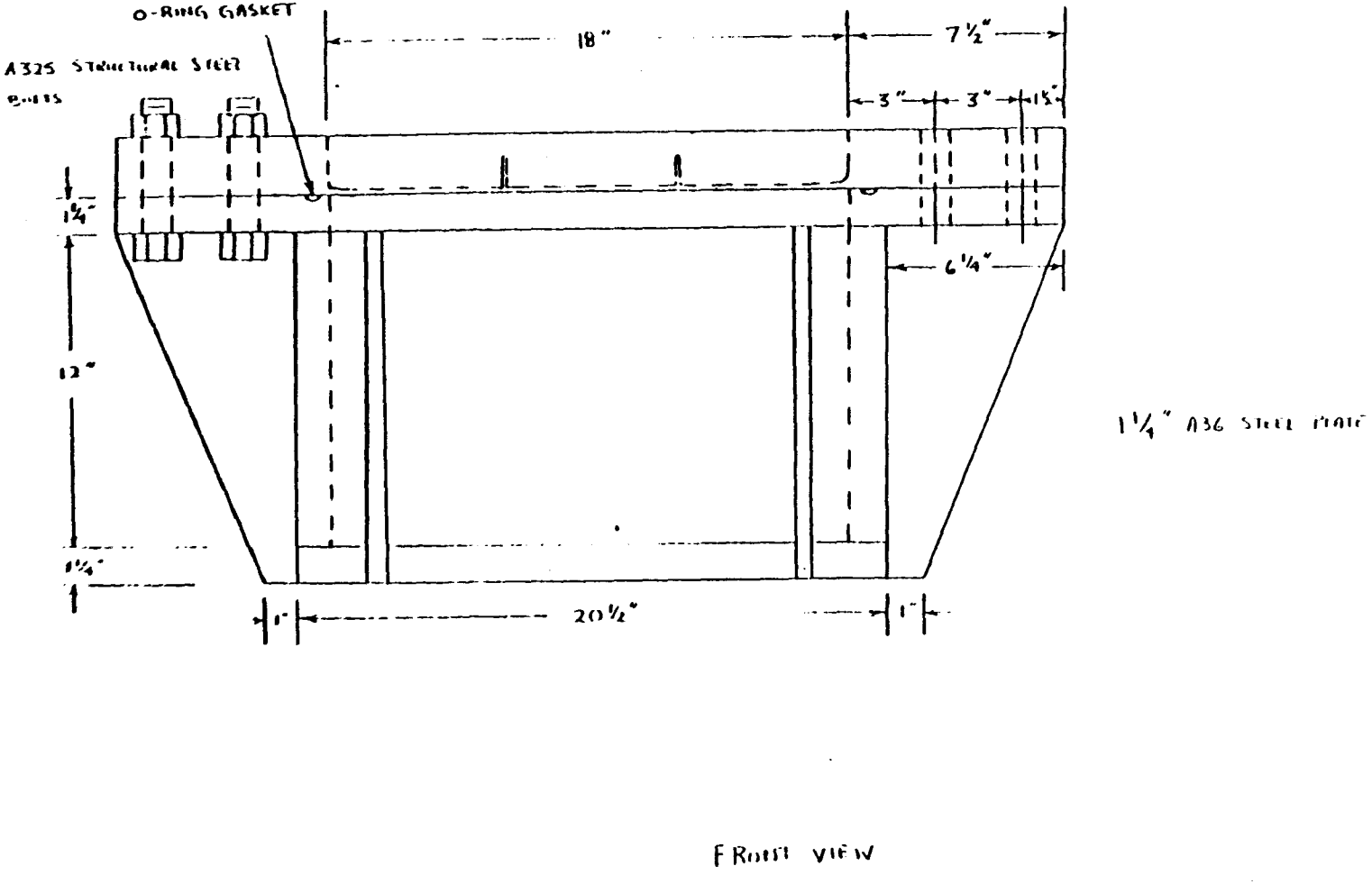

Figure B.3 Front View of the Structure

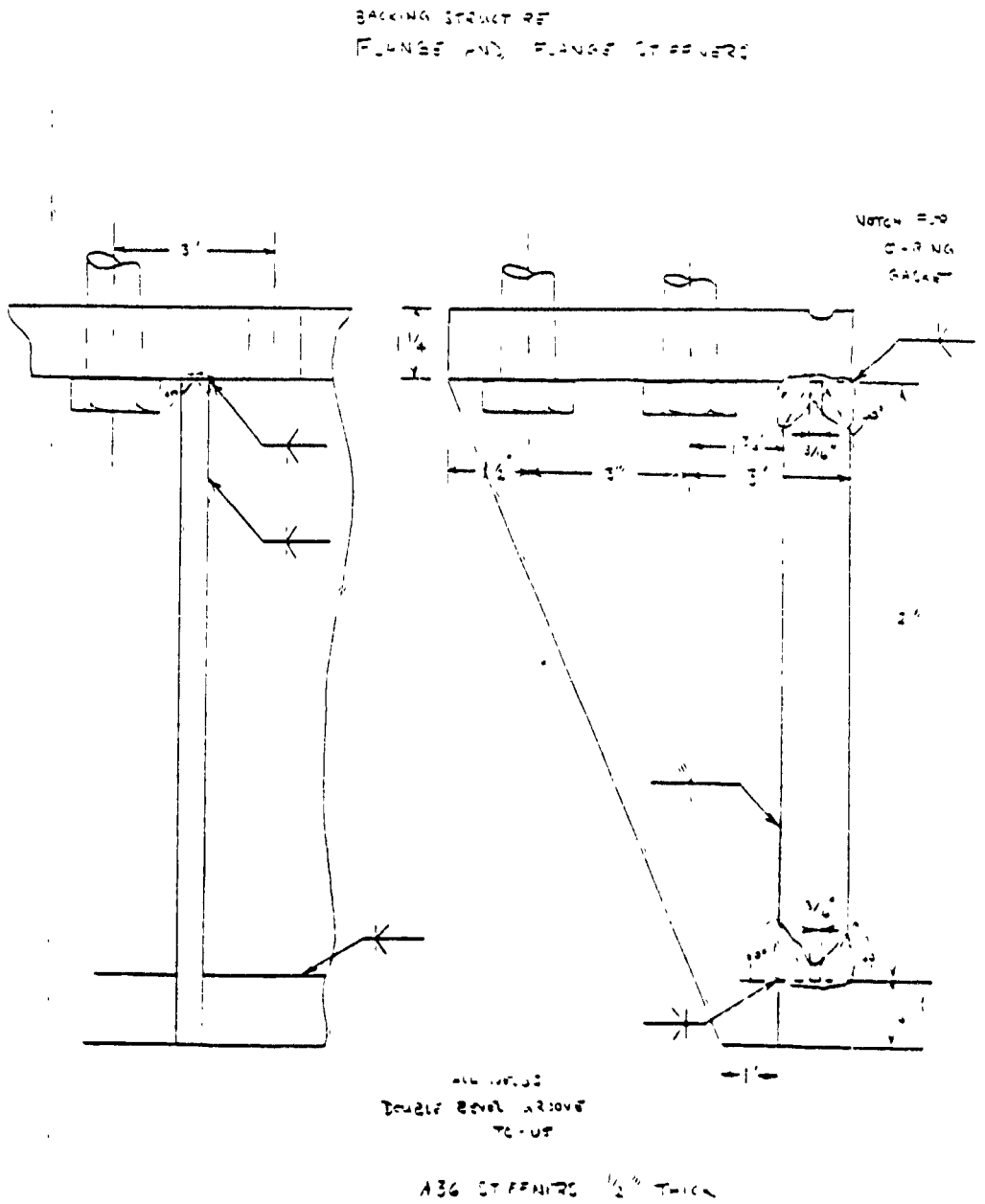

Figure B.4 Flange and Stiffener Details

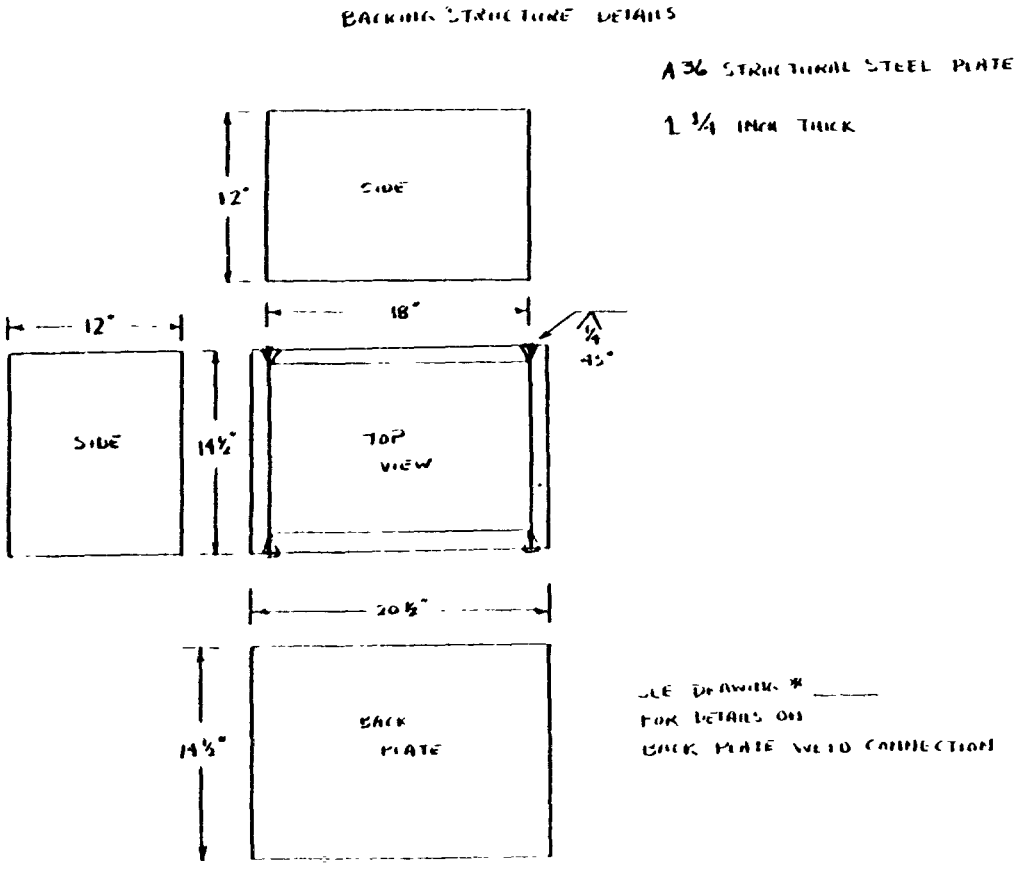

Figure B.5 Backing Structure Details

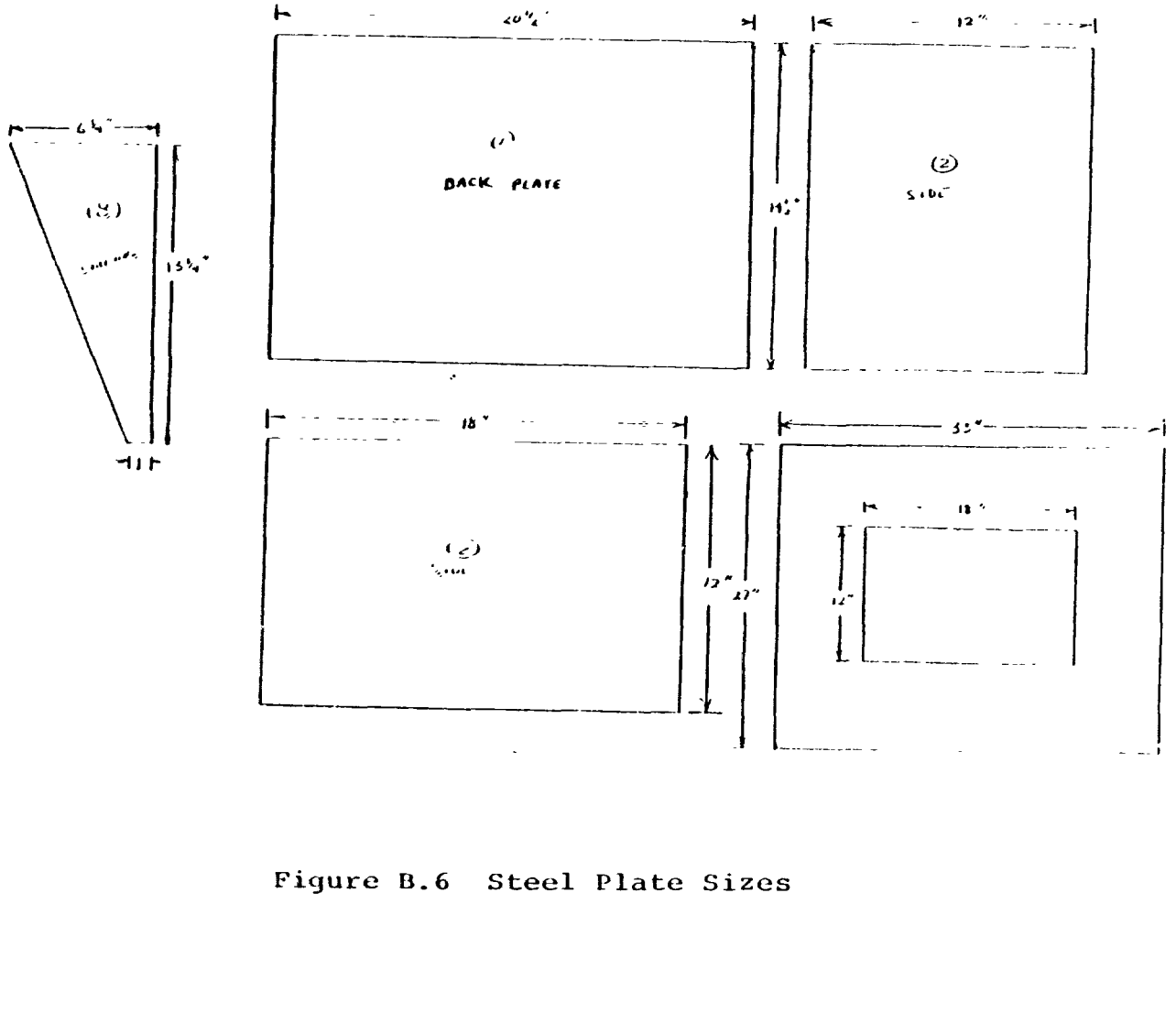

Figure B.6 Steel Plate Sizes

APPENDIX C

EPSA ON THE VAX

The EPSA User's Manual titled "Underwater Shock Response of Submerged Shells" [Ref. 9] presents the commands necessary to execute an EPSA job on a VAX computer. Francois Daube's thesis [Ref. 10] also shows how to run EPSA at NPS and how to generate and view the PATRAN files. The intent of this appendix is to cover some of this material again and, hopefully, bring out some helpful information that was previously omitted.

The input deck used for the pre-shot analysis is shown again on the following page as Figure C.1, the name of this input data file is CPLT.DAT. Most of the input is adequately described in Reference 9 ; those modifications to EPSA which deal will the PATRAN interface are not found in the reference, but are described in Figure C.2.

To access PATRAN, two numbers at the end of line 2 must be added to the input deck. This specifies the number of PATRAN files to be created. The only limitations on the numbers are that they be positive integers and do not exceed the number of time steps requested. However, it is advised to keep them small due to the additional memory allocation these files require.

```
NPS PLATE- 2 REC STIF  STRN TOP
4000  1  0  0  0  100  0  0  4  4
.0000005     1  4000  100
1  1  17  1  16
16  10  4  1  1  0  27  20  26  14  1  1  0
0  0
10000000.  .3  .000255  40000.  .18750  0.0  0.00001
'stif' 1  0  1
-1   1   1
187  0
1  0  0  0.0  0.0
17  1  0  9.0  0.0
-17 17  10  0.0  0.6
0/
160  1  1  16  10
1   1  17  0  1  0  1  0
2   1  11  1  0  0  1  0
3   1  17  1  1  1  1  0
4   1  11  1  1  1  1  0
1   1  1  1  0.0  0.0  0.0
0.0  0.0  0.0  0.0  0.0  0.0  0.0  0.0/
1  1  1  1  1  2  1  1  3  17 1  1  17 1  2
17 1  3  6  7  1  6  7  2  6  7  3  17 11 1
17 11 2  17 11 3  12 7  1  12 7  2  12 7  3
1  11 1  1  11 2  1  11 3  6  1  1  6  1  2
6  1  3  12 1  1  12 1  2  12 1  3  17 5  1
17 5  2  17 5  3/
1  1  1  1  1  2  1  1  4  1  1  5  16 1  1
16 1  2  16 1  4  16 1  5  6  7  1  6  7  2
6  7  4  6  7  5  16 10 1  16 10 2  16 10 4
16 10 5  11 10 1  11 10 2  11 10 4  11 10 5/
11 5  10 10 1  9  11 1  10 12 1  9  12 10 10
16 5  9  16 5  10 16 1  9  16 1  10 11 1  10
10 1  10 12 8  9  11 8  10 10 8  9  16 1  7
16 1  8  11 1  11 11 2  11 11 3  11 11 4  11
11 5  11 11 6  11 11 7  11 11 8  11 11 9  11
11 10 11/
1  1  3  17 1  3  17 11 3  1  11 3  5  7  3
5  11 3  12 2  3  12 7  3  12 11 3  17 7  3
11 1  3  11 3  3  11 5  3  11 7  3/
0.5625   0.1875  1.000
11       1/
0/
9.0   0.0000945   60000.0
1   108.0   0.0    9.0
8.0   22505.0    1.18   0.058   -0.185  0.0008/
0   0   0   0   0
```

Figure C.1 EPSA Input Deck for Pre-Shot Analysis

End of line 2:

4	4
number of Patran displacement plots	number of Patran stress/strain plots

End of line 3:

1	4000	100
timestep number to start time history plot	time step number to stop plotting	number of increments

Entire line 4:

1	1	17	1	16
number of nodes to be plotted	number of elements	node identifer first row, number 17		element number

Figure C.2 Modifications to the Input Deck

The numbers added to the end of line three will cause EPSA to create a file of data points during a run. The subroutines PLOTEN and BIGPLOT were added to EPSA to do this. These data points may be plotted on the Tektronics 4013 terminal by using a separate Fortran program to produce either a displacement or strain history. If this is requested by adding the numbers to line three, then an entire line four must also be input. The data files created are: FOR022.DAT for displacements, FOR021.DAT for Y

strains, FOR024.DAT for X strains, and FOR023.DAT for velocities. Although four files are created, a program to access the velocity history at a node (the FOR023.DAT file) has not been written. To access the displacement and strain history files, the following Fortran programs were written: PLOTD2, PLOTSX, and PLOTSY. Listings of these files are at the end of this appendix. To plot one of these histories from a Tektronics terminal, simply type the command, "RUN PLOTD2" (or PLOTSX or PLOTSY).... and return.

An example of a strain history is presented in Figure C.3, and the data file which created it is found in Figure C.4. However, it is the executable version of these files which is run. These are created by compiling the Fortran file, then linking to PLOT 10 by the following commands:

```
$ FOR PLOTD2.FOR
$ LINK PLOTD2.OBJ 'PLOT10'
```

Any changes made to these routines must be supported by the PLOT10 software package--see a PLOT10 User's Manual for details.

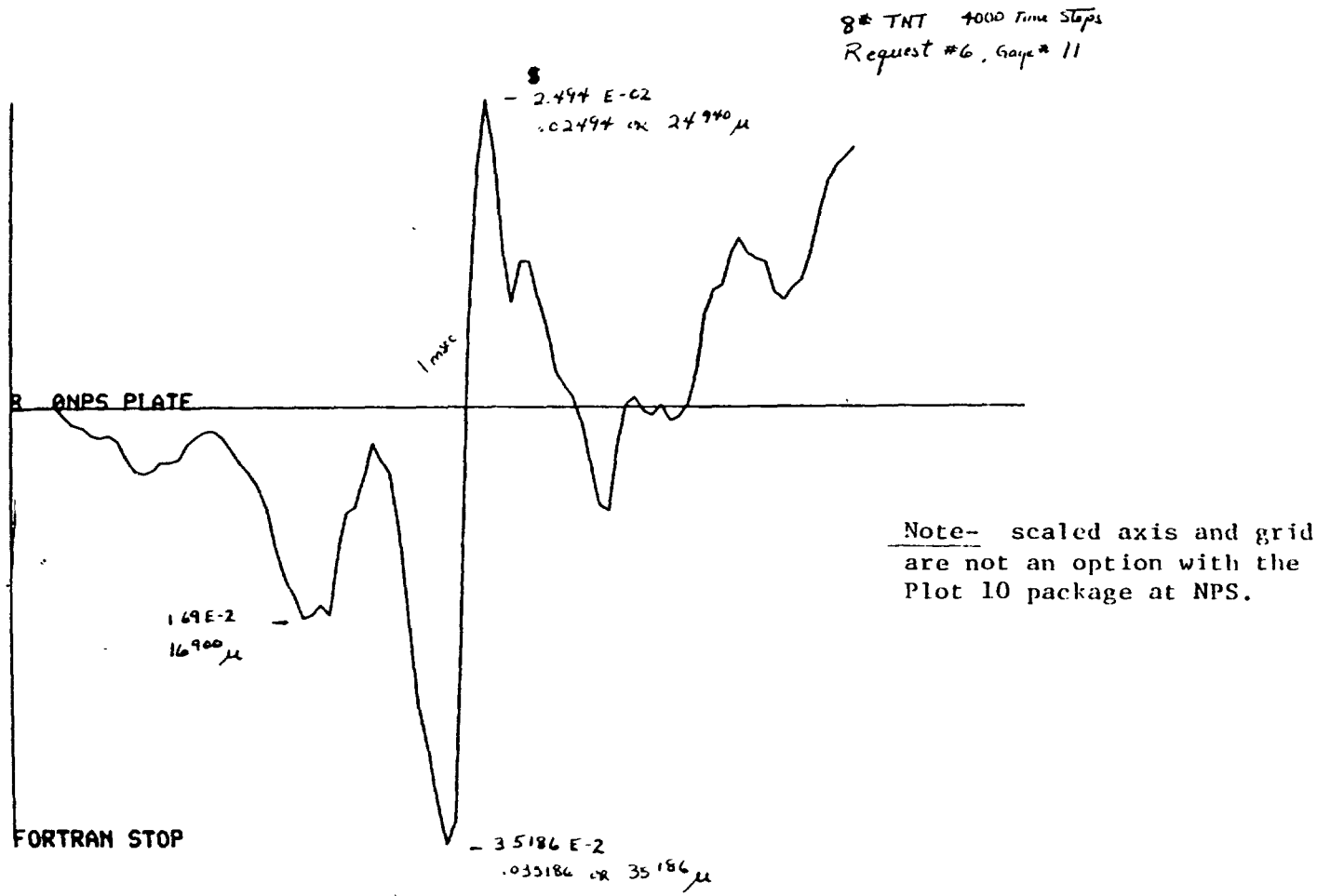

Note- scaled axis and grid are not an option with the Plot 10 package at NPS.

Figure C.3 Strain History Plotted on Tektronics 4013

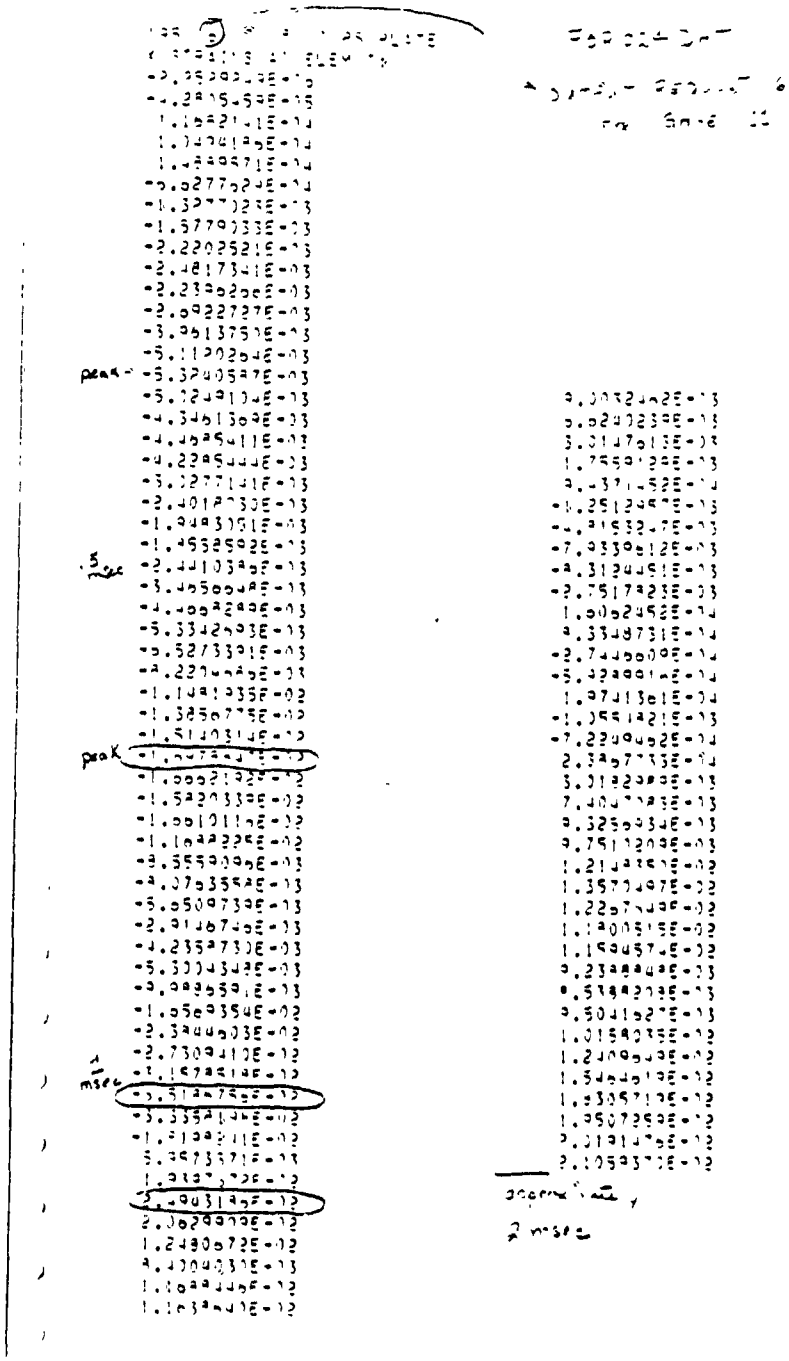

Figure C.4 Strain History Data File, FOR024.DAT

After the creation of the input deck, the commands required to execute the EPSA job are shown in the figures below. Figure C.5 shows the queries and responses necessary for an interactive EPSA run. Note that the request for a Virtual Mass Array filename is returned empty. This is done only for the case of a flat plate model where only the Plane Wave Approximation is used. If a cylinder were being modeled, the proper response would have been EPM.VMA.

```
$ @epsa1
     VAX/VMS COMMAND PROCEDURE FOR AN
     INTERACTIVE EPSA INITIAL RUN

EXECUTABLE FILE NAME: epsa5804i.exe
INPUT FILE NAME: cplt.dat
OUTPUT FILE NAME: cplt.out
VIRTUAL MASS ARRAY FILE NAME:
```


Figure C.5 Commands for an Interactive EPSA Run

Another comment about the interactive runs is to be aware that interactive runs should be made only if the user intends on executing only a small number of time steps and wants to remain at the terminal during the run. Otherwise, a batch job is more appropriate. This also has the advantage of allowing the user to access and work with his other files during the run; the terminal screen is not busy wiwth the EPSA run. The commands for the batch execution are shown in Figure C.6.

```
$ @bepsai
        VAX/VMS COMMAND PROCEDURE TO SUBMIT
        AN INITIAL EPSA RUN TO THE BATCH QUEUE.

EXECUTABLE FILE NAME: epsa5804i.exe
INPUT FILE NAME: cplt.dat
OUTPUT FILE NAME: cplt.out
TIME HISTORY FILE NAME: for010.th1
CORE TAPE FILE NAME: for011.cr1
VIRTUAL MASS FILE NAME:
```


Figure C.6 Commands for an EPSA Batch Run

In Figure C.7, note that the time history and the core tape file names are requested. The file names input are consistent with those names used by the authors of EPSA. The time history file would be used for the plotting of output data. The specific plotting routine to do this is not available at NPS. An example of its use may be found in Reference 11. The core tape file is used for a restart of EPSA--if it was desired to start the computation process at the same timestep which a job terminated. An example of this procedure is found in the User's Manual. Another feature of the batch process is illustrated in Figure C.7. A file name BEPSAI.LOG is generated during execution, but it cannot be accessed until the job is terminated. Should a request to view (type) this file be made before job termination, the DCL symbol $ is returned, meaning "not ready yet". This is a positive signal that the job submission has gone through and computation is in progress. The BEPSAI.LOG file contains only system control messages from the VMS level, such as the date and time completed and CPU time required for execution.

An example of other DCL commands not covered adequately in the VAX/VMS literature is shown in Figure C.8 on the following page. A request is made to display all the files in the user's directory of name FOR018.DAT with the version unspecified (;*). A second example follows the first. Note

that the EPSA run had created the previously unmentioned files FOR015.DAT and FOR017.DAT. These two data files are not used, they are in machine language, and their creation was meant to be eliminated by Francois Daube.

```
$ @bepsa1
        VAX/VMS COMMAND PROCEDURE TO SUBMIT
        AN INITIAL EPSA RUN TO THE BATCH QUEUE.

EXECUTABLE FILE NAME: epsa5804i.exe
INPUT FILE NAME: cplt.dat
OUTPUT FILE NAME: cplt.out
TIME HISTORY FILE NAME: for010.th1
CORE TAPE FILE NAME: for011.th1
VIRTUAL MASS FILE NAME:
  Job 1718 entered on queue SYS$BATCH
$ ty bepsa1.log
$
```


Figure C.7 Request to View Status of Batch Job

```
$
$ dir for018.dat;*

Directory _DUA0:[RENTZ]

FOR018.DAT;13       FOR018.DAT;12       FOR018.DAT;11       FOR018.DAT;10
FOR018.DAT;9        FOR018.DAT;8        FOR018.DAT;7        FOR018.DAT;6
FOR018.DAT;5        FOR018.DAT;4        FOR018.DAT;3        FOR018.DAT;2
FOR018.DAT;1

Total of 13 files.
$ dir for*.dat;*

Directory _DUA0:[RENTZ]

FOR015.DAT;13       FOR015.DAT;12       FOR015.DAT;11       FOR015.DAT;10
FOR015.DAT;9        FOR015.DAT;8        FOR015.DAT;7        FOR015.DAT;6
FOR015.DAT;5        FOR015.DAT;4        FOR015.DAT;3        FOR015.DAT;2
FOR015.DAT;1        FOR016.DAT;13       FOR016.DAT;12       FOR016.DAT;11
FOR016.DAT;10       FOR016.DAT;9        FOR016.DAT;8        FOR016.DAT;7
FOR016.DAT;6        FOR016.DAT;5        FOR016.DAT;4        FOR016.DAT;3
FOR016.DAT;2        FOR016.DAT;1        FOR017.DAT;13       FOR017.DAT;12
FOR017.DAT;11       FOR017.DAT;10       FOR017.DAT;9        FOR017.DAT;8
FOR017.DAT;7        FOR017.DAT;6        FOR017.DAT;5        FOR017.DAT;4
FOR017.DAT;3        FOR017.DAT;2        FOR017.DAT;1        FOR018.DAT;13
FOR018.DAT;12       FOR018.DAT;11       FOR018.DAT;10       FOR018.DAT;9
FOR018.DAT;8        FOR018.DAT;7        FOR018.DAT;6        FOR018.DAT;5
FOR018.DAT;4        FOR018.DAT;3        FOR018.DAT;2        FOR018.DAT;1
FOR019.DAT;117      FOR019.DAT;116      FOR021.DAT;196      FOR021.DAT;195

FOR021.DAT;194      FOR022.DAT;55       FOR022.DAT;54       FOR022.DAT;53
FOR023.DAT;45       FOR023.DAT;44       FOR023.DAT;43       FOR024.DAT;21
FOR024.DAT;20       FOR024.DAT;19       FOR099.DAT;1

Total of 67 files.
```

Figure C.8 Specific Fortran Files within a Directory

```
$ patran
.....................................................................

P D A / P A T R A N - G          RELEASE 1.5

CUSTOMER - NAVAL POSTGRADUATE SCHOOL   -   MONTEREY, CALIFORNIA

For information on new features in release 1.5
obtain a printout of file PATRAN$DIR:RELEASE1.5

PLEASE INPUT THE DEVICE NAME (OR 'REPORT'): TEK
```


Figure C.9 Commands to Access PATRAN

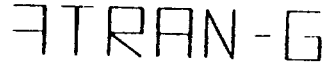


```
NAVAL POSTGRADUATE SCHOOL   -   MONTEREY, CALIFORNIA
INPUT GO, SES, HELP, OR PDA/PATRAN-G EXECUTIVE DIRECTIVE
>GO
```

Figure C.10 PATRAN Accessed

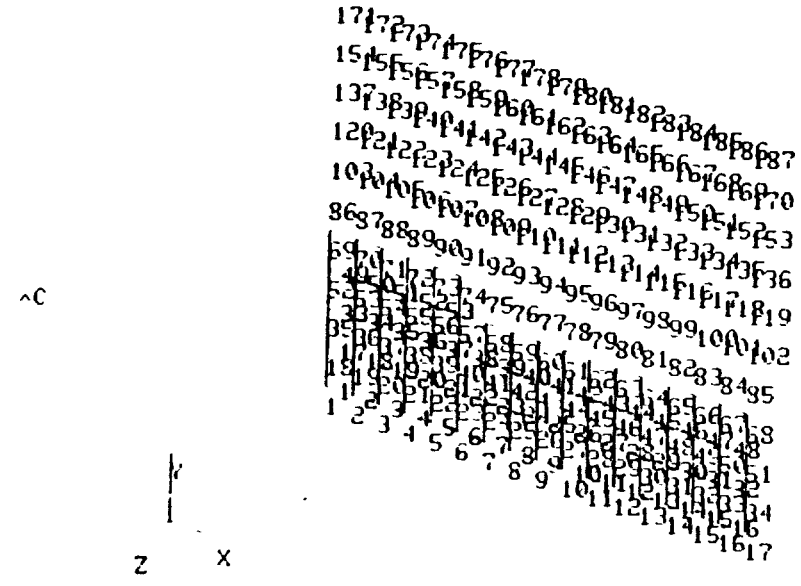

^CONTROL/C ABORT OF FUNCTION
MODE? 1.GEOMETRY MODEL 2.ANALYSIS MODEL 3.DISPLAY 4.NEUTRAL SYS. 5.END
>

Figure C.11 Control C Command

To access PATRAN, follow the procedure in Figure C.9. The work TEK is input when using a Tektronics graphics terminal and it must be in upper case letters. The screen will clear and follow with what is shown in Figure C.10. Answer with GO. The other commands and options necessary to utilize the PATRAN graphics are adequately covered in Francois Daube's thesis. Refer to reference 15. However, one feature of the PATRAN package not discussed is illustrated in Figure C.11. To stop the plotting of a view which is not desired or incorrect, simply hit the Control and C keys simultaneously. This will abort the function without losing the PATRAN session files. A control Y will cause an exit from PATRAN altogether and a loss of all session files.

Should it be necessary to make changes in EPSA, or any other executable file on the VAX, the procedure is shown on page 29 of the User's Guide [Ref. 16]. An example is now given. The required changes would be made in the edit mode to the Fortran version of the file or subroutine. An example would be to change the line CX = -CX to read CX = CX in the subroutine CPTSTRN. Now the corrected version of EPSA5804.FOR must be compiled. To do this without a request for debugging type

```
$FORTRAN EPSA5804.FOR
```

An object file is created named EPSA5804.OBJ. For ease in making future changes to EPSA, a library file named EPSA5804.OLB should be created. This is done by the command

```
$LIBRARY/CREATE EPSA5804.OLB EPSA5804.OBJ
```

Next the library file, or the object file if none was created, must be linked to the main program to produce an executable file. Type in

```
$LINK EXE=EPSA5804I.EXE EPSAI,EPSA5804/LIBR
```

if linking to the library, or

```
$LINK EXE=EPSA5804I.EXE EPSAI,EPSA5804.OBJ
```

if none was created. The purpose and value of a library file is that if one were created and another change be necessary to subroutine CPTSTRN, the entire EPSA code would not have to be recompiled and linked. Simply "cut and paste" the subroutine from EPSA5804.FOR so that it is a separate Fortran file, CPTSTRN.FOR. Make the necessary corrections, then compile this smaller file to produce CPTSTRN.OBJ. Now link this object file to the EPSA library and it will replace the older version of the routine. A form of the command which achieves this is

```
$LINK EXE=EPSA5804I.EXE EPSAI,CPTSTRN,EPSA5804/LIBR
```

Of course there will not be a correct Fortran file of the current executable version (EPSA580_I.FOR) within the directory. Either a printout must be kept updated through manual changes, or the Fortran file on the computer should be changed but not compiled.

If a change were made to one of the Fortran files which plot the output histories on the Tektronics terminals, the compiling and linking is achieved by typing

```
$FOR PLOTD2
$LINK PLOTD2,'PLOT10'
```

Plot10 is the plotting package that contains commands used by these routines. As mentioned earlier in this chapter, to plot one of these histories on the Tektronics, type in RUN PLOTD2.

APPENDIX D

STRAIN GAGE INSTALLATION TECHNIQUE

The procedure used for this test is presented here as a reference for future work and possible improvement. The procedure proved successful as all gages indicated some strain. It is based upon the BLH-SR-4 application kit (part 103158) manufactured by BLH Electronics, 42 Fourth Avenue, Waltham, MA 02254. The figures used are from the BLH instruction sheet. The materials required are

- -Permabond 910 catalyst P/N 215203 in jar with brush applicator (red)
- -Permabond 910 P/N 223012 in squeeze bottle (clear)
- -Sheet of teflon film
- -Tweezers, razor blades, silicon carbide 400 grit sandpaper
- -Scotch Magic Brand transparent tape
- -Tissues or Kimwipes
- -Rubbing alcohol and acetone in plastic squirt bottles

A. SURFACE PREPARATION

1) Clean general gage area to be bonded so it's free of dirt and grease.

2) Scribe lightly crosshairs over the center position, using care not to score severely or it will create a stress concentrator. Use a lead pencil if you don't want to use a

metal scribe, but remember that it will be erased during the cleaning process and must be redone before the laying of the gages.

3) Use silicon carbide paper to smooth out the surface. Wipe clean with Kimwipes.

4) Saturate a tissue with acetone and rub well. Now, use alcohol to remove the acetone.

5) Repeat the above steps until you are certain that the surface is absolutely clean and free of dust and oxidation. The wiping tissue should not be discolored.

B. BONDING INSTRUCTIONS

1) Using clean tweezers, remove a strain gage from its package and lay it down in the exact position where it is to be bonded. Do not touch the back of the gage with your fingers or allow it to be contaminated in any way. Most strain gages have crosshairs embedded in the backing material which are specifically made for this alignment process. For future use, cut a section of teflon film about 2 inches by 3 inches and have it available.

2) Remove a length of scotch tape about 3 inches and carefully fix one end of it down on the surface and straighten it out so that the tape will extend beyond the gage about one inch. Now lay the tape down evenly proceeding from the fixed end until the gage is now picked up by and securely stuck to the tape. Double the tape back

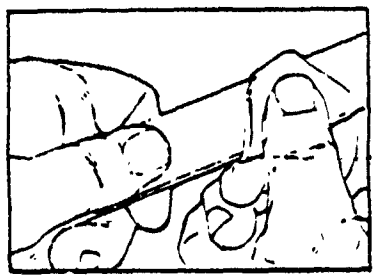

Figure 1

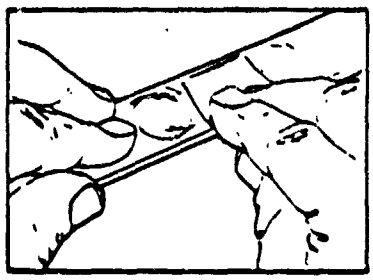

Figure 2

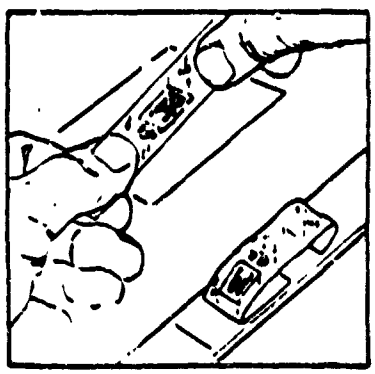

Figure 3

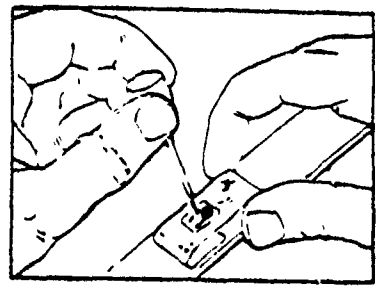

Figure 4

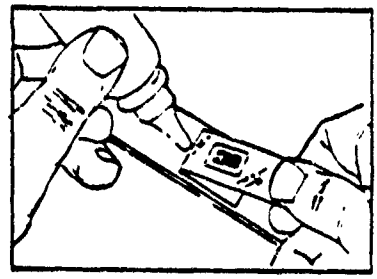

Figure 5

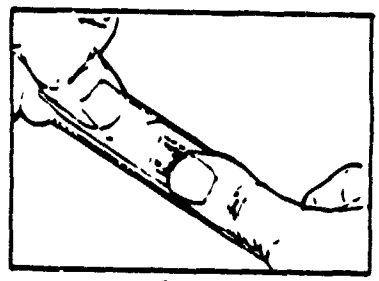

Figure 6

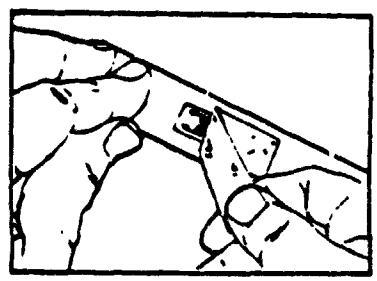

Figure 7

Figure D.1 Strain Gage Bonding Technique

over itself to form a loop and secure the other end of the loop to the plate. This tape will be used to replace the gage in the exact position after the adhesive is applied.

3) Apply a catalyst to the back of the gage sparingly, yet ensure the entire gage is covered. It should dry quickly.

4) Now lift up the working end of the tape and re-lay it so the gage is over its final position, but not quite touching the surface. While holding the tape with one hand, position the precut piece of teflon film so that it is now between the back of the tape and the fingers you will use to rub the tape after the adhesive is applied (this is the same hand as the one still holding the tape above the surface). This can be tricky.

5) Apply the catalyst by placing only a few drops onto the surface close to where the tape is now attached so that it will spread through the area where the gage will lay. Be careful not to touch the tip of the applicator to anything or it will contaminate the entire contents.

6) Now continue laying down the tape so that the gage contacts the surface, first only one end of it, then proceeding to the other end. Permabond will ooze out from under the surface. This is the reason for the Teflon film--to prevent your fingers from becoming glued together. Use the film to rub the backing of the tape to make a good bond

between the gage and the surface, and press down on the gage for 45 seconds.

7) Allow the permabond to set about 5 minutes, then carefully peel up the working end of the Scotch tape. Pull backwards and to the side at a ninety degree angle to the line of the tape. Work the tape back until it is entirely removed. Be particularly careful that you do not exert enough force on the edge of the gage to cause it to detach in the process.

8) Now the gage is bonded securely in place. Keep in mind that during this procedure the accuracy of the strain gage is entirely dependent on a complete and thorough bonding to the surface which is to be measured.

9) After attachment of the lead wires to the gage terminals, an application of "Gage Cote" to the surface of the gage will provide additional protection. This is advisable in a workshop environment where the test plate is exposed to rough treatment.

C. IMPROVED METHODS

In the study of impulsively loaded structures performed by E.A. Witmer at MIT, an improved method of strain gage application was devised and reported as Appendix A of reference 2. Although the test arrangement was quite different from that studied in this paper, the gage installation technique proved successful for the measurement

of transient strains. Dr. Witmer presents an "enhanced survival" method of protecting the gages under severe impulse loading conditions. To prevent the gages from becoming detached from the surface, a covering patch of polyimide sheet was cemented over the entire gage and a portion of the lead wires. Figure D.2 is a reproduction of his illustration, followed by his description as found on page 101 of reference 2.

"From a 0.001 inch thick sheet of polyimide, cut a 'cover patch' of the size indicated in Figure A-7 (Figure D-2 here). Roughen and clean this patch as in Step 5 (using a 400 grit silicon-carbide paper and clean with N5). Apply a thin coat of AE-15 cement to (a) the gage area, (b) the polyimide insulator patch, and (c) both sides of the polyimide cover patch. Position as shown in Figure A-7 and cover the entire region with a strip of 0.003 x 1 x 1 inch of teflon film. Secure the teflon in place with cellophane tape. Repeat Step 8 to complete the cementing/curing process (this step describes the curing of the bonded gage with proper pressure and heat). The teflon cover does not adhere and is hence removed. The result is a multilayer cover of cement/polyimide/cement, with an exterior layer of AE-15 cement."

Dr. Witmer used special, high elongation strain gages manufactured by Micro-Measurement Co., Romulus, Michigan. His gage data follows:

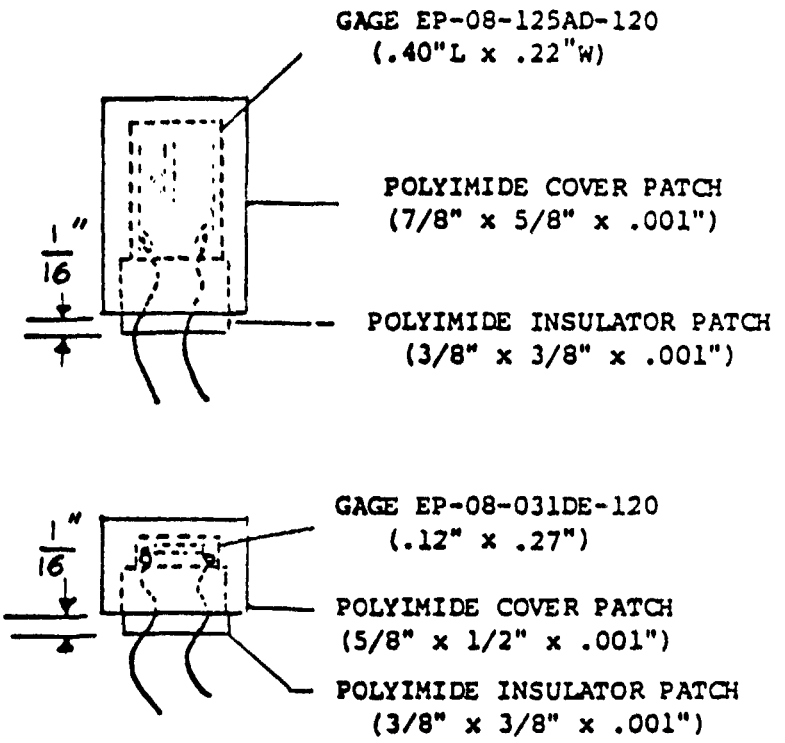

FIG. A,7 POLYIMIDE COVER PATCH DIMENSIONS AND LOCATION

Figure D.2 Improved Strain Gage Mounting [Ref. 2]

Gage	EP-08-031DE-120	EP-08-125AD-120
length (in.) without tabs	0.031	0.125
length (in.) with tabs	0.140	0.250
width (in.)	0.032	0.125
Polyimide backing		
length (in.)	0.27	0.40
width (in.)	0.12	0.22
thickness (in.)	0.001	0.001

Special consideration to lead wire arrangement is also given in reference 2. In an effort to make the lead wires as nearly massless as possible, very fine (0.003 inch diameter) varnish covered copper lead wires (AWG 40) were used. They were suspended above the structure in a "soft coil" arrangement to reduce the forces on the wires and the connection.

Although a configuration such as this appears necessary to properly measure transient strains, this particular method is not feasible for external gages in an underwater shock test. Attention must be given to this matter in future tests. As recommended earlier, a tube or sheath arrangement to permit the lead wires to extend seems plausible.

APPENDIX E

INSTRUMENTATION AND EQUIPMENT AT WCSF

The following list identifies the electronic equipment used in the instrumentation. The components listed are located at the West Coast Shock Facility, San Francisco, CA.

Unit	Quantity
Ampex FR 1300 tape recorder	2
Ampex magnetic oxide coated tape	2
General Radio Co. 1952 Universal Filters (high pass/low pass)	-
Bell and Howell DC amplifer CEC 1-168	16
Endevco signal conditioner model 4470 Current Regulated Bridge Conditioners	15
Systron Donner Time Code Reader/Search Unit 8134	1
Honeywell Universal Bridge Balance Unit Model #B2-6, six channels each unit	2
Honeywell 1858 Visicorder	1
Firing Circuit, 800 volts DC Relay operated, capacitive discharge	1
Dupont EBW Detonators X-175	4
Tourmaline pressure gages, 1/4 inch, four pile with a 50 foot cable attached	2
Micro Measurements 120 OHM strain gages EA-06-250BG-120	21
Endevco piezoresistive accelerometer model 2262-2000, range $\pm$2000 g	1

Seacon Connector, 24 pin XSM-CCP with 50 foot cable, Boston insulated wire and cable co. MWF-19 NEOP		1
Seacon Penetrator, XSM-BCR		1
Bellfoil Shielded Cables,	Belden 8424, 1/4 inch	1-200 feet
	Belden 9776, 1/2 inch 16 gage	2-200 feet
Standard U.S. Navy Brass Connection Boxes one on side of backing structure one floating 50 feet from the test rig and 200 feet from pier		2

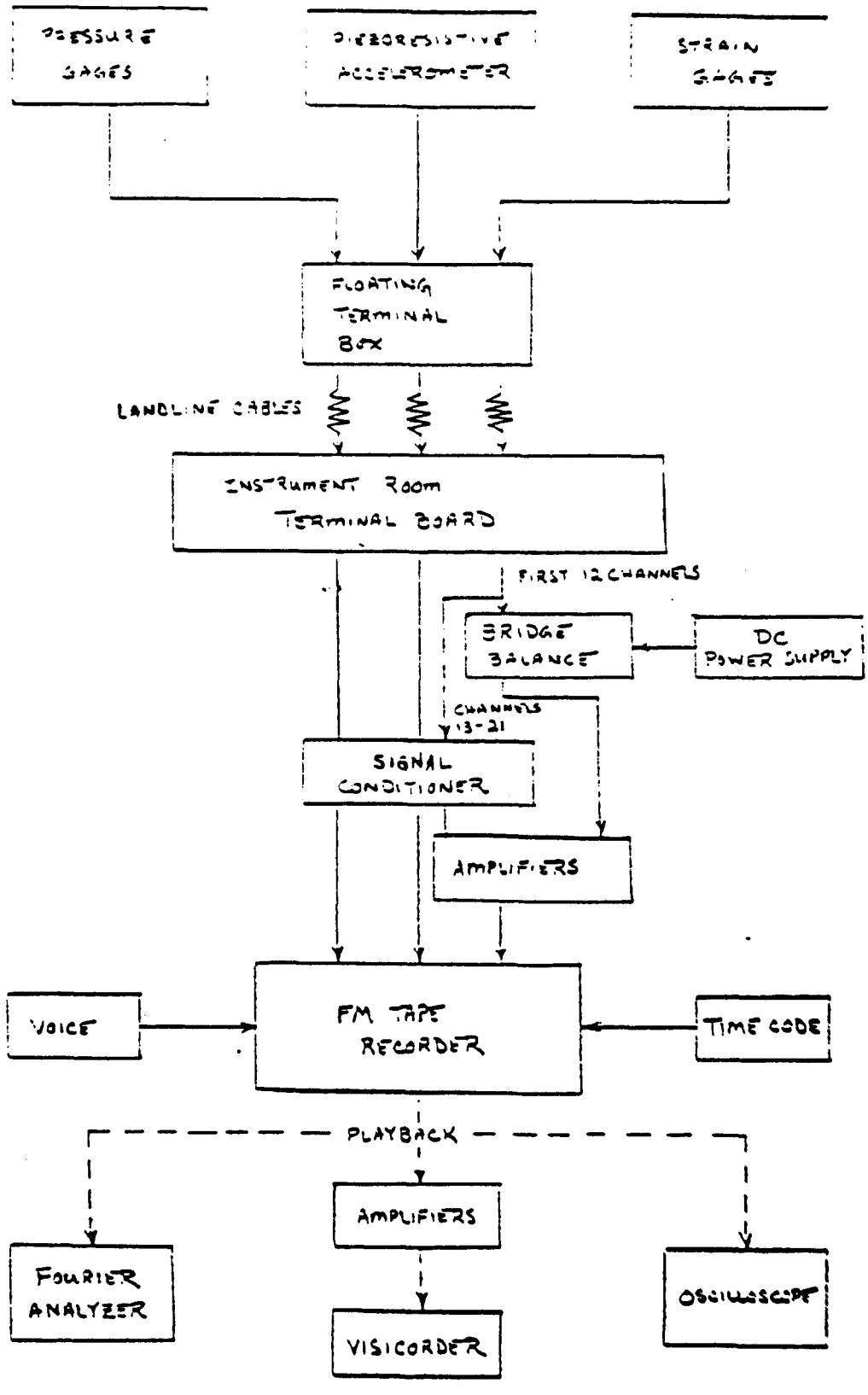

Figure E.1 Flow Chart for Electronic Setup

APPENDIX F

SELECTED DATA RECORDS

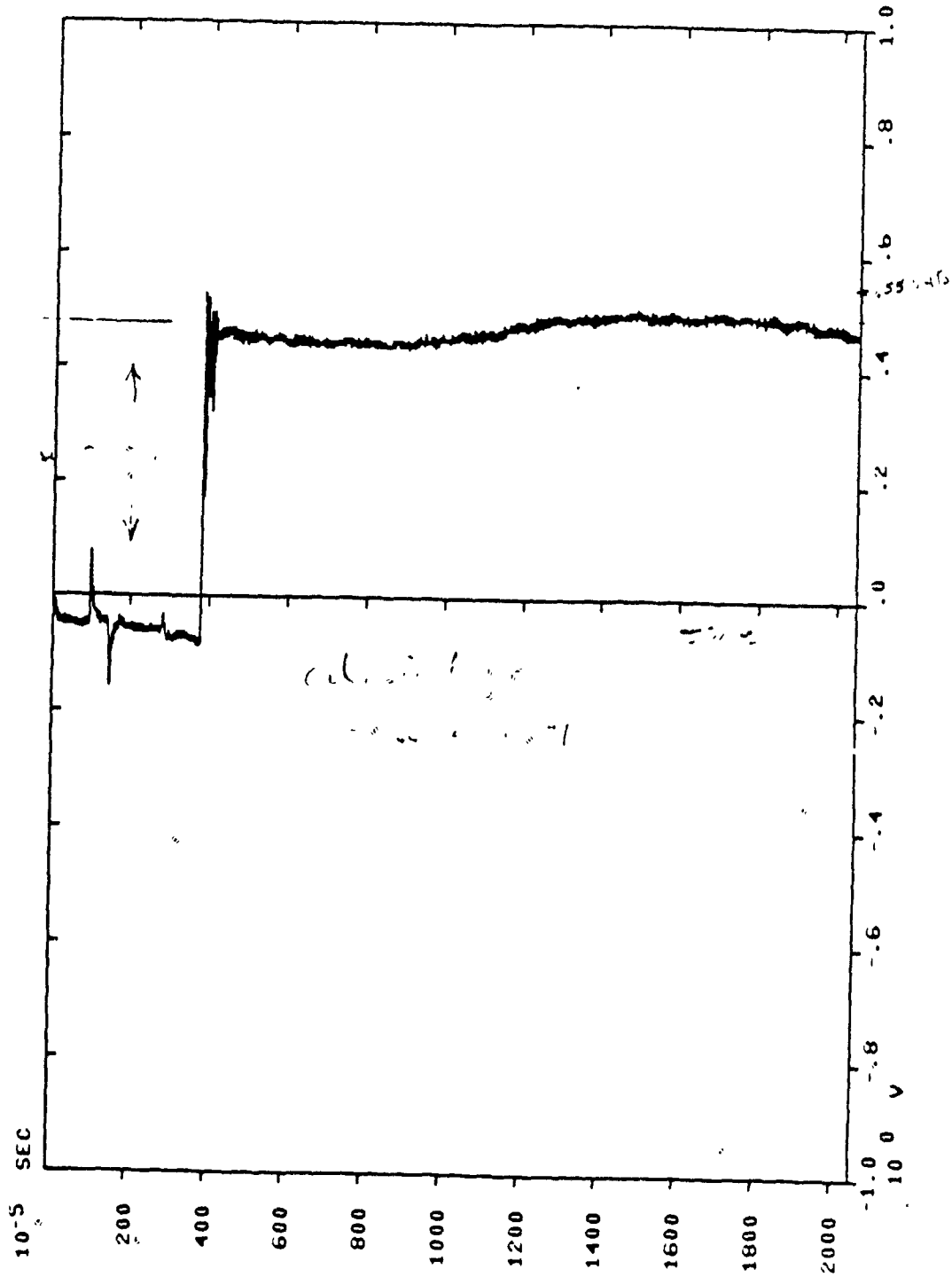

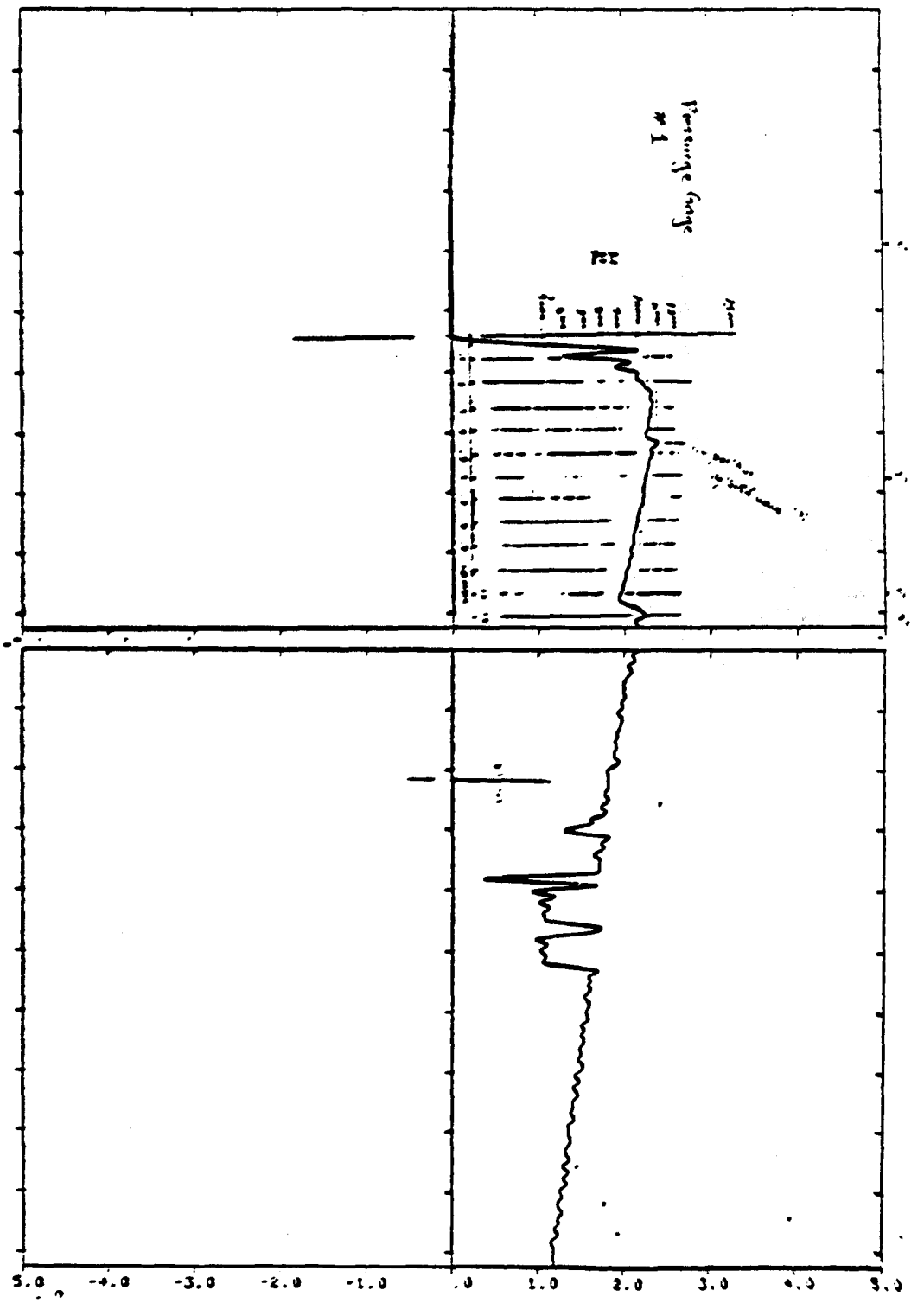
-5.0
-4.0
-3.0
-2.0
-1.0
1.0
2.0
3.0

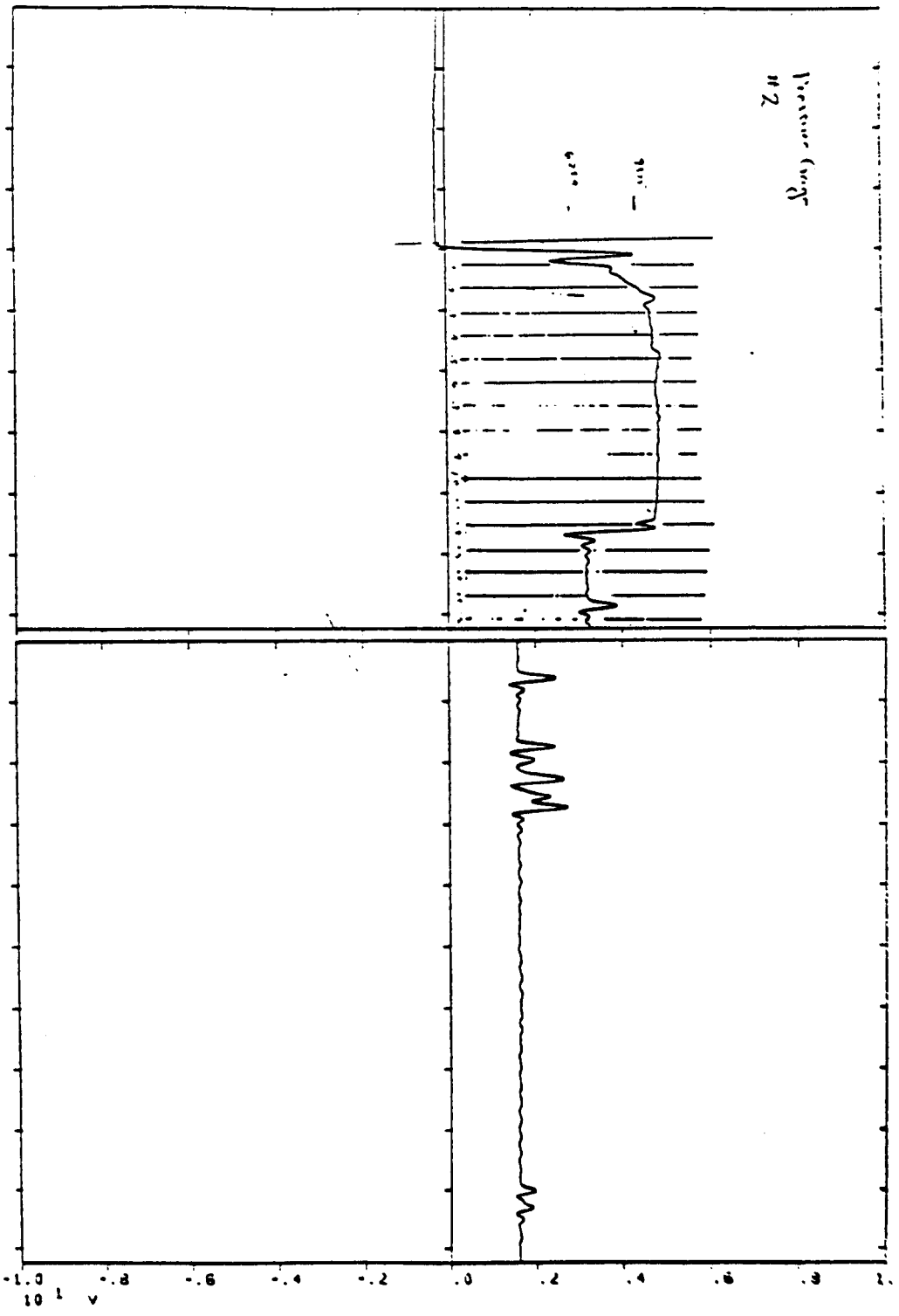
-1.0
-.8
-.6
-.4
-.2
.0
.2
.4
.6
.8
1.
10 1 V

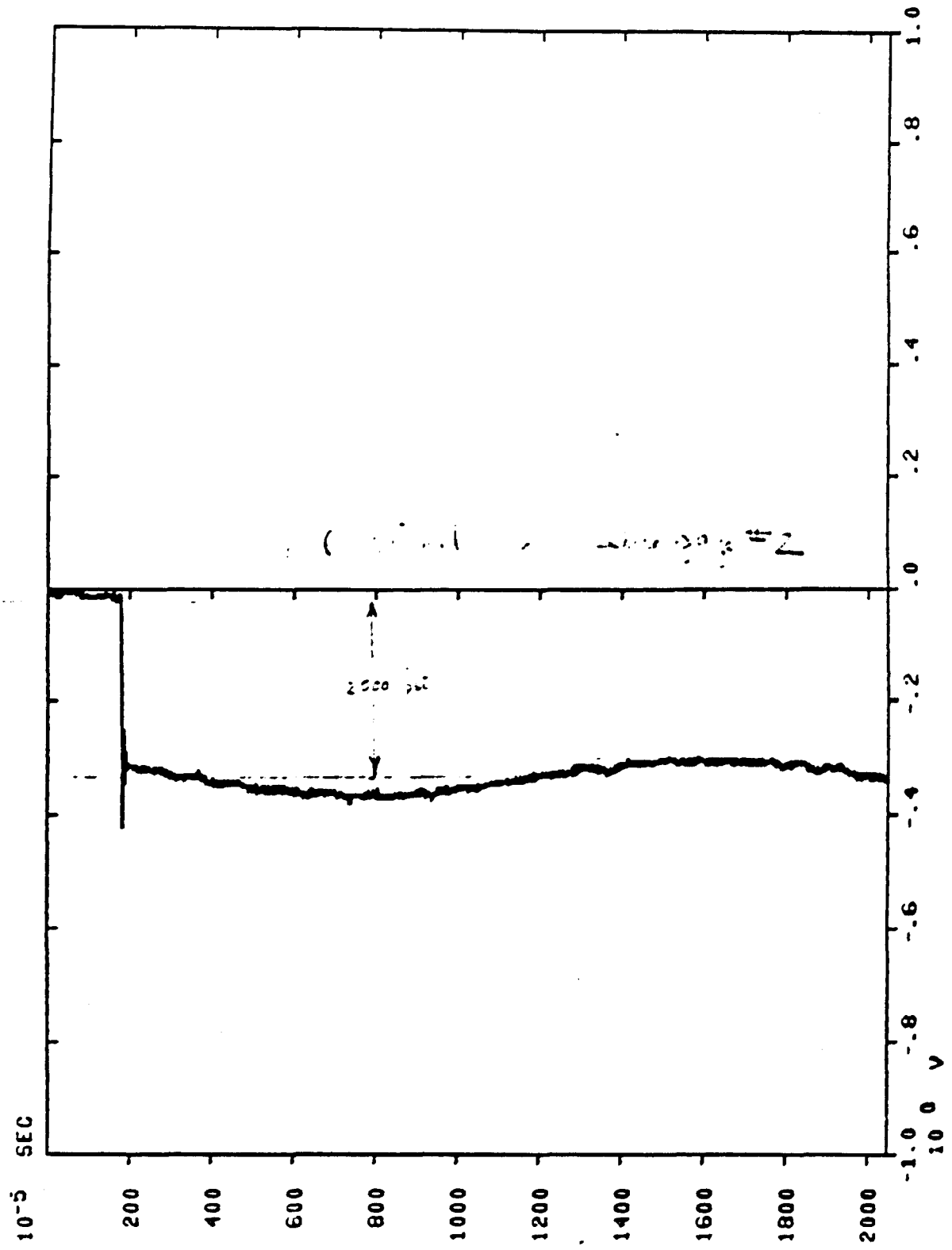
10^-5 SEC
200
400
600
800
1000
1200
1400
1600
1800
2000
-1.0
-.8
-.6
-.4
-.2
0
.2
.4
.6
.8
1.0
V

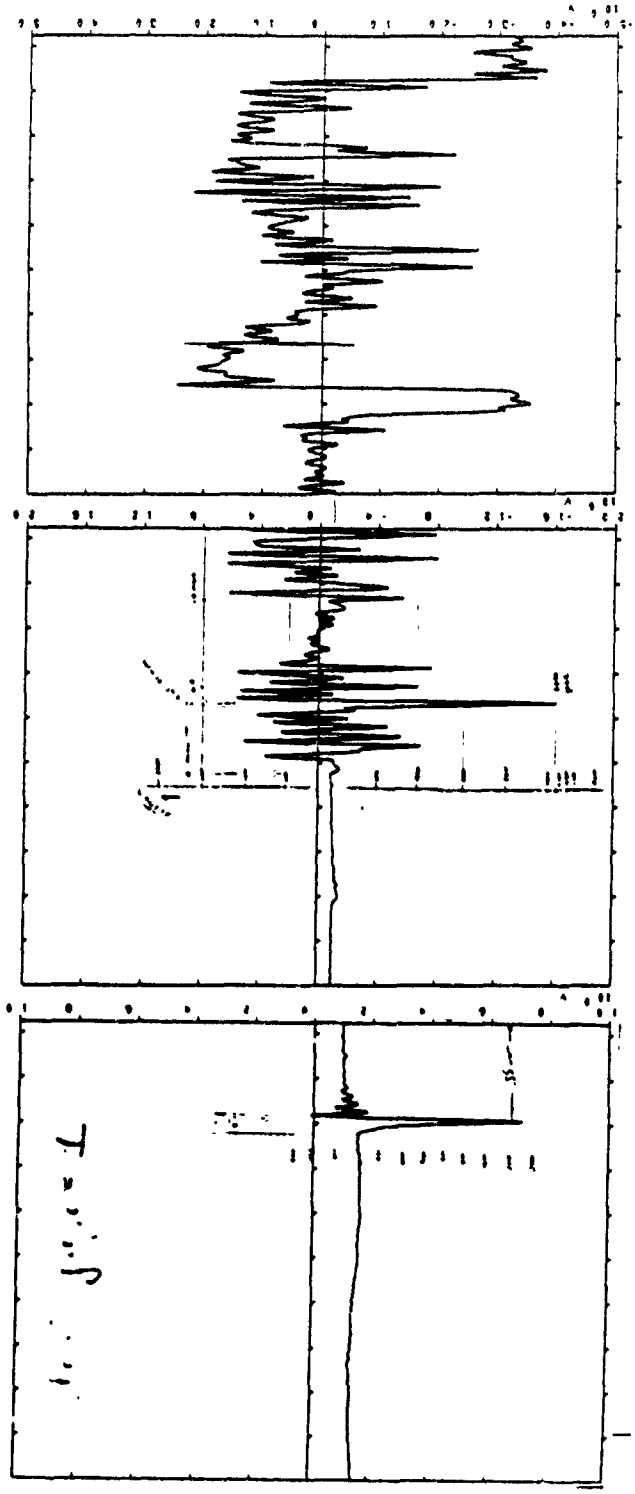

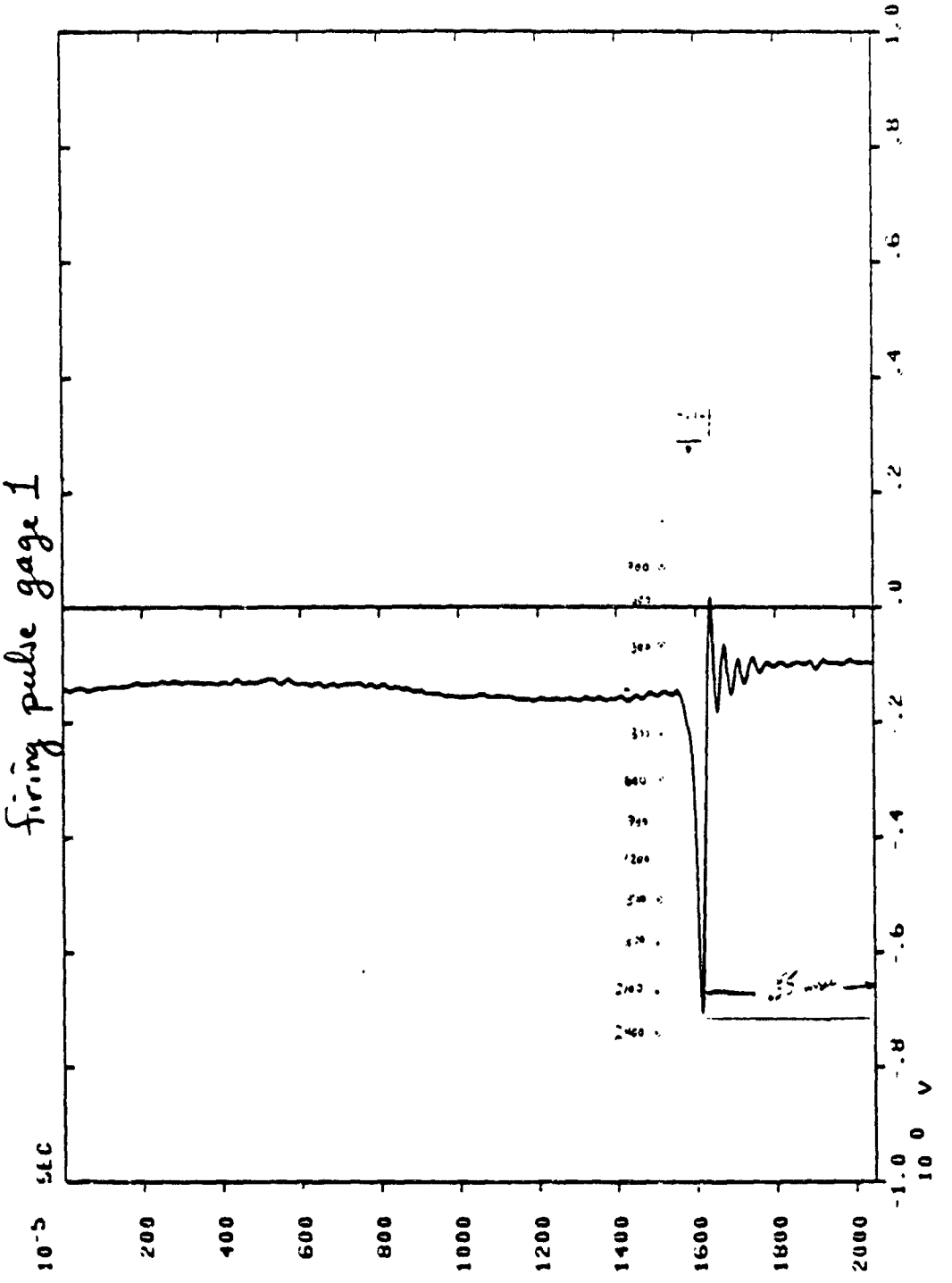
firing pulse gage 1
10⁻⁵ SEC
200
400
600
800
1000
1200
1400
1600
1800
2000
1.0
.8
.6
.4
.2
0
.2
.4
.6
.8
-1.0
10 0 V

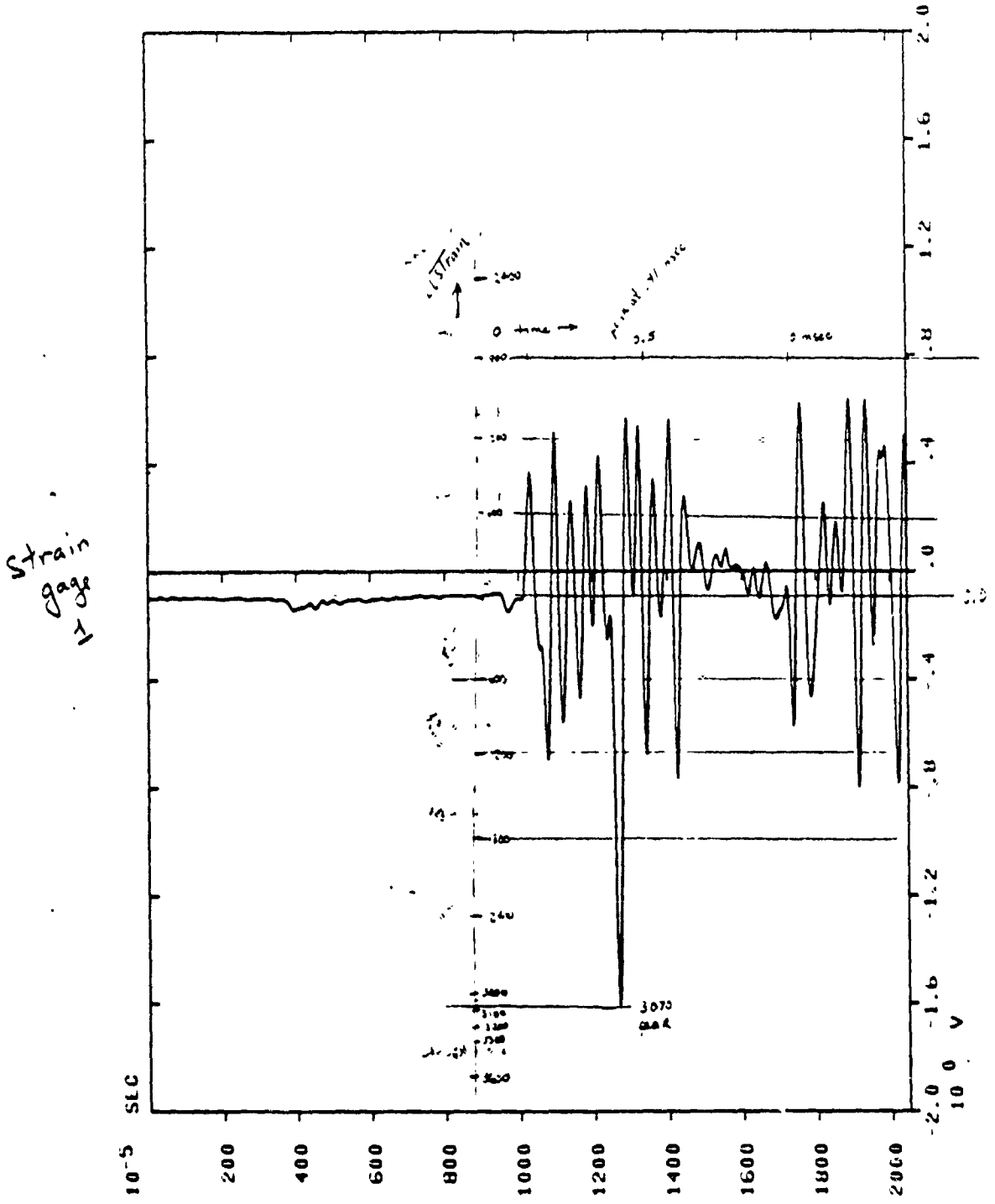
Strain gage 1
SEC
10⁻⁵
200
400
600
800
1000
1200
1400
1600
1800
2000
2.0
1.6
1.2
.8
.4
0
-.4
-.8
-1.2
-1.6
-2.0
V
3070

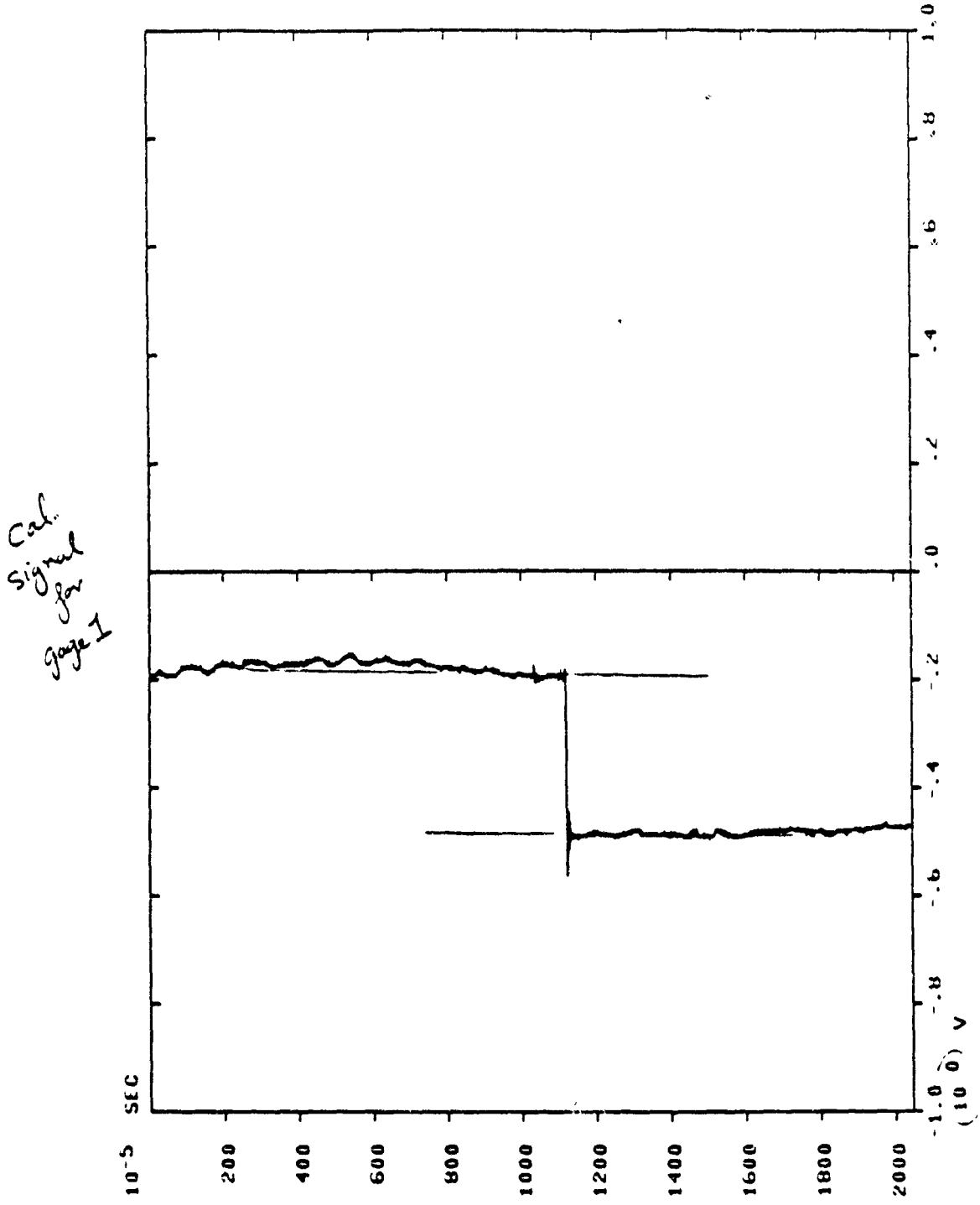
Cal. signal for gage 1
10⁻⁵ SEC
200
400
600
800
1000
1200
1400
1600
1800
2000
1.0
.8
.6
.4
.2
.0
-.2
-.4
-.6
-.8
-1.0
(10 0) V

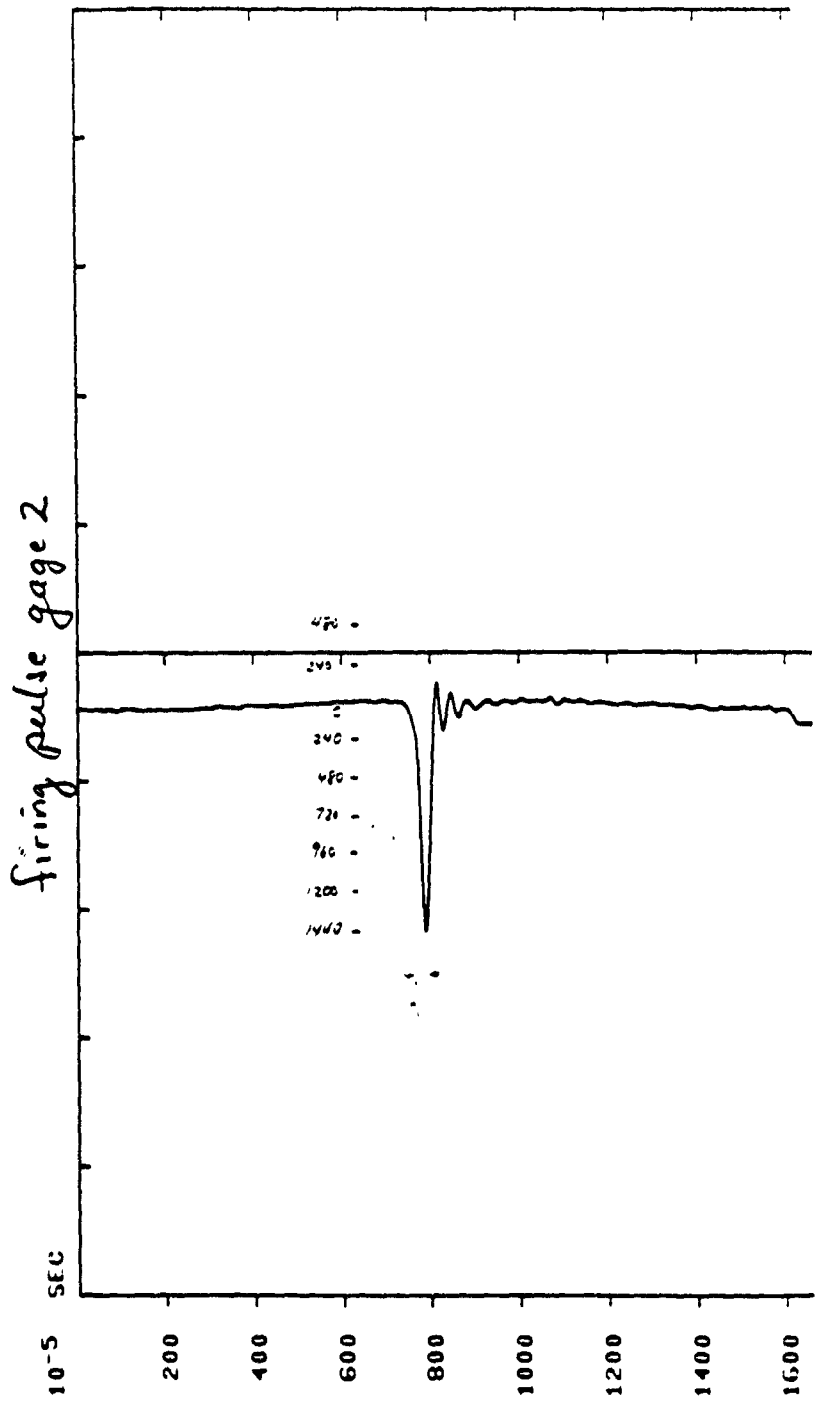
firing pulse gage 2
10⁻⁵ SEC
200
400
600
800
1000
1200
1400
1600

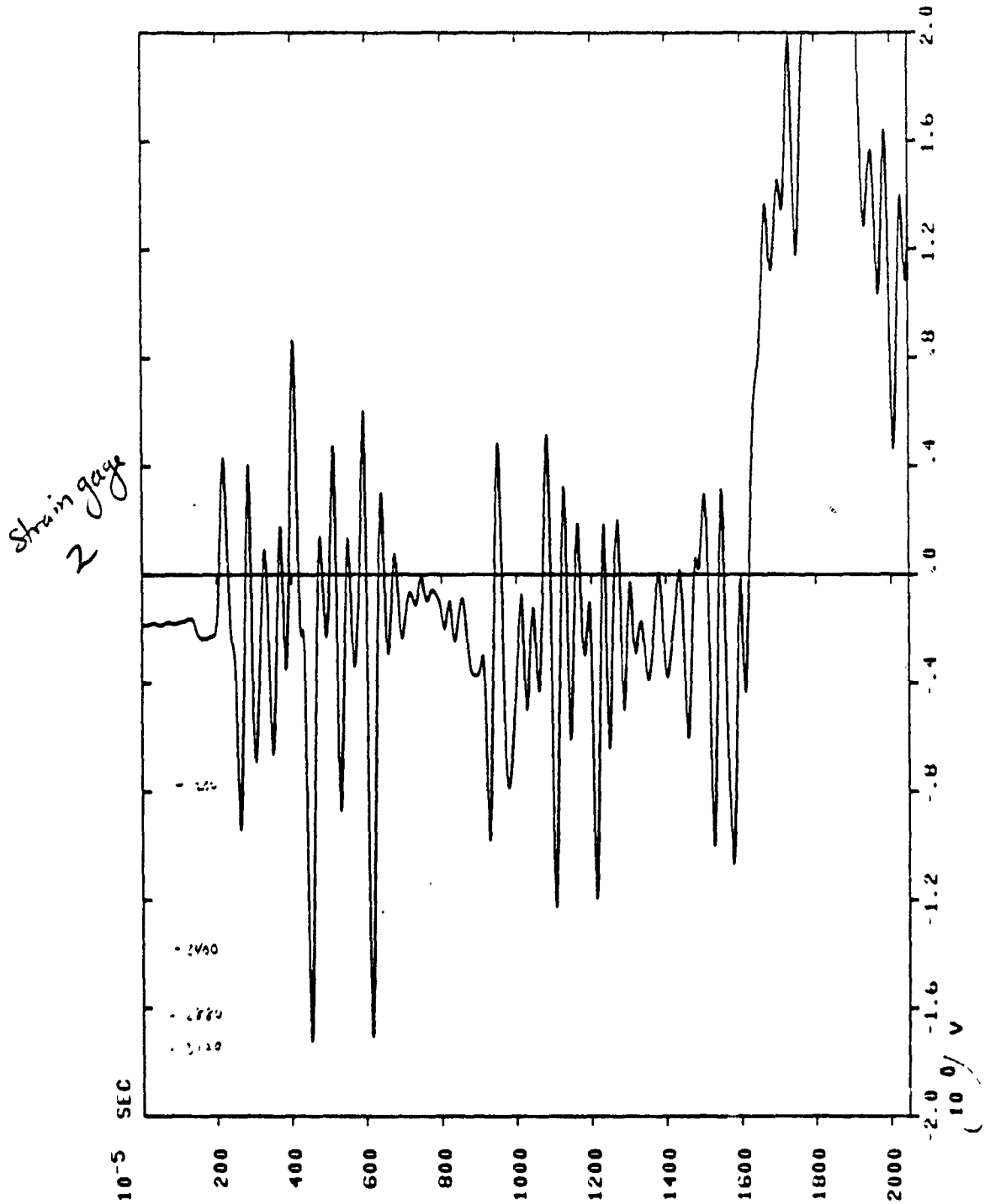
Strain gage
2
10^-5 SEC
200
400
600
800
1000
1200
1400
1600
1800
2000
2.0
1.6
1.2
.8
.4
0
-.4
-.8
-1.2
-1.6
-2.0
(10 0/ V

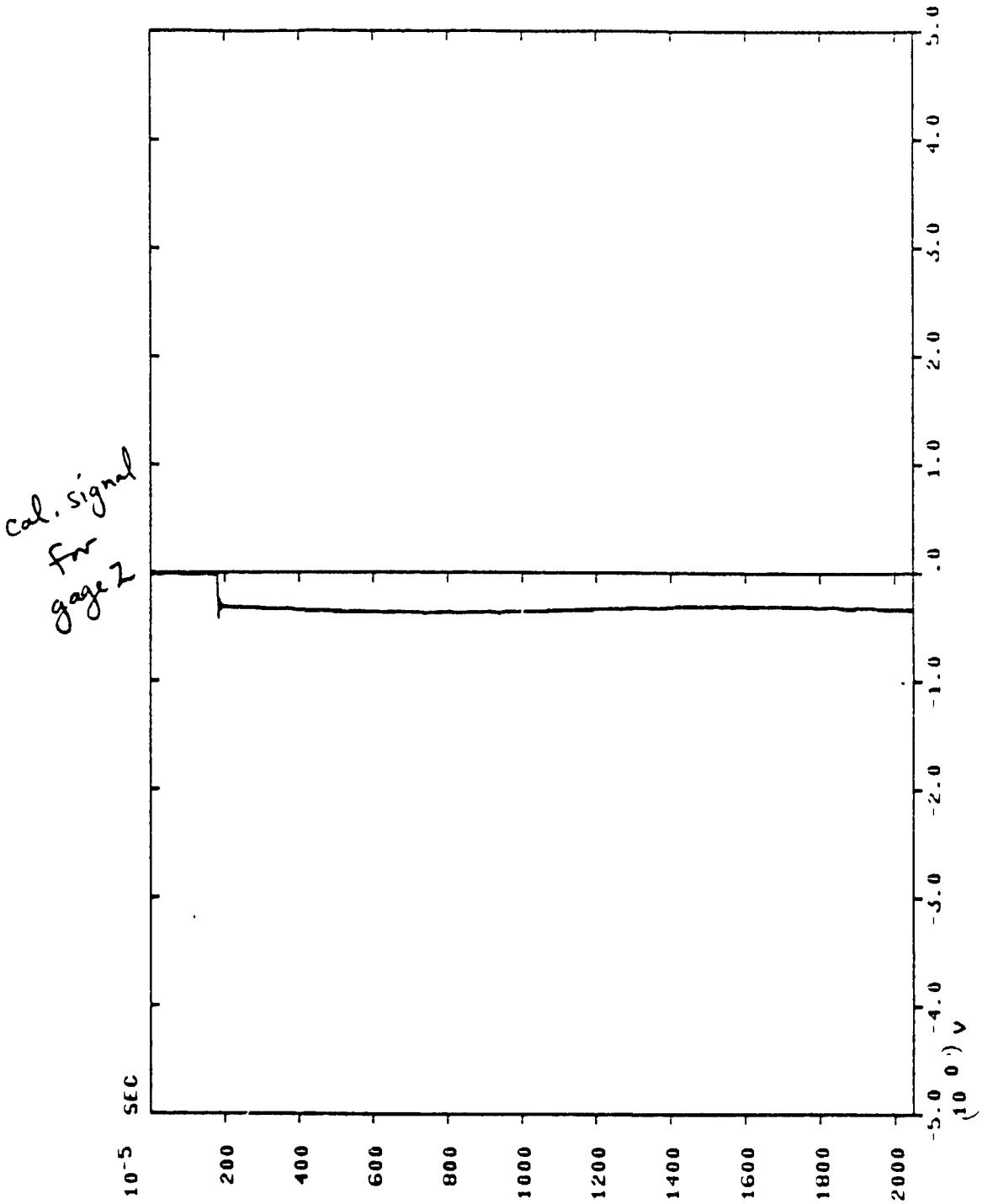
cal. signal
for
gage 2
10⁻⁵ SEC
200
400
600
800
1000
1200
1400
1600
1800
2000
5.0
4.0
3.0
2.0
1.0
.0
-1.0
-2.0
-3.0
-4.0
-5.0
(10 0) V

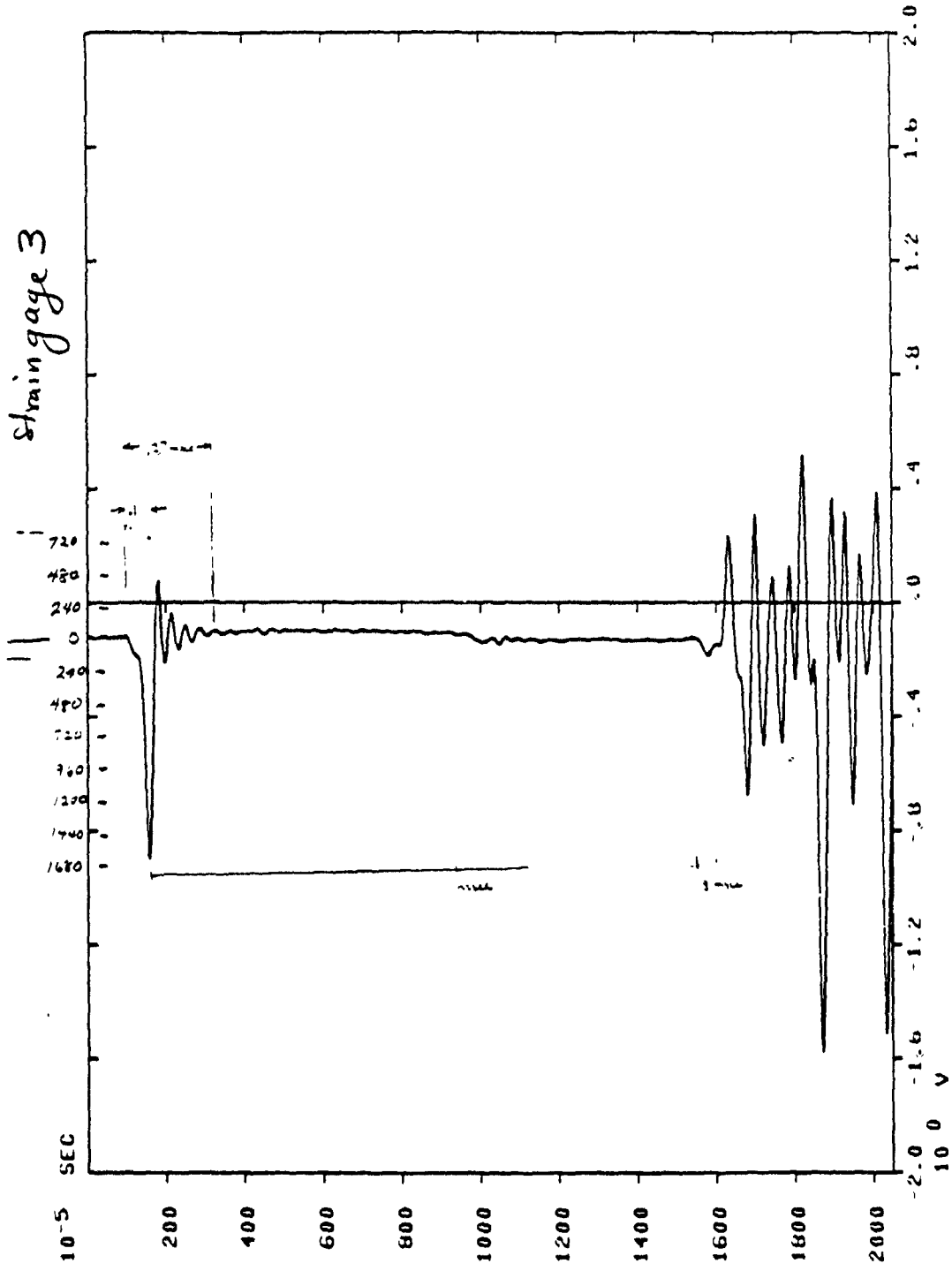
Strain gage 3
720
480
240
0
240
480
720
960
1200
1440
1680
SEC
10⁻⁵
200
400
600
800
1000
1200
1400
1600
1800
2000
2.0
1.6
1.2
.8
.4
.0
.4
.8
1.2
1.6
2.0
V
10 0

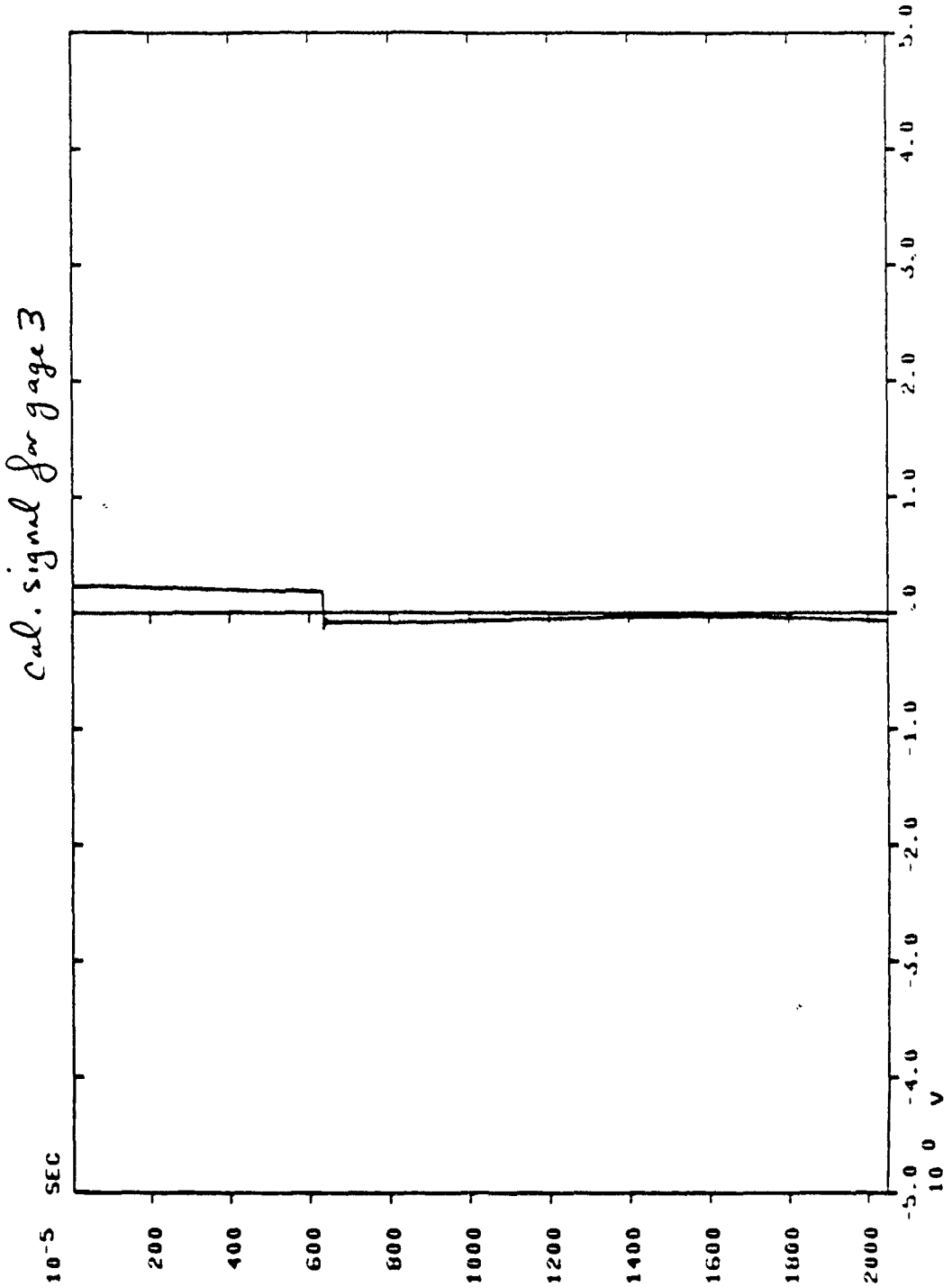
cal. signal for gage 3
10⁻⁵ SEC
200
400
600
800
1000
1200
1400
1600
1800
2000
-5.0
-4.0
-3.0
-2.0
-1.0
0
1.0
2.0
3.0
4.0
5.0
10 0 V

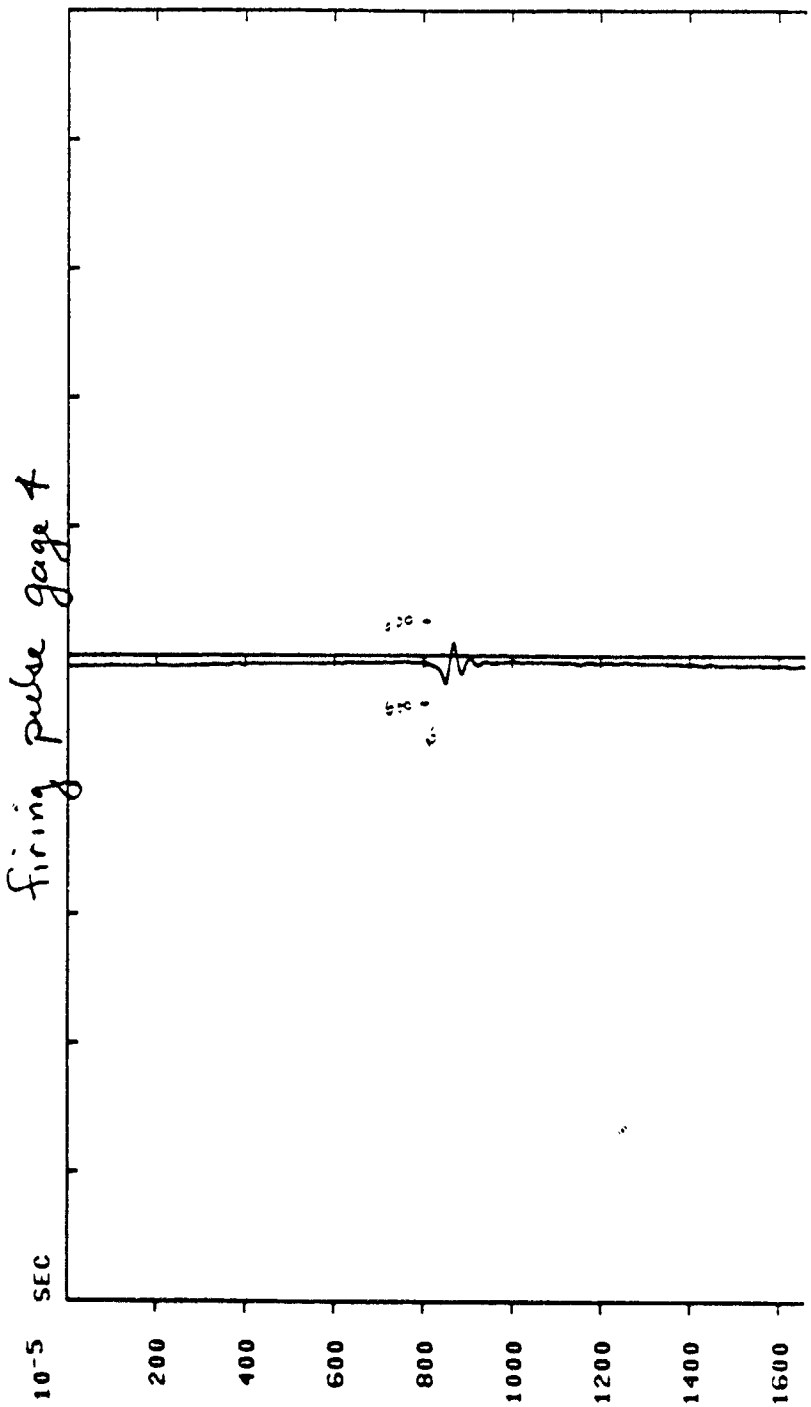
firing pulse gage 4
10-5 SEC
200
400
600
800
1000
1200
1400
1600

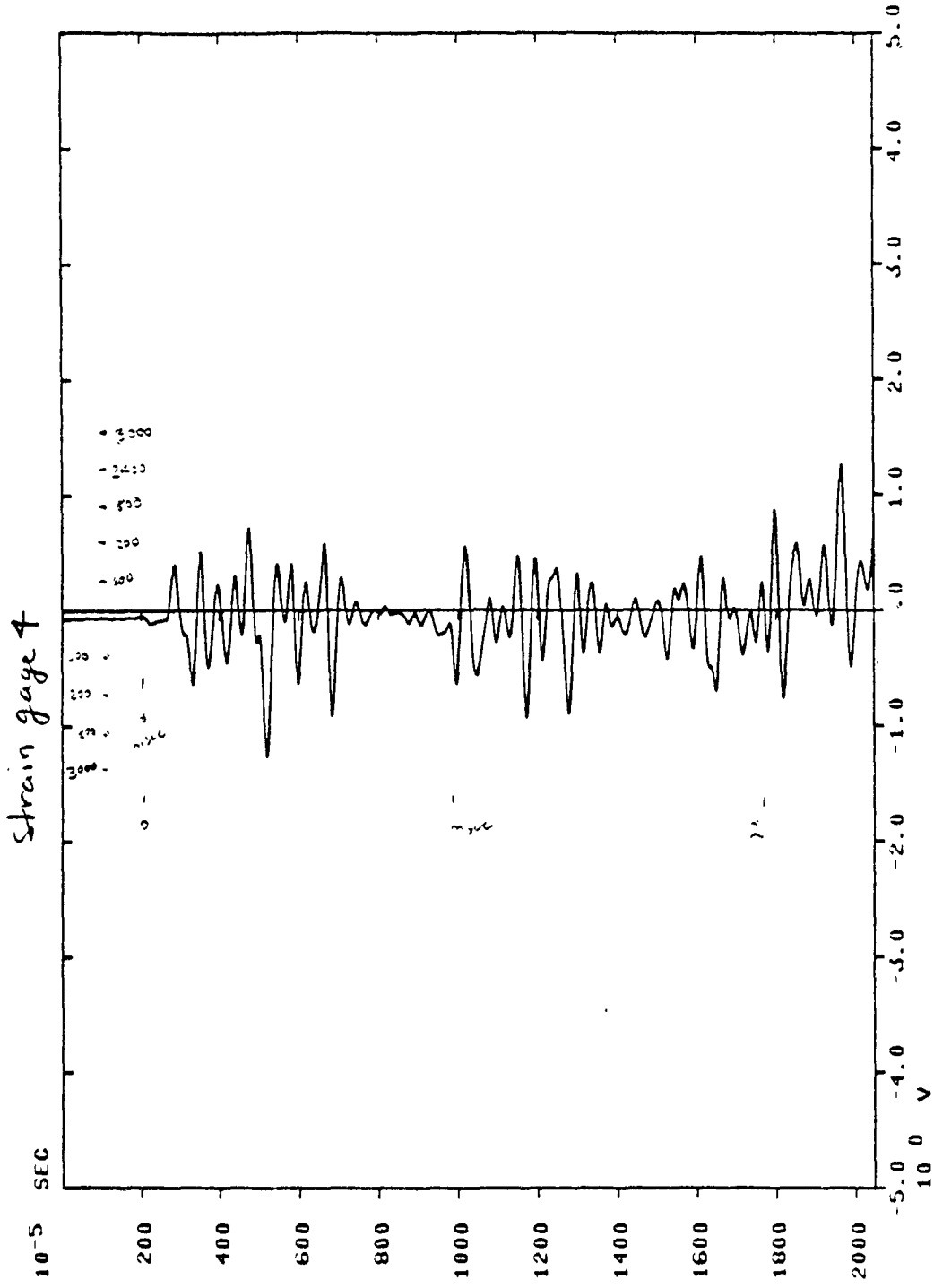
Strain gage 4
10⁻⁵ SEC
200
400
600
800
1000
1200
1400
1600
1800
2000
5.0
4.0
3.0
2.0
1.0
.0
-1.0
-2.0
-3.0
-4.0
-5.0
10 0 V

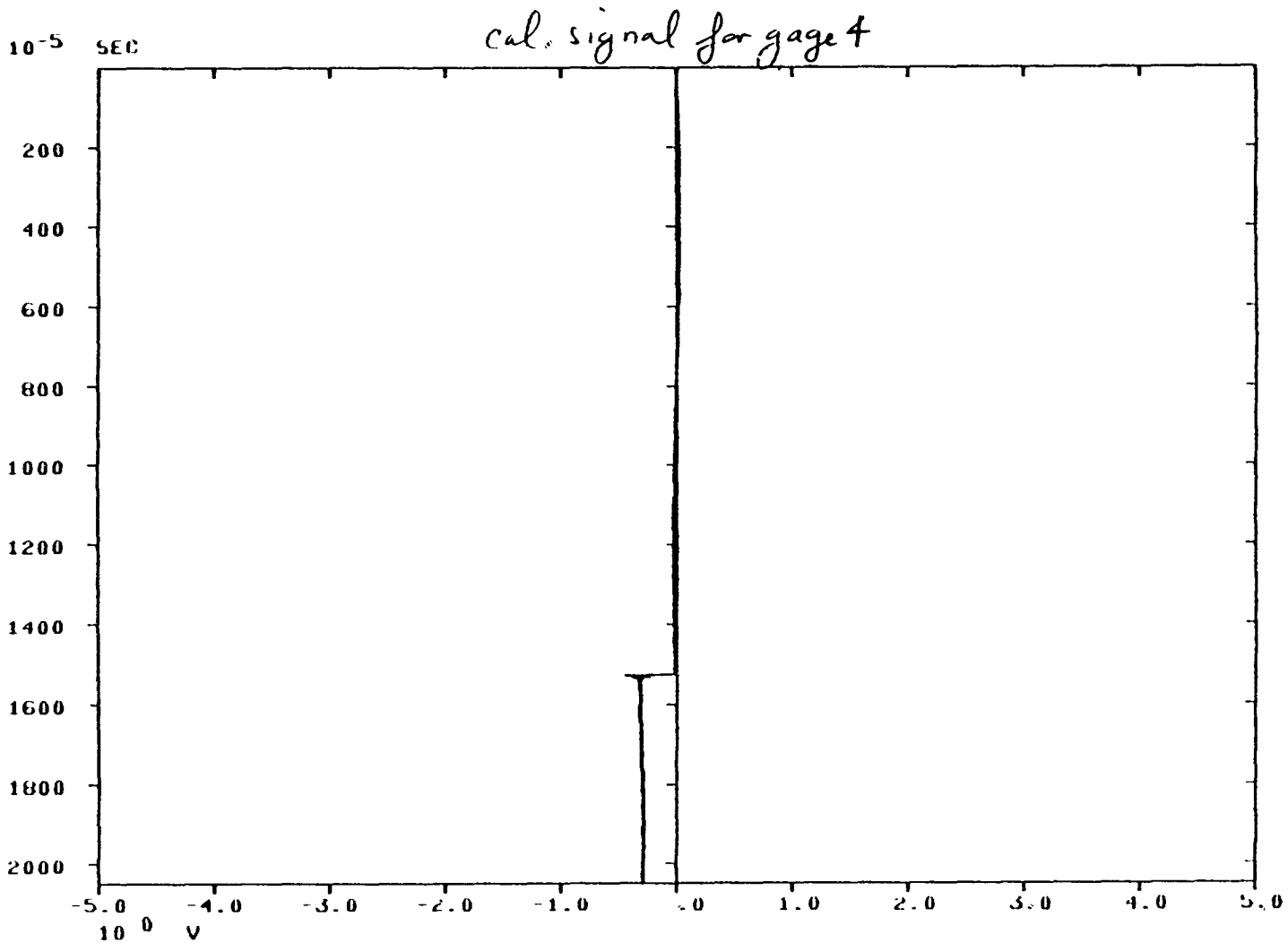
cal. signal for gage 4
10⁻⁵ SEC
200
400
600
800
1000
1200
1400
1600
1800
2000
-5.0
-4.0
-3.0
-2.0
-1.0
.0
1.0
2.0
3.0
4.0
5.0
10 0 V

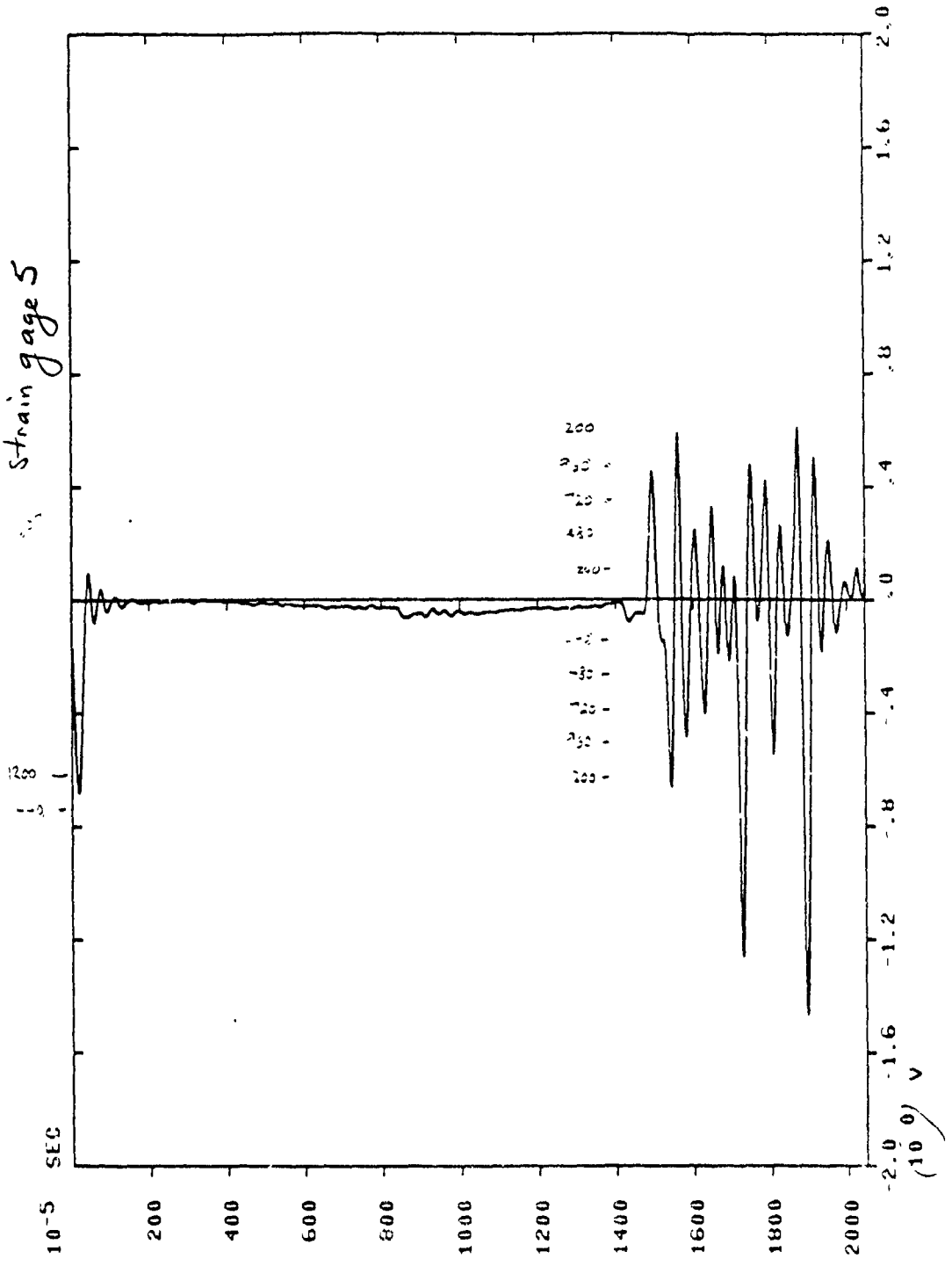
strain gage 5
SEC
10-5
200
400
600
800
1000
1200
1400
1600
1800
2000
2.0
1.6
1.2
.8
.4
0
-.4
-.8
-1.2
-1.6
-2.0
(10 0) V

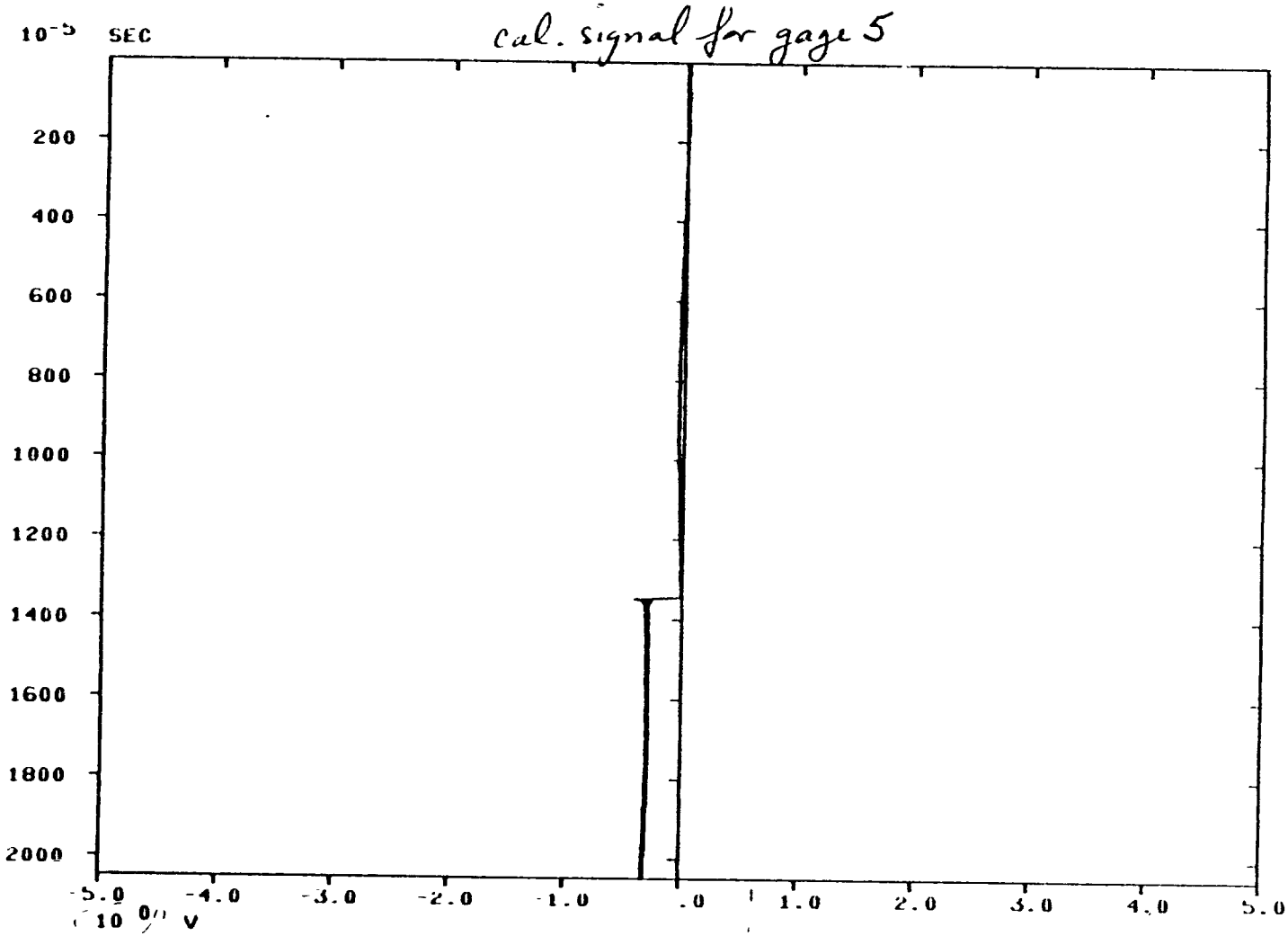
cal. signal for gage 5
10⁻⁵ SEC
200
400
600
800
1000
1200
1400
1600
1800
2000
-5.0
-4.0
-3.0
-2.0
-1.0
.0
1.0
2.0
3.0
4.0
5.0
10 0/ V

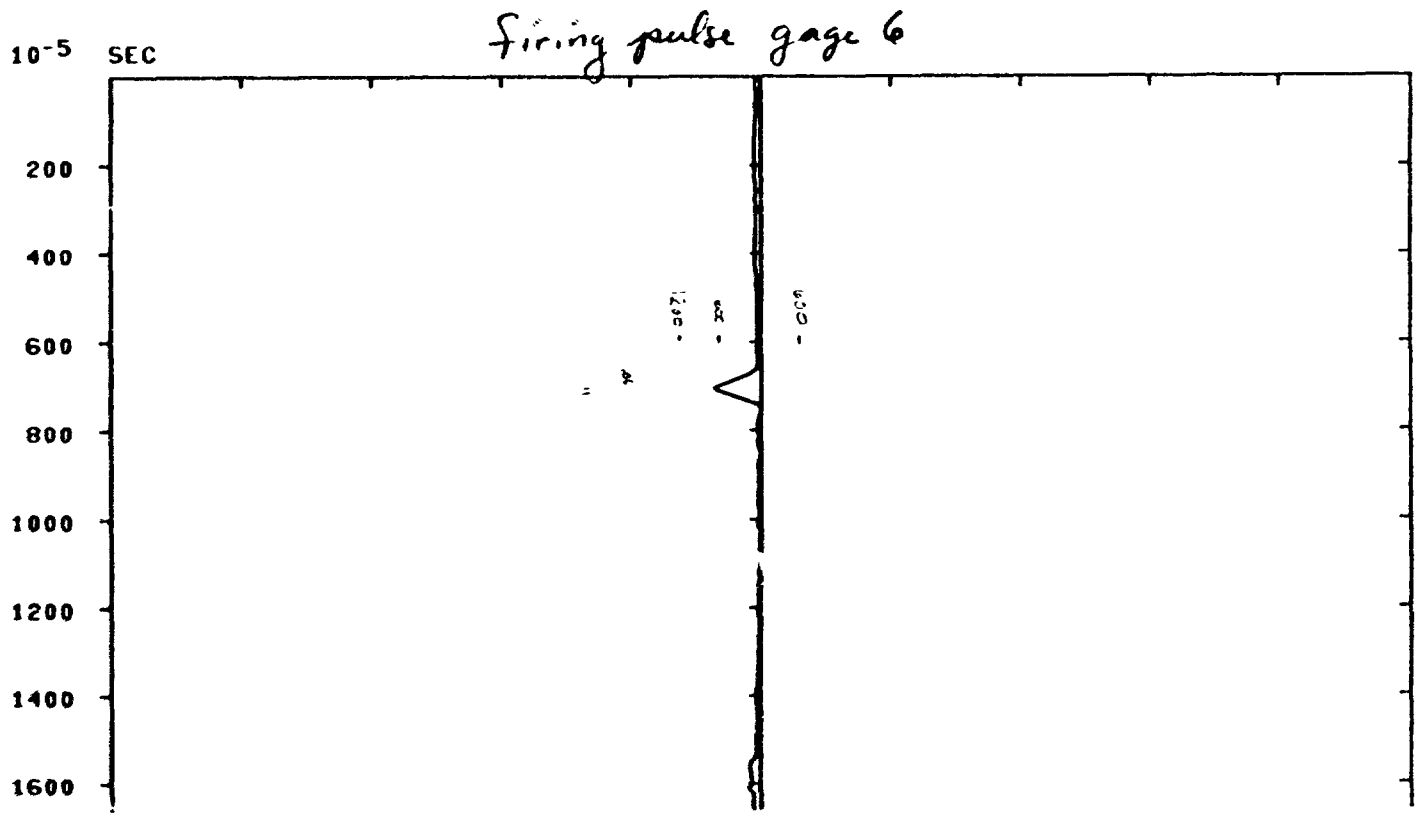
Firing pulse gage 6
10-5 SEC
200
400
600
800
1000
1200
1400
1600

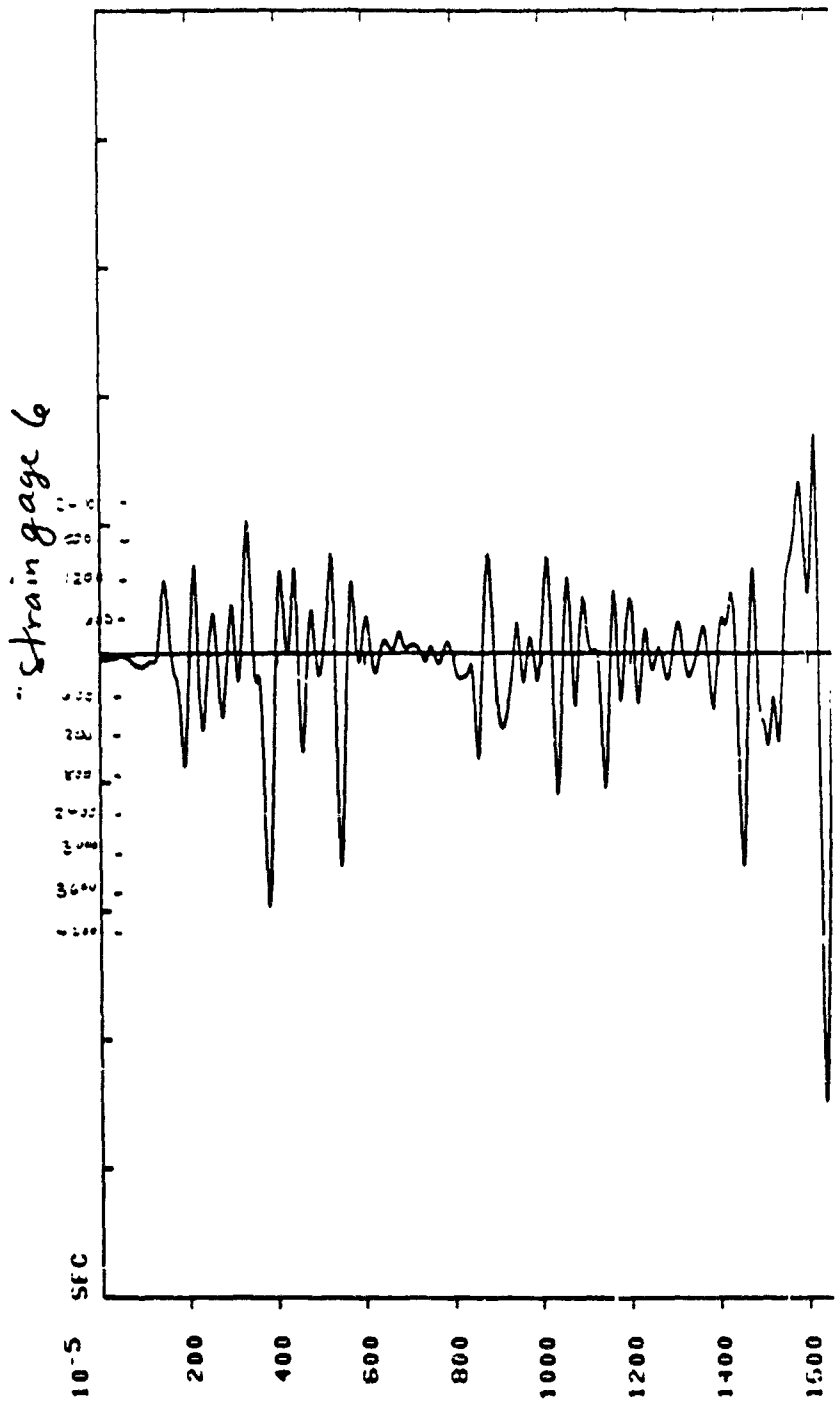
strain gage 6
10⁻⁵ SEC
200
400
600
800
1000
1200
1400
1600

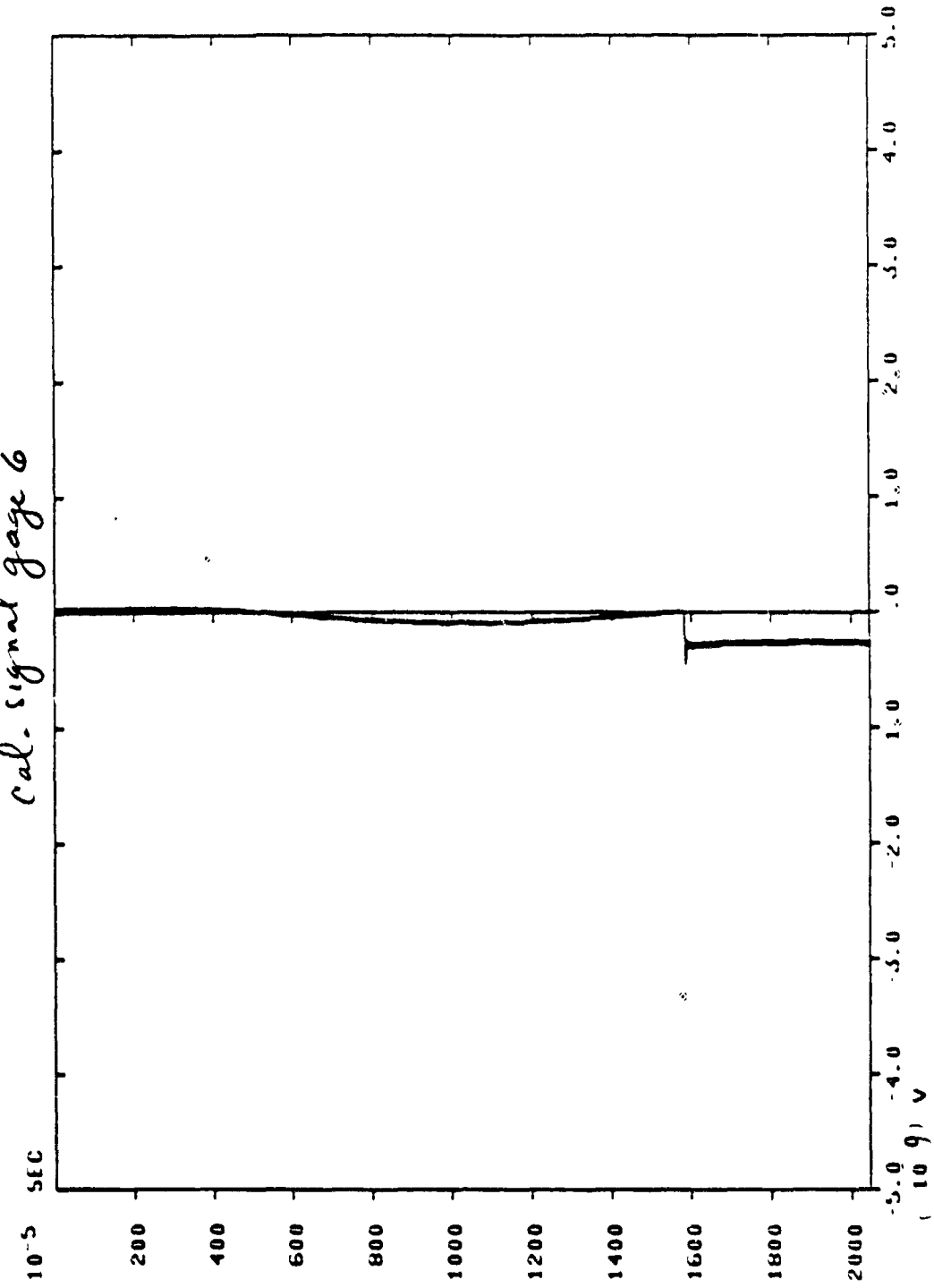
cal. signal gage 6
10⁻⁵ SEC
200
400
600
800
1000
1200
1400
1600
1800
2000
-5.0
-4.0
-3.0
-2.0
1.0
.0
1.0
2.0
3.0
4.0
5.0
(10 9) V

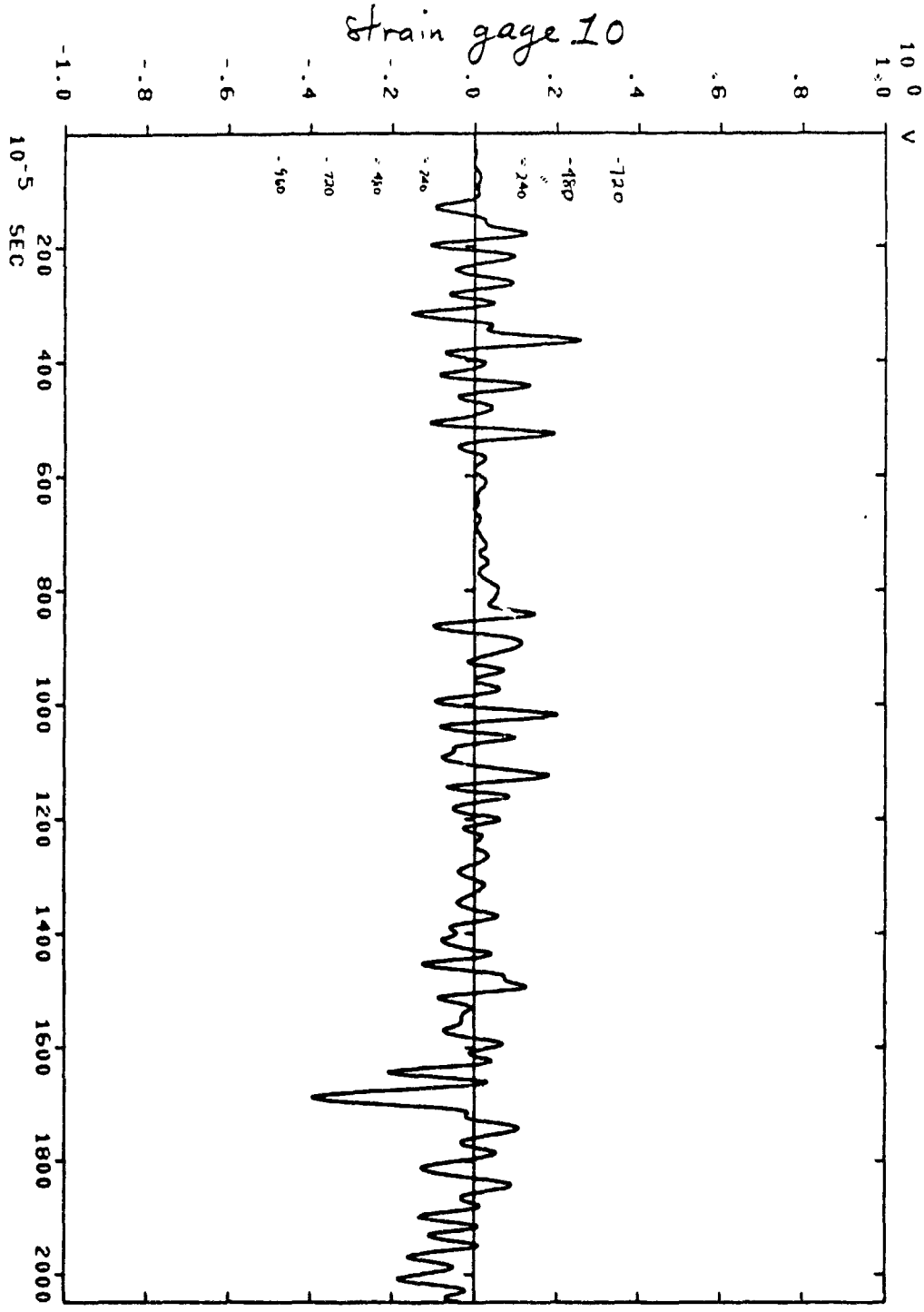
Strain gage 10
10 0
1.0 V
-1.0
-.8
-.6
-.4
-.2
.0
.2
.4
.6
.8
-720
-480
-240
-160
-240
-480
-720
10^-5 SEC
200
400
600
800
1000
1200
1400
1600
1800
2000

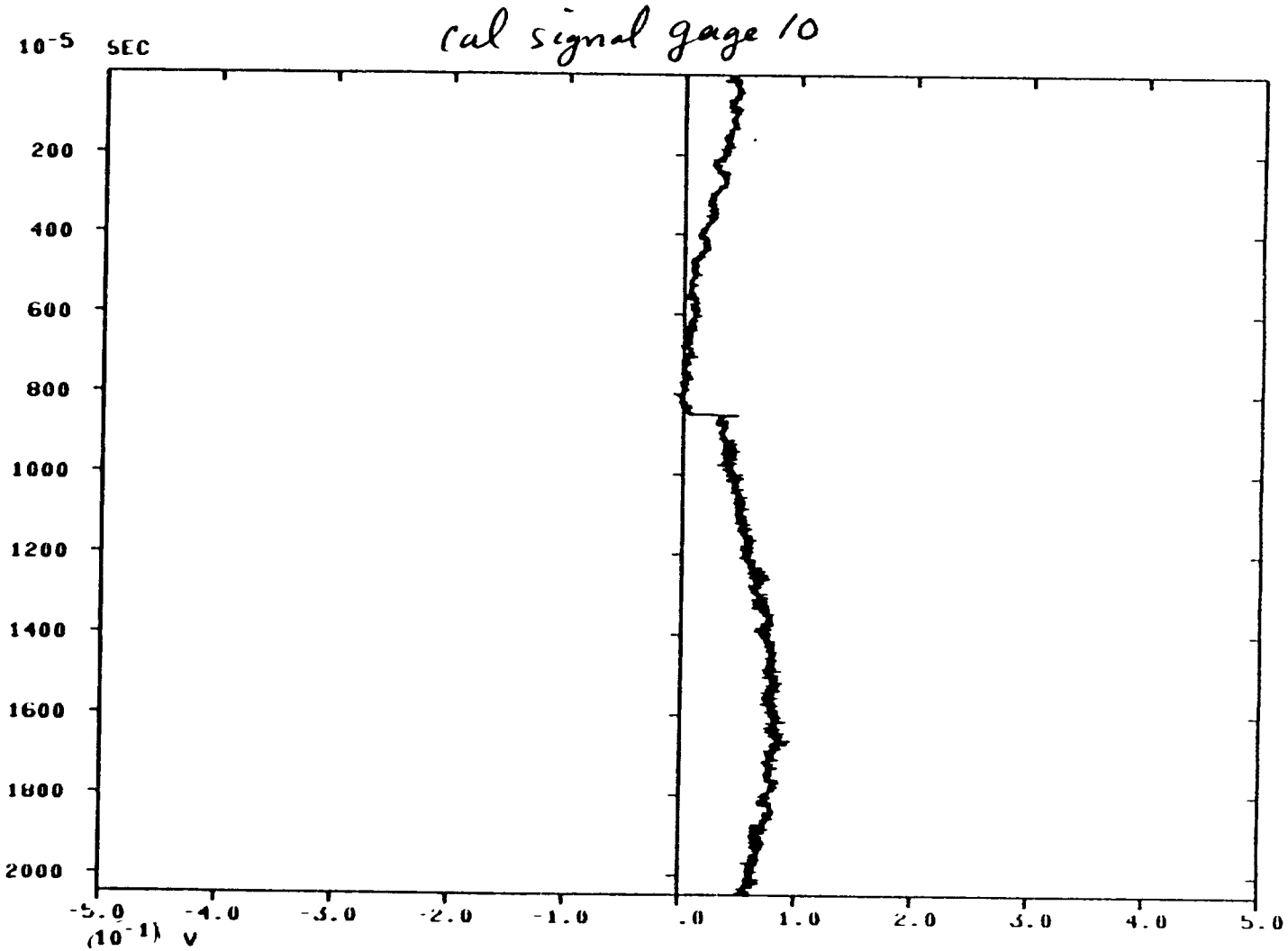
cal signal gage 10
10⁻⁵ SEC
200
400
600
800
1000
1200
1400
1600
1800
2000
-5.0
-4.0
-3.0
-2.0
-1.0
.0
1.0
2.0
3.0
4.0
5.0
(10⁻¹) V

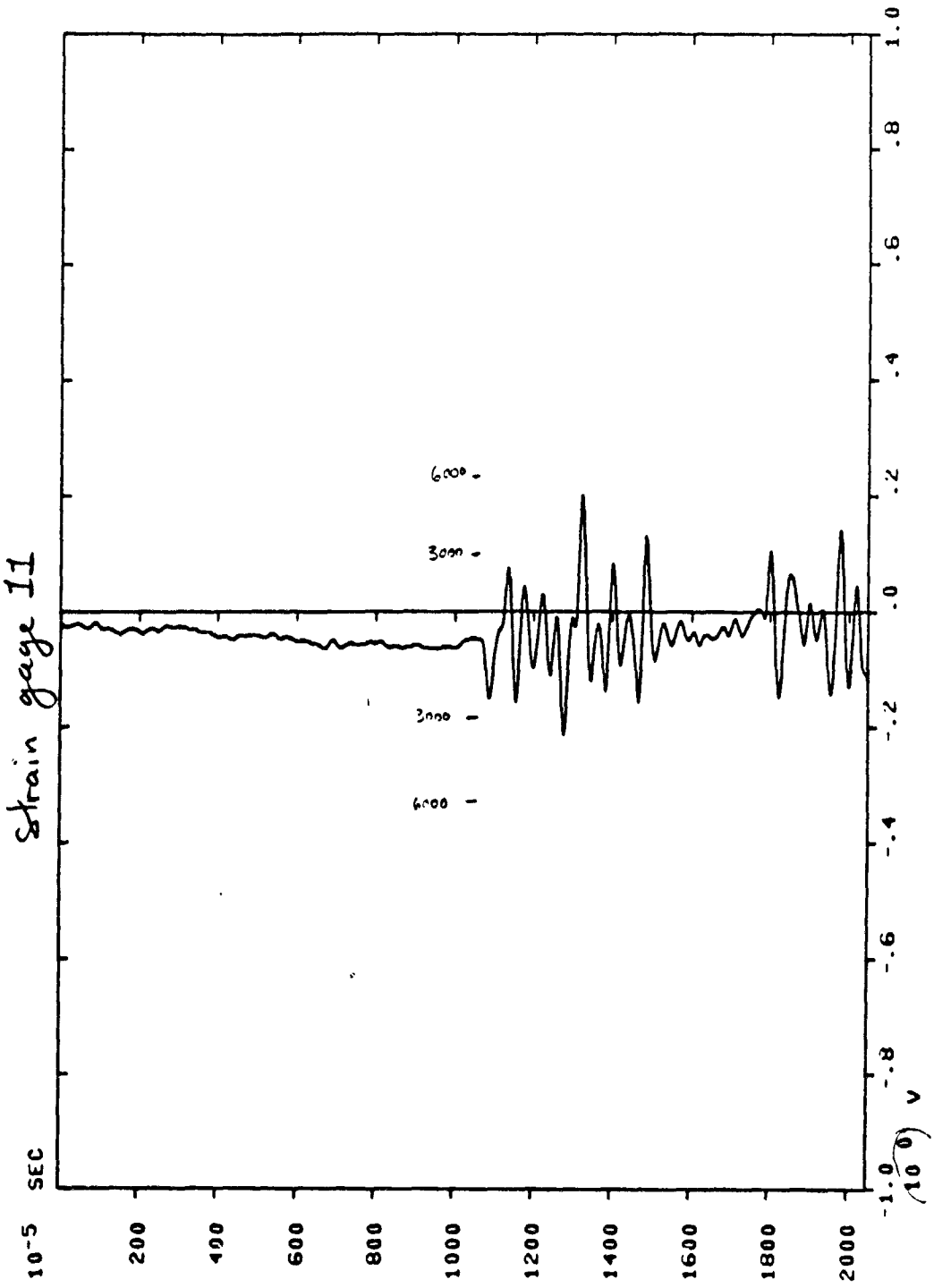
Strain gage 11
6000
3000
3000
6000
10^-5 SEC
200
400
600
800
1000
1200
1400
1600
1800
2000
1.0
.8
.6
.4
.2
.0
-.2
-.4
-.6
-.8
-1.0
(10^0) V

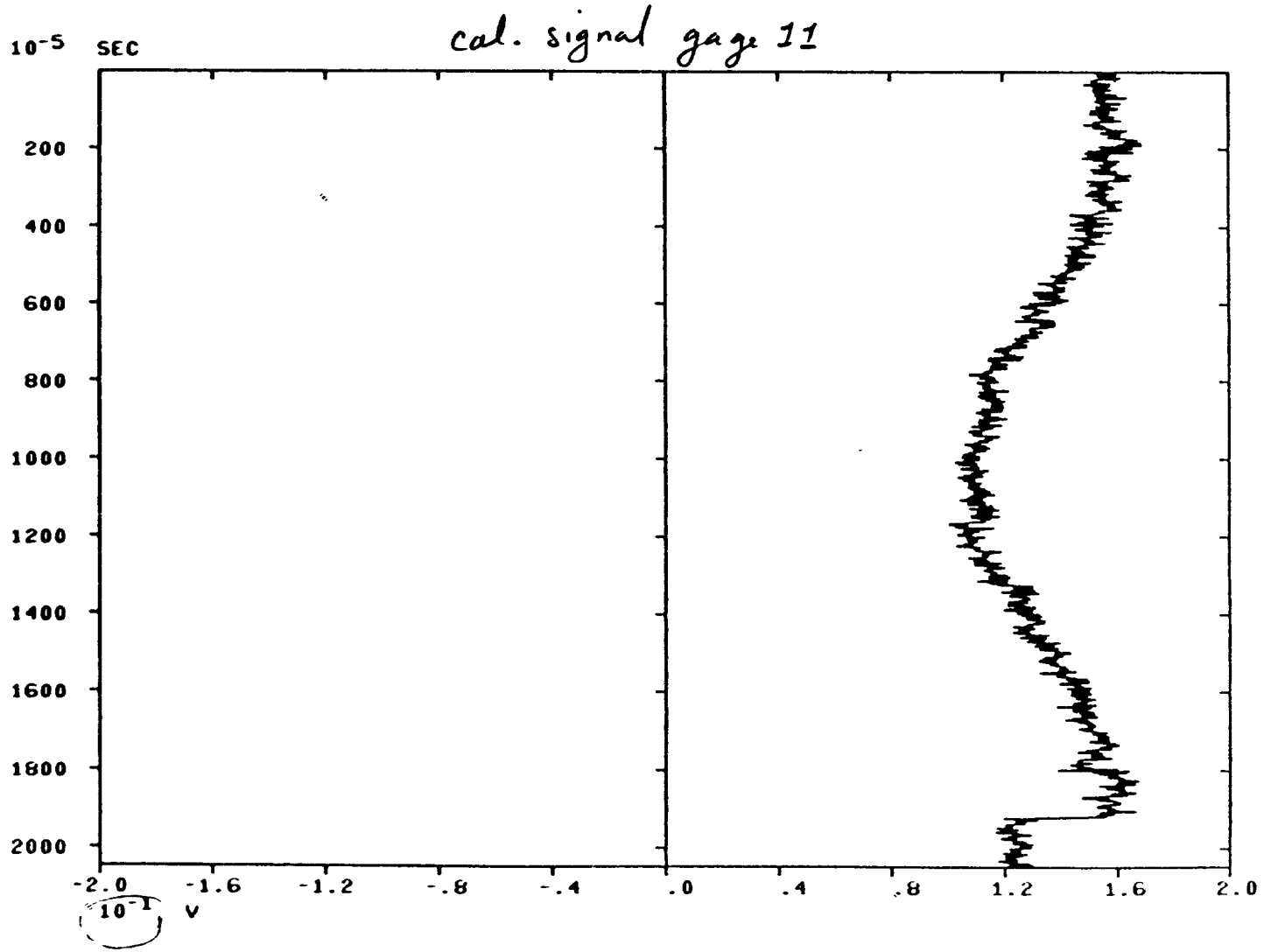
cal. signal gage 11
10-5 SEC
200
400
600
800
1000
1200
1400
1600
1800
2000
-2.0
-1.6
-1.2
-.8
-.4
.0
.4
.8
1.2
1.6
2.0
10-1 V

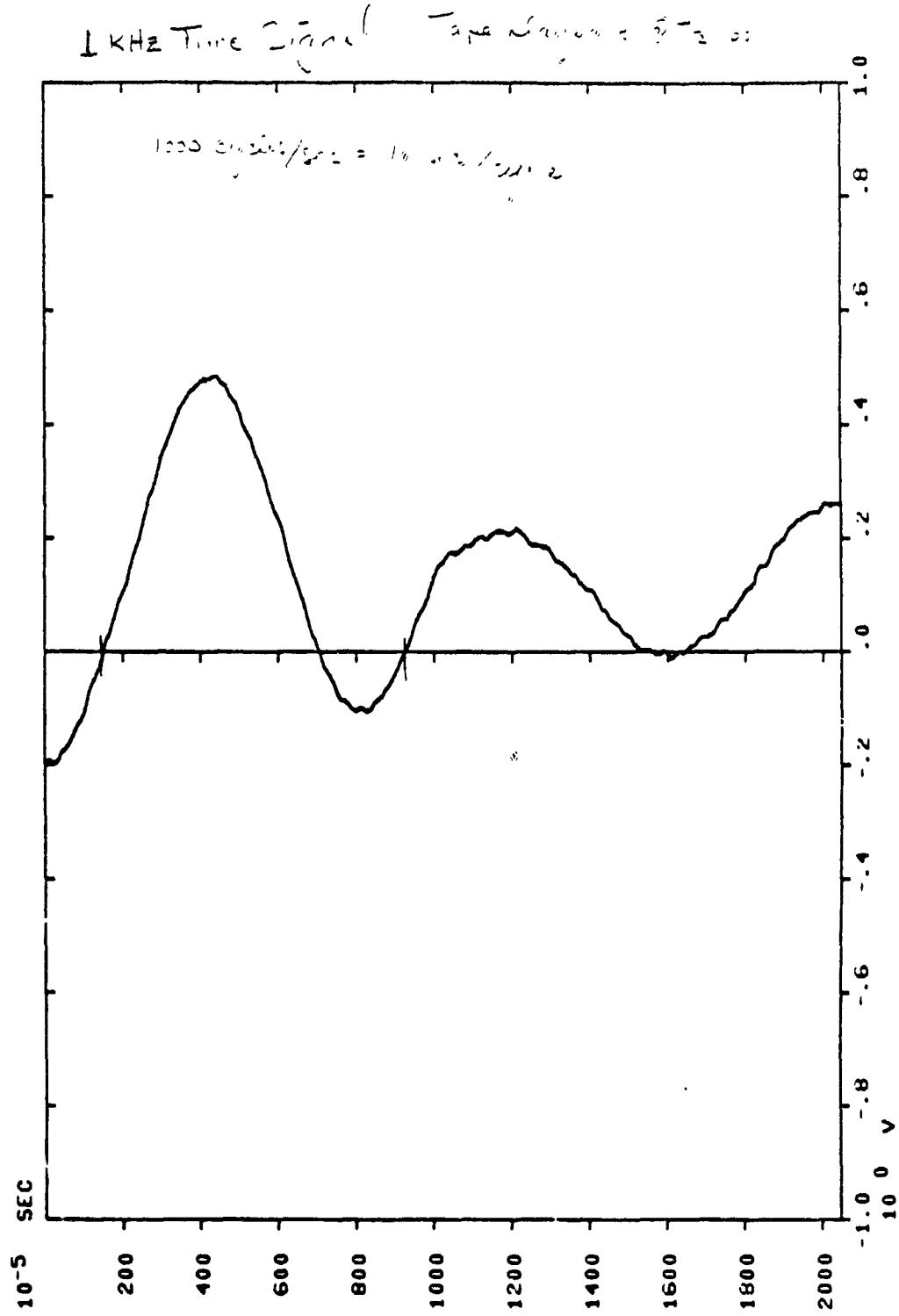
1 KHz Time Signal
SEC
10^-5
200
400
600
800
1000
1200
1400
1600
1800
2000
1.0
.8
.6
.4
.2
.0
-.2
-.4
-.6
-.8
-1.0
10 0 V

LIST OF REFERENCES

1. David, W. Taylor Naval Ship Research Center Report 79/064, Design Equations for Tripping of Stiffeners Under Inplane and Lateral Loads, by John C. Adamchak, p. 2, October 1979.

2. Wu, R., and Witmer, E., "Analytical and Experimental Studies of Nonlinear Transient Responses of Stiffened Cylindrical Panels," AIAA Journal, Vol. 13, No. 9, pp. 1171-1178, September 1975.

3. Army Materials and Mechanics Research Report 74-29, Experimental Transient and Permanent Deformation Studies of Impulsively-Loaded Rings and Cylindrical Panels, both Stiffened and Unstiffened, by E. A. Witmer, R. W-H. Wu and F. Merlis, p. 2-3, April 1974.

4. Smith, C.S., "Compressive Strength of Welded Steel Ship Grillages," Journal of the Royal Institute of Naval Architects, No. 4, October 1975.

5. Manual of Steel Construction, Eighth Edition, American Institute of Steel Construction, 1980.

6. Stultz, K., et.al., Preliminary Analysis of the Response of Structural Elements of a Minesweeper Hull to Underwater Explosion Shock Wave Loading, Weidlinger Associates Testing Services, Chesapeake, VA, November 1982.

7. Cole, R.H., Underwater Explosions, Princeton University, Princeton, New Jersey, 1948.

8. Geers, T.L., "Residual Potential and Approximate Methods for Three-Dimensional Fluid Structure Interaction Problems," J. Acoustic Soc. Am., Vol. 49, No. 5, p. 1505-1510, May 1971.

9. Daddazio, R. and Atkatsh, R., Underwater Shock Response of Submerged Shells an Introduction to the EPSA Computer Program, Weidlinger Associates, New York, NY, June 1983.

10. Daube, R., Underwater Shock-Induced Responses of Submerged Cylindrical Structures, Master's Thesis, Naval Postgraduate School, Monterey, CA, Dec. 1983.

11. Atkatsh, R. and Daddazio, R., Supplement to the EPSA User's Manual, Weidlinger Associates, New York, NY, October 1982.

12. Office of Naval Research Report 27, Dynamic Elasto-Plastic Response of Shells in an Acoustic Medium User's Manual for the EPSA Code, by R. Atkatsh and R.P. Daddazio, March 1980.

13. Butt, L.T., Naval Ship Shock Design Analysis, lecture notes presented at N.P.S. for Naval Ship Shock Course, winter quarter, Vol. 2, p. 31, Jan. 1984.

14. Naval Surface Weapons Center Report 82-294, Accuracy and Response of Tourmaline Gages for Measurement of Underwater Explosion Phenomena, by Ronald B. Tussing, 1 July 1982.

15. Booker, A. and Harrington, C., "The Multiple Charge Effect," Under water Explosion Research, A Compendium of British and American Reports, Office of Naval Research, Department of the Navy, Vol. 1, p. 1121, 1950.

16. Crede, C.E. and Harris C.M., Shock and Vibration Handbook, 2nd ed., McGraw-Hill Book Company, 1976.

17. United States Army Ballistics Research Laboratories Report 134, Experimental Studies of Explosively-Induced Large Deformations of Flat Circular 2024-0 Alumimun Plates with Clamped Edges and of Free Thin Cylindrical 6061-T6 Shells, by E.A. Witmer, et.al., Jan. 1974.

INITIAL DISTRIBUTION LIST

		No. Copies
1.	Defense Technical Information Center Cameron Station Alexandria, Virginia 22314	2
2.	Library, Code 0142 Naval Postgraduate School Monterey, California 93943	2
3.	Professor Y. S. Shin, Code 69Sg Department of Mechanical Engineering Naval Postgraduate School Monterey, California 93943	5
4.	Department Chairman, Code 69 Department of Mechanical Engineering Naval Postgraduate School Monterey, California 93943	1
5.	R. P. Daddazio Weidlinger Associates 333 Seventh Avenue New York, NY 10001	1
6.	M. L. Baron Weidlinger Associates 333 Seventh Avenue New York, NY 10001	1
7.	A. Misovec Weidlinger Associates 5202 West Military Highway Chesapeake, Virginia 23321	1
8.	L. Butt Weidlinger Associates 5202 West Military Highway Chesapeake, Virginia 23321	1
9.	T. L. Geers Lockheed Missile and Space Company 3251 Hanover Street Palo Alto, California 94304	1

10. J. Gagorik, Code 03R24 — 1
Naval Sea Systems Command
Washington, D.C. 20362

11. B. Whang, Code 1750.2 — 1
Hull Group Head, Submarine Protection Division
David Taylor Naval Ship Research and Development Center
Bethesda, Maryland 20814

12. LCDR J. White, USN — 1
SSPS
Defense Nuclear Agency
Washington, D.C. 20305

13. J. Sevin — 1
Defense Nuclear Agency
Washington, D.C. 20305

14. J. V. Meyer, Code 290 — 1
West Coast Shock Test Facility
Supervisor of Shipbuilding, Conversion and Repair
San Francisco, California 94135

15. R. Fuss — 1
David W. Taylor Naval Ship Research and Development Center
Underwater Explosions Research Division
Portsmouth, Virginia 23709

16. R. Tussing — 1
Naval Surface Weapons Center, White Oak
Silver Spring, Maryland 20910

17. LT H. Reams, USN — 1
Public Works Department
Bldg. 210-2
Washington Navy Yard
Washington, D.C. 20374

18. LT Thomas R. Rentz, USN — 1
RD3 Box 224
Oswego, New York 13126